February 1996 • NREL/TP-411-20794

Automated Solar Cell Assembly Teamed Process Research

Final Subcontract Report
6 January 1993 - 31 October 1995

M. J. Nowlan, S. J. Hogan, W. F. Breen,
J. M. Murach, S. F. Sutherland,
J. S. Patterson, G. Darkazalli
Spire Corporation
Bedford, Massachusetts

National Renewable Energy Laboratory
1617 Cole Boulevard
Golden, Colorado 80401-3393
A national laboratory of the U.S. Department of Energy
Managed by Midwest Research Institute
for the U.S. Department of Energy
under Contract No. DE-AC36-83CH10093

NREL/TP-411-20794 • UC Category: 1250 • DE96000537

Automated Solar Cell Assembly Teamed Process Research

Final Subcontract Report
6 January 1993 - 31 October 1995

M.J.Nowlan, S.J. Hogan, W.F. Breen,
J.M. Murach, S.F. Sutherland,
J.S. Patterson, G. Darkazalli
Spire Corporation
Bedford, Massachusetts

NREL technical monitor: Holly Thomas

National Renewable Energy Laboratory
1617 Cole Boulevard
Golden, Colorado 80401-3393
A national laboratory of
the U.S. Department of Energy
Managed by Midwest Research Institute
for the U.S. Department of Energy
under contract No. DE-AC36-83CH10093

Prepared under Subcontract No. ZAG-3-11219-01

February 1996

NOTICE

Available to DOE and DOE contractors from:
Office of Scientific and Technical Information (OSTI)
P.O. Box 62
Oak Ridge, TN 37831
Prices available by calling (615) 576-8401

Available to the public from:
National Technical Information Service (NTIS)
U.S. Department of Commerce
5285 Port Royal Road
Springfield, VA 22161
(703) 487-4650

Printed on paper containing at least 50% wastepaper, including 10% postconsumer waste

TABLE OF CONTENTS

LIST OF ILLUSTRATIONS

LIST OF ILLUSTRATIONS (Concluded)

LIST OF TABLES

ACKNOWLEDGMENTS

This work was made possible by support from the U. S. Department of Energy's National Renewable Energy Laboratory (NREL) through the Photovoltaic Manufacturing Technology (PVMaT) program. The authors gratefully acknowledge the support of Holly Thomas, the program technical monitor at NREL.

The authors wish to thank Jean Hummel and Theresa Jester, Siemens Solar Industries, and John Wohlgemuth, Solarex, for providing solar cells for assembly process evaluations and for performing module qualification tests. The authors also thank Ronald Gonsiorawski and Brian Mackintosh of ASE Americas for providing solar cells for assembly process evaluations and for assistance in final processing evaluations (Task 16).

SECTION 1
INTRODUCTION

This is the Final Technical Report for a program entitled "Automated Solar Cell Assembly Teamed Process Research," funded by the U. S. Department of Energy under National Renewable Energy Laboratory (NREL) subcontract No. ZAG-3-11219-01. The program duration was 34 months, from January 6, 1993, to October 31, 1995. The total program budget was $1.52M, cost-shared between NREL and Spire. The Technical Monitoring Team members were Holly Thomas (NREL), Alex Maish (Sandia National Laboratories), and Joseph Burdick (NREL).

This program was part of Phase 3A of the Photovoltaic Manufacturing Technology (PVMaT) project, which addressed the generic needs of the photovoltaic (PV) industry for improved quality, accelerated production scale-up, and substantially reduced manufacturing cost. Crystalline silicon solar cells (Czochralski monocrystalline, cast polycrystalline, and ribbon polycrystalline) are used in the great majority of PV modules produced in the U. S., accounting for 95% of all shipments in 1994.[1] Spire's goal in this program was to reduce the cost of these modules by developing high throughput (5 MW per year) automated processes for interconnecting solar cells made from standard and thin silicon wafers. Spire achieved this goal by developing a completely new automated processing system, designated the SPI-ASSEMBLER™ 5000, which is now offered as a commercial product to the PV industry. A photograph of the Assembler is provided in Figure 1.

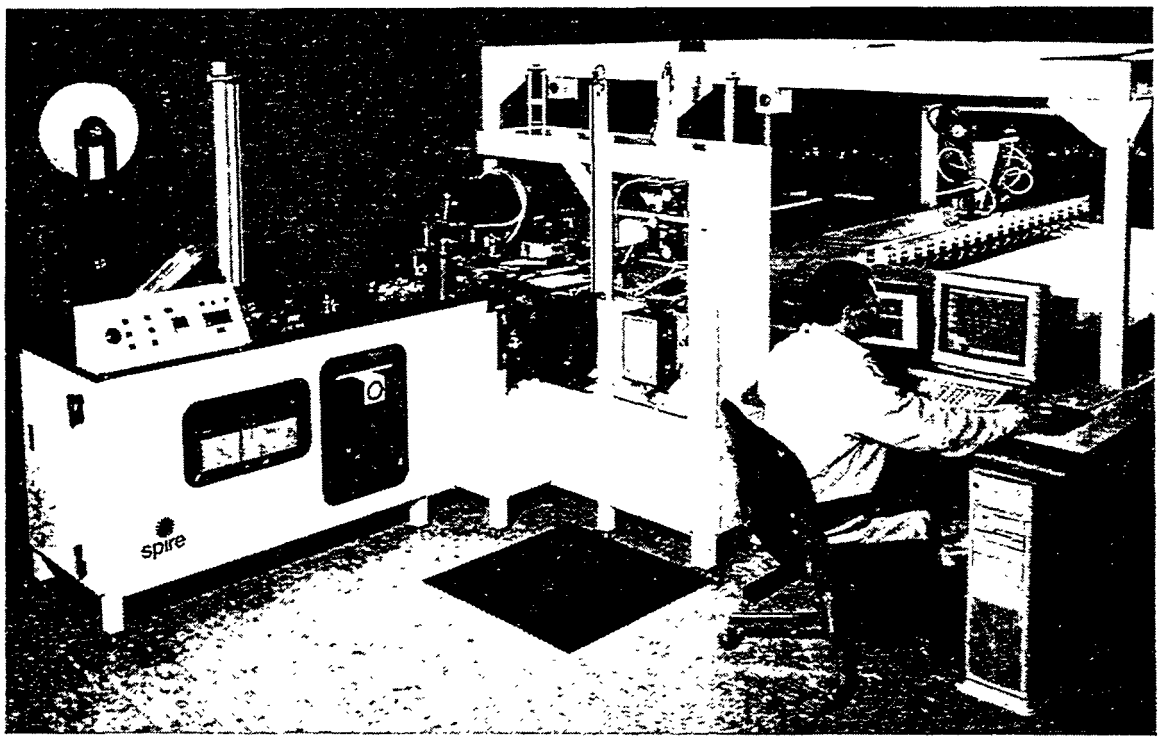

Figure 1 *The SPI-ASSEMBLER 5000 automated solar cell interconnecting system.*

An operator loads stacks of solar cells, reels of copper interconnect ribbon, and liquid soldering flux into the Assembler. The Assembler produces multiple cell strings, where each string is a number of cells connected together in series. New automated processes were developed for cell loading, cell aligning, ribbon handling (ribbon feeding, forming, cutting to length), flux application, ribbon-to-cell soldering, cell string handling, and in-line string I-V testing. Flexible automation techniques were incorporated to enable production of a variety of module designs with minimal mechanical adjustments or tooling changes. During preliminary processing evaluations, Spire successfully processed more than 15,000 cells from six major PV manufacturers.

Significantly more thin (200 μm) wafers can be produced per kilogram of polysilicon feedstock than conventional (350 to 400 μm) wafers, substantially reducing cell cost. However, unacceptably high breakage in processing normally makes such thin cells impractical. In this program, Spire achieved high yields (>98%) with these fragile cells by developing processes with reduced mechanical and thermal stress.

Key process improvements made during this program are summarized in Table 1, which compares features of the Assembler with Spire's previous cell tabbing and interconnecting equipment. As Table 1 indicates, the Assembler has higher throughput, processes larger and thinner cells, applies less mechanical and thermal stress to cells, and performs a number of new functions not done by the previous equipment.

Table 1 *Assembler improvements over previous equipment.*

Feature	Previous Equipment	SPI-ASSEMBLER 5000
Cycle time	8 s/cell	5 s/cell
Cell size capacity	103 mm (4")	150 mm (6")
Cell thickness	≥300 μm	≥200 μm
Cell alignment method	Mechanical edge contact	Non-contact, machine vision
Automated visual inspection	None	Machine vision system
Automated flux dispensing	Front of cell only	Front & back of cell
Heating cycle for soldering	2 cycles, front & back	1 cycle with preheating
String testing	None	Illuminated I-V curve
Labor requirements	4 operators	1 operator
Maximum module size	78 cm x 144 cm	137 cm x 200 cm

Several systems based on the new technology developed in this program have already been sold to PV manufacturers. A semi-automated system based on the Assembler concept, the SPI-STRINGER™ 500, was developed for manufacturers starting at lower volume production levels. As of October, 1995, Spire had sold three Assemblers and two Stringers, generating total sales of $1.6M.

A detailed cost analysis was done to compare the cost of the Assembler's automated processes to the semi-automated Stringer's processes and to manual processes.[2] The costs, not including cells, were calculated to be $0.445/W for the manual case, $0.163/W for the Stringer, and $0.087/W for the Assembler.

Spire teamed with Solec International (Hawthorne, CA), a PV module manufacturer, and the University of Massachusetts Lowell's Center for Productivity Enhancement (UML, Lowell, MA), automation specialists, who were lower-tier subcontractors. Solec produced thin (200 μm) cells used to evaluate the cell interconnection processes, while UML provided vision system and software support for cell loading and aligning processes. A number of additional PV manufacturers, including ASE Americas (Billerica, MA), Siemens Solar Industries (Camarillo, CA), Solarex (Frederick, MD), Ebara Solar (Large, PA), and Texas Instruments (Dallas, TX), participated in process evaluations in the course of the program. The Assembler was shipped and installed at ASE Americas, which served as the site for production evaluations. A program organization chart is provided in Figure 2.

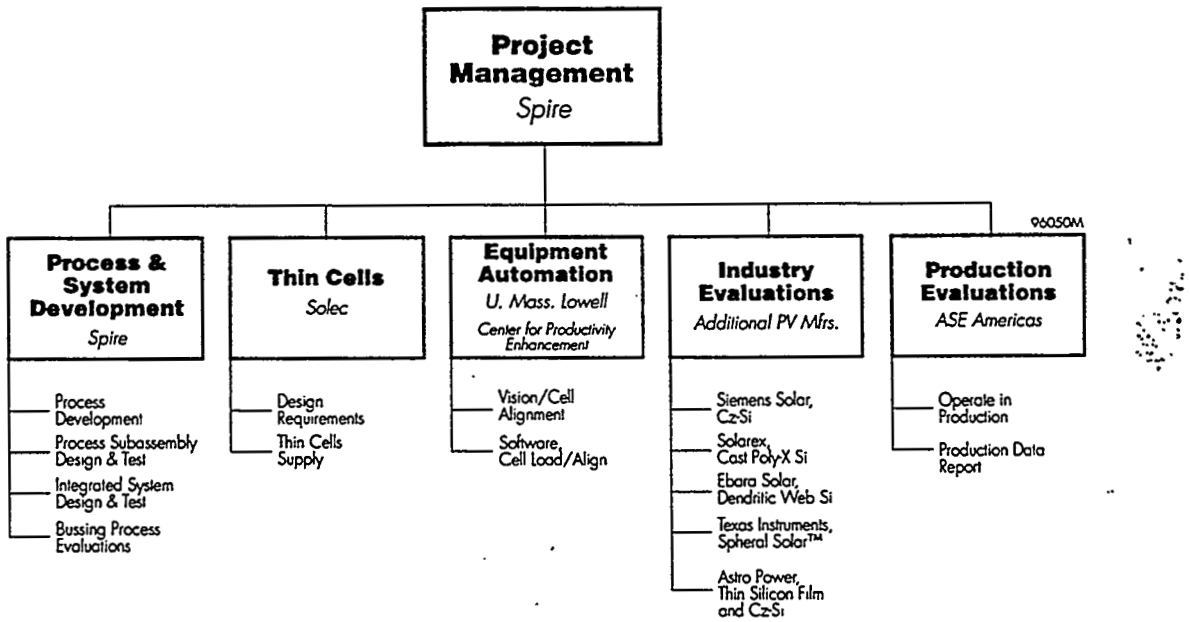

Figure 2 *Project team organization, PVMaT Phase 3A for Automated Solar Cell Assembly Teamed Process Research.*

The program was divided into two phases and twenty tasks, as listed in Table 2. Phase I comprised Tasks 1 through 12, extending from January 6, 1993, to December 31, 1993. Phase II comprised Tasks 13 through 20, extending from December 6, 1993, to October 31, 1995.

An organization chart showing Spire's project team for this program is provided in Figure 3.

Table 2 *Program tasks.*

Phase		Task
I	1	Design Definition
	2	Cell Loading Process Development
	3	Cell Alignment Process Development
	4	Interconnect Ribbon Handling Process Development
	5	Solder Flux Application Process Development
	6	Ribbon to Cell Soldering Process Development
	7	Cell String Handling Process Development
	8	In-Line I-V String Testing Development
	9	Process Subassembly Design
	10	Process Subassembly Test
	11	Integrated System Design
	12	Information Dissemination
II	13	In-Line I-V String Testing Development
	14	System Integration and Test
	15	Preliminary Processing Evaluations (at Spire)
	16	Final Processing Evaluation (at ASE Americas)
	17	Information Dissemination
	18	System Design Definition for Novel Cells & Bussing
	19	Bonding Interconnects for Novel Cells
	20	Bus Ribbon Bonding

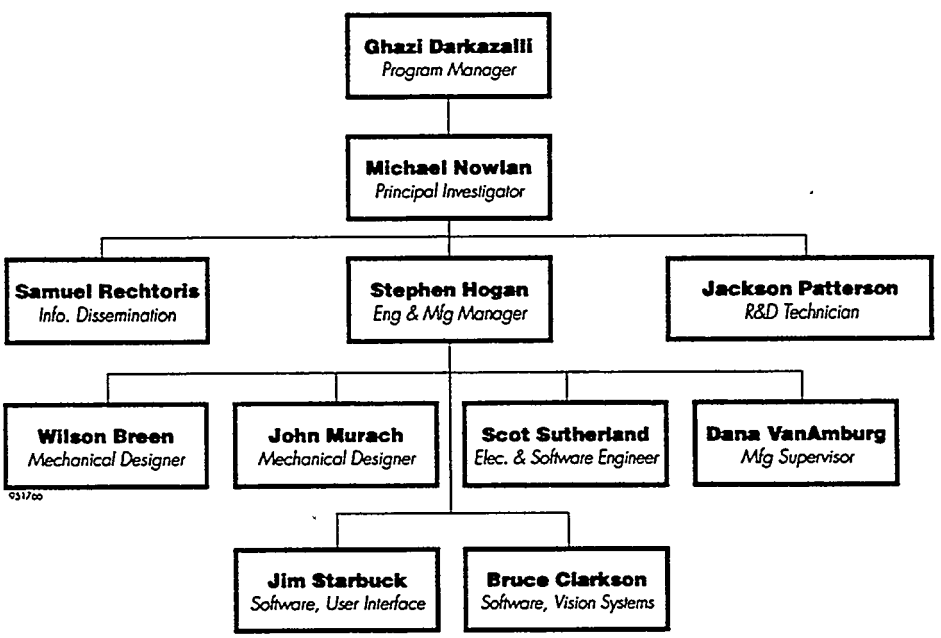

Figure 3 *Spire's project team for the PVMaT Phase 3A program.*

SECTION 2
TECHNICAL DISCUSSION

Spire attained its program objective of developing high throughput (5 MW/yr) automated processes for interconnecting standard and thin silicon solar cells. High yield was achieved with fragile cells through the development of low mechanical stress and low thermal stress processes. For example, a machine vision system was developed for aligning cells without making mechanical contact to the cell edges, while a new soldering process was developed that solders metal interconnect ribbons simultaneously to a cell's front and back contacts, eliminating one of the two heating steps normally used for soldering each cell. Simultaneous front and back soldering has the additional benefit of eliminating the labor intensive task of transferring tabbed cells onto alignment fixtures, previously required for separate tabbing and interconnecting processes.

Flexible automation techniques were incorporated wherever practical to enable production of a variety of module designs with minimal mechanical adjustments or tooling changes. This flexibility is provided through software control of the tab (cut ribbon) length, the tab stress-relief bend location, the soldering cycle, the cell-to-cell spacing, the number of cells per string, the number of strings per module, the string-to-string spacing, and the arrangement of strings in a series, parallel, or combined configuration.

The processing system has the capacity to handle round, square, or pseudo-square (round with four large flats) cells up to 15 cm across. Strings up to 2.0 m long can be assembled and placed side-by-side to create two-dimensional module-size cell arrays up to 1.4 m wide. A layout drawing of the system is provided in Figure 4.

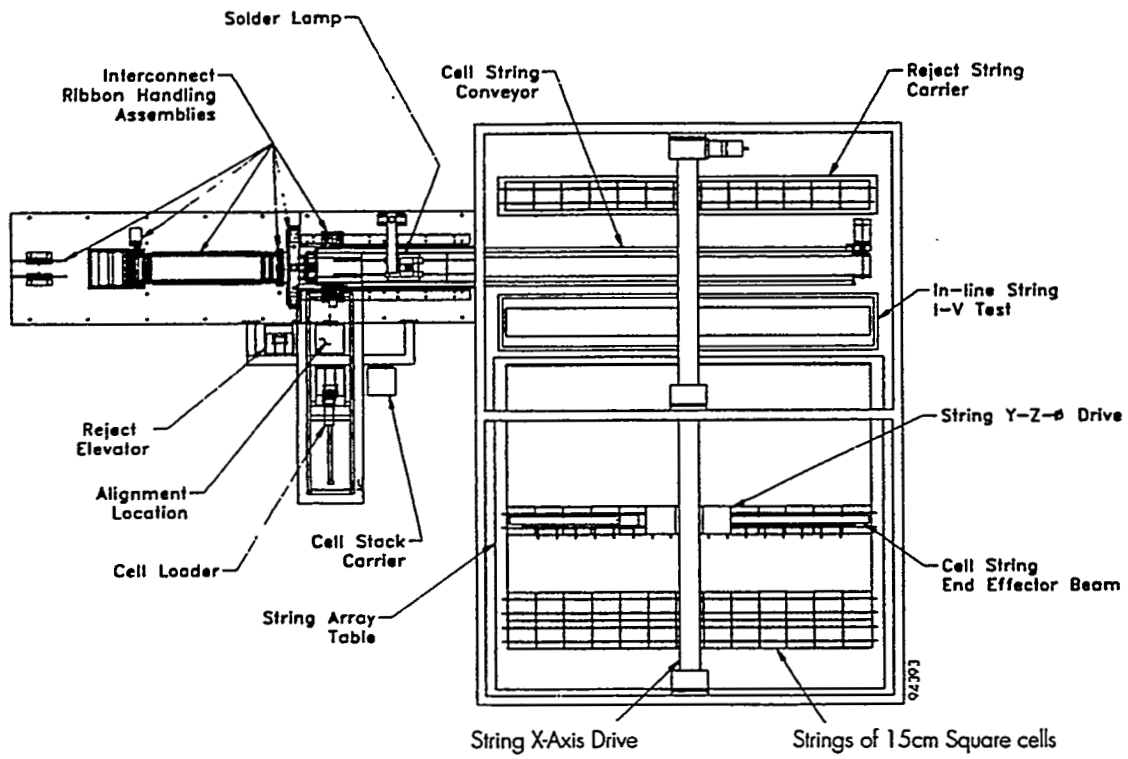

Figure 4 *Lay-out drawing of the automated cell assembly system (plan view).*

A process flow chart illustrating the flow of materials (solar cells and interconnect ribbon material) through the cell assembly system is shown in Figure 5.

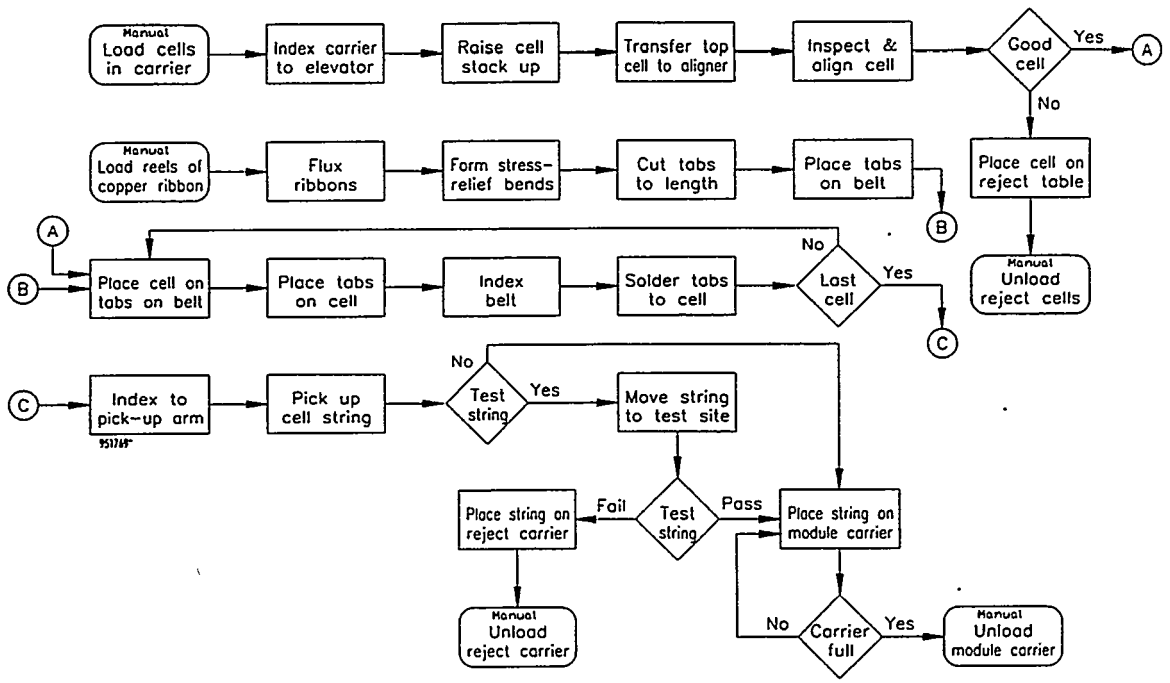

Figure 5 *Process flow chart, automated solar cell assembly system.*

2.1 Process Throughput

The annual throughput is a function of the processing rate, the system up-time, the cell efficiency, the cell area, the hours of operation, and the process yield. It can be calculated by the following expression:

$$T = Rt\eta ALn_s n_d Y \qquad \textbf{(1)}$$

where
- T = annual throughput (W/yr)
- R = processing rate in cells/minute x 60 min/hr x 8 hr/shift (cells/shift)
- t = system up-time, the ratio of (operating time)/(total time)
- η = average cell efficiency in production at Standard Test Conditions
- A = cell area (cm^2)
- L = solar insolation = 0.100 (W/cm^2)
- n_s = number of operating shifts per day (shifts/day)
- n_d = number of operating days/week x 52 weeks/year (days/year)
- Y = process yield, the ratio of (good cells out) / (cells in)

As an example, for R = 5760, t = 80%, η = 14.5%, A = 100 cm^2, n_s = 3, n_d = 260, and Y = 0.98, the annual throughput, T, is 5.11 MW/yr. This processing rate, R, is equivalent to 12 cells/ minute, or a process cycle time of 5.0 s/cell. (This value of T is conservative in that, with 5 day/week operation, there is a weekend downtime of 2/7 = 28.6% in addition to the 1-t = 20% downtime allowed for in the calculation.) Annual throughput is plotted as a function of cell efficiency for various cell sizes in Figure 6. The impact of uptime and yield on cost is discussed in Section 3.

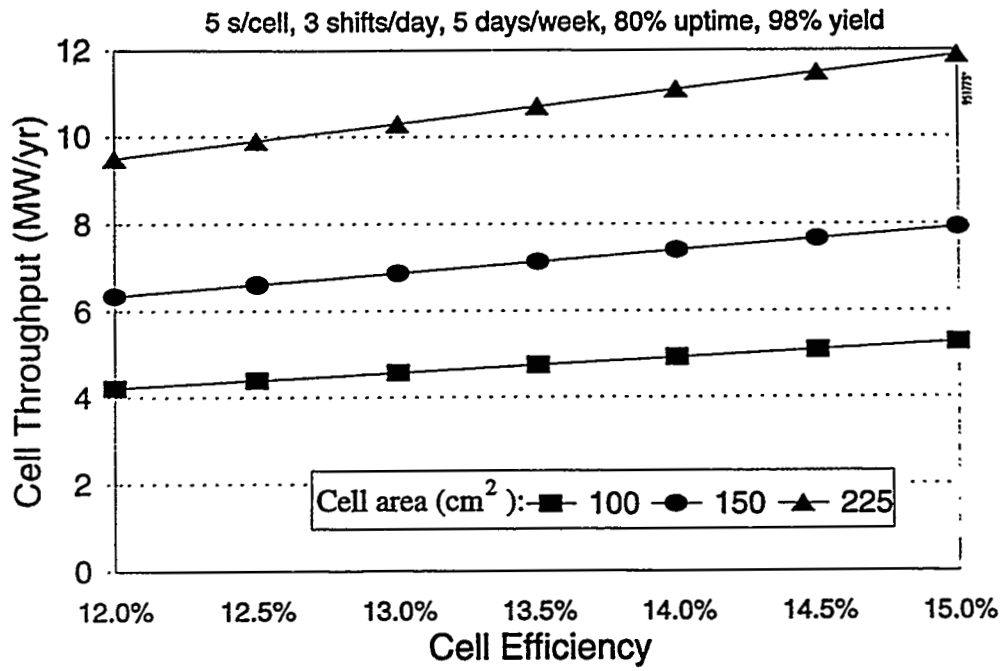

Figure 6 *Cell assembler capacity vs. cell efficiency for three cell sizes. Assumes R = 5760 cells/shift, t = 80%, n_s = 3, n_d = 260, and Y = 0.98.*

2.2 Program Tasks

2.2.1 Task 1 - Design Definition

Spire engineers met with several PV module manufacturers during the first four months of the program to solicit design input for cell interconnection processes. This information guided subsequent design and development work to ensure that the systems and processes would meet the specific needs of as many manufacturers as possible.

The manufacturers that participated in the survey were Solec, Siemens Solar, ASE Americas (then Mobil Solar), and Texas Instruments. Spire presented its baseline concepts for manufacturing interconnected assemblies of solar cells, which were formulated in the PVMaT Phase 1 program.[3] Discussions of the baseline concept gave valuable insights from the manufacturer's perspective to the Spire design team. Detailed input was gathered on the manufacturers' specific cell assembly requirements, including cell sizes, contact configurations, interconnect ribbon materials, coatings, and sizes, solder flux or paste requirements, string lengths, required process yield, *etc.*

The information obtained from these manufacturers was used by Spire to develop cell interconnection processes that are compatible with the majority of photovoltaic module manufacturers. The information is summarized in Table 3.

Table 3 *PV module manufacturers' requirements for cell interconnecting.*

Category	Parameter	Requirements
Solar cell characteristics	Cell shapes	Round, square, pseudo-square, rectangular
	Maximum cell size	100 to 125 mm square; 150 mm in future
	Cell thickness	300 to 450 μm; 200 μm in future
	Loading arrangement	Coin stack, two for continuous feeding
Interconnect ribbon characteristics	Material	Copper, ETP or OFHC*
	Width	1.5 to 2.5 mm
	Thickness	50 to 125 μm
	Coating	$Sn_{60}Pb_{40}$ or other solder alloy
	No. of ribbons/cell	2; possibly 3 in future
Solder flux or paste requirements	Flux	Low-solids "no clean" flux used with thick (12 μm) SnPb coating on ribbon
	Paste	"No clean" SnPbAg paste used with thin (1.6 μm) SnPb coating on ribbon
Other requirements	Maximum string length	2.0 m
	Throughput	4 to 5 s/cell
	Minimum yield	98% to 99%
	Minimum system up-time	75% to 80% in 3-shift 7-day operation
	Pre-soldering inspection	Desirable
	Post soldering string test	Desirable

*ETP is electrolytic tough pitch copper, alloy C110; OFHC is oxygen-free high conductivity copper, alloy C102.

A significant recommendation which came out of these discussions was the need for an in-line string I-V test. This test is done after string fabrication and prior to string placement on the module carrier, as a quality control measure. Spire and NREL agreed to add two tasks (Tasks 8 and 13) to the program to implement this in-line test.

2.2.2 Task 2 - Cell Loading Process Development

A process for automatically loading standard and thin cells with high throughput was developed under this task. A vendor survey was done to determine the availability of wafer handling equipment in the commercial marketplace. Information on wafer handling, wafer transport, and cassette (slotted wafer carrier) handling systems was obtained and reviewed. A list of vendors was compiled to summarize and compare the types of products offered.

After reviewing the product literature, discussions were held with representatives from seven companies whose handling systems were best suited for this application. As a result of these discussions, four general types of loading systems were defined, as illustrated in Figure 7.

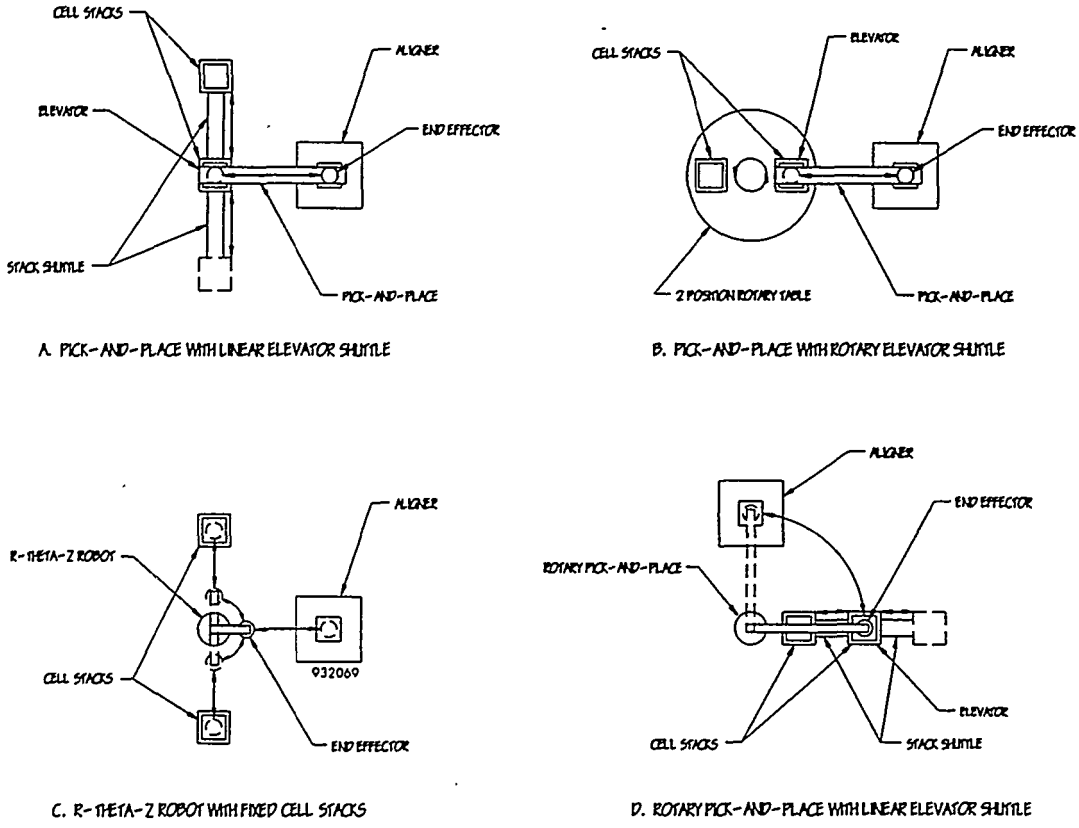

Figure 7 *Solar cell loading options.*

Option A (in Figure 7) has a linear pick-and-place mechanism with x and z motions to pick up a cell from a stack elevator and place it at the aligner. Two cell stacks are mounted on a linear shuttle which transports each stack to the elevator. Option B is similar to option A except the linear shuttle is replaced with a rotary table. Option C uses an r-θ-z robot to transfer cells from fixed stacks to the aligner. In this case, no elevator is required, since the robot has sufficient z travel. Option D has a rotary pick-and-place mechanism (θ and z motions) and a linear shuttle for cell stacks similar to option A.

Slotted cassette unloading systems, commonplace in the semiconductor industry, have been eliminated from consideration in favor of cell stack unloaders. The ability of solar cells to tolerate stacking without yield or performance degradation and the processing of cells in high volumes, on the order of millions per year, encourages PV module manufacturers to handle cells in a stack format to minimize the volume of space taken up by cells in process. For example, a typical cassette for holding twenty-five 100 mm square wafers has overall dimensions of 143 mm by 123 mm by 114 mm.[4] A stack carrier of the same dimensions can hold a stack of cells 130 mm high, equivalent

to 520 cells with a thickness of 250 μm, or more than 20 times the number of cells in the same volume. (A 250 μm cell thickness was chosen for this example to allow 50 μm for the front and back contacts, in addition to the silicon thickness.)

All four options (A through D) have the capacity to hold two stacks of cells to allow the operator to manually load a stack of cells while the system is automatically feeding from another stack. Thus the loading process can proceed indefinitely without interruptions, resulting in increased product throughput.

The r-θ-z robot approach (option C) is used for wafer loading by the semiconductor industry. This approach is elegant in that it eliminates all other loading process mechanisms (elevator and shuttle mechanisms). Its flexibility in motion exacts a price in throughput, however, since almost all of its motions must be done in series. The process required to load a cell requires 11 separate r, θ, and z motions estimated to take five to six seconds per cell. Since this cycle time is too slow to meet the four second per cell throughput goal, the r-θ-z robot approach was eliminated from consideration.

Options A, B, and D are all potentially faster than option C since the cell stack vertical motion is done concurrently with the cell pick-and-place operation. A version of option D is commercially available and is typically used to load ceramic substrates into screen printers for hybrid circuit applications. This loader should be able to meet the four seconds per cell requirement. However, the largest cell size which the system can handle is 114 mm (4.5 inch) square, smaller than our requirement of 150 mm (6 inch) square. As a result, this system was not selected.

The stack loader which Spire designed and builds for its SPI-TAB™ 1000 tabbing machine was also evaluated for use in this program. The loader has a single elevator with multiple shelves for cell stacks and an optical sensor to maintain the proper stack height. A rotary pick-and-place arm (θ and z motions) with vacuum cups picks up cells from the top of the stack. A compressed air jet and a cell flexer (which slightly bends the top cell as it is being picked up) are used to separate the top cell from those under it in the stack, since quickly picking up a cell creates a low pressure region under the cell which tends to lift additional cells in the stack, especially if they are thin. While this loader works well and has a number of good features (the optical stack height sensors, the air jet, and the cell flexer), it was not selected for use because it has no stack shuttle, which requires that the loading process be interrupted for inserting cell stacks into the elevator.

Since no commercial system was found which satisfies all the requirements for this application, Spire designed a custom system for loading cells. Option A (in Figure 7) was selected over option B because the linear stack shuttle is a simpler mechanism than the rotary shuttle. A lay-out drawing of the cell loading system is provided in Figure 8. The drawing also shows the cell aligner system, which is mounted on the same frame.

Quick-release stack carriers were designed for holding cell stacks on the shuttle mechanism. Each carrier has the capacity to hold a stack up to 25 cm high, equivalent to 714 cells with a thickness of 350 μm per cell. At a processing rate of 5.0 s/cell, a full stack will take 59.5 minutes to unload.

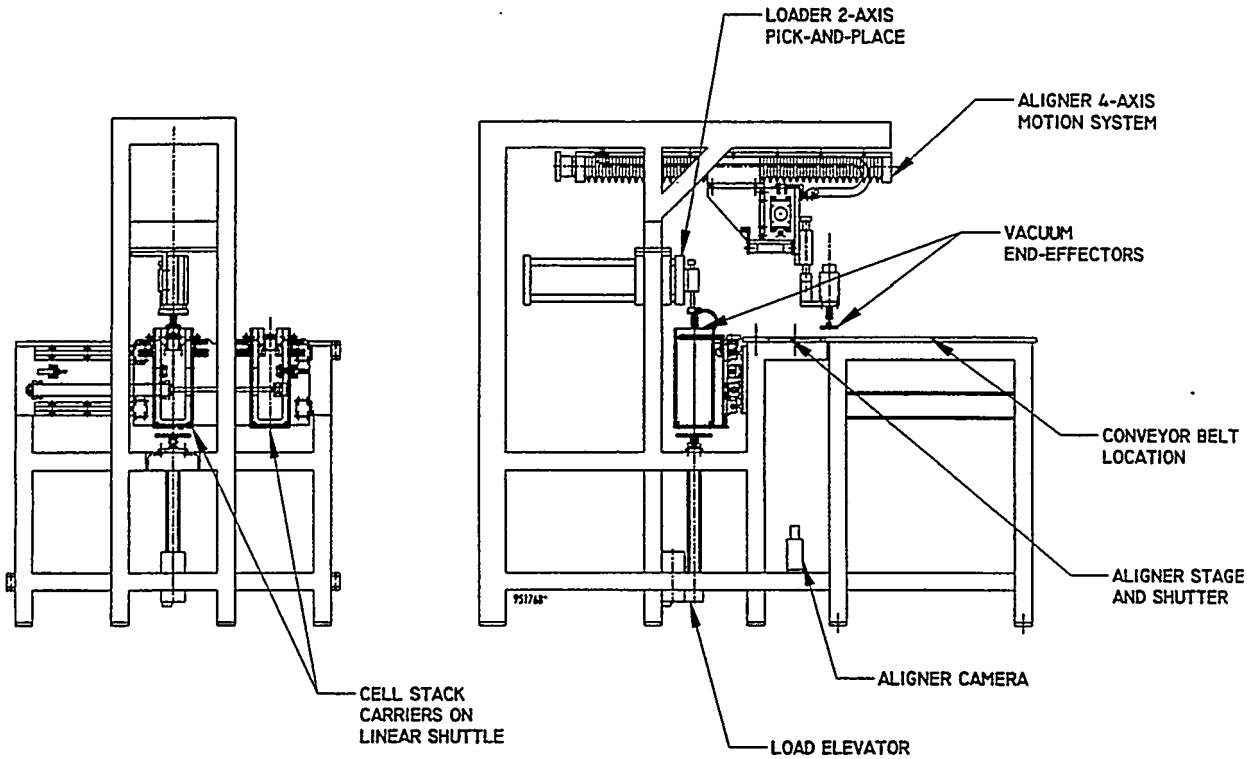

Figure 8 *Lay-out of the cell loading and alignment systems.*

The stack shuttle is mounted on linear ball bushings and driven by an air cylinder. The shuttle transports two stack carriers back and forth between the load elevator and locations on either side of the elevator for removing empty carriers and inserting full ones.

The load elevator is driven by a linear electric cylinder (lead screw type) controlled by optical sensors. As cells are withdrawn from a stack by the pick-and-place mechanism, a broken-beam optical sensor directs the load elevator to raise the stack, thus maintaining the top of the stack at the proper height. An additional optical sensor detects when a carrier on the load elevator is empty.

Air knives (a series of air jets arranged in a line) were designed to separate the top cell from the others in the stack. The jets direct streams of compressed air at opposite sides of the cell stack to fill the low pressure region created under the cell by the pick-up operation.

The cell pick-and-place mechanism (also called the cell manipulator) uses air actuated linear slides with ball bushing mounts for moving the cell in x and z axes. Hydraulic cushions allow higher speed operation by reducing end-of-stroke vibrations. A vacuum pick-up end-effector with a mechanically floating mount was designed to minimize stress on thin cells during pick up and placement. Vacuum is provided to the end effector by a vacuum aspirator assembly, which includes a venturi vacuum pump, a filter, a vacuum switch to indicate the presence of a cell, and a vacuum breaking valve for rapid release of the cell.

Position sensors are installed on all mechanisms (cell pick-and-place, stack shuttle, and elevator) to prevent collisions. The sensors also increase processing speeds, since they signal the process controller to execute the next step in a sequence as soon as conditions are safe. Safety mats are provided in the two stack carrier loading areas to prevent operator injury during stack loading. The stack shuttle and the stack elevator are interlocked so they will not move when an operator is standing on either mat.

2.2.3 Task 3 - Cell Alignment Process Development

A new solar cell alignment process was developed that uses a machine vision system to locate and inspect each cell and a 4-axis (x-y-z-θ) robot with a vacuum end-effector for cell alignment and transport. Unlike mechanical alignment systems, no contact is made to the wafer edges. The vision system includes a monochrome CCD video camera, lighting, an alignment stage with a shutter, and a vision processor board installed in a personal computer (PC). A black and white video monitor displays camera images and vision board output. Software was developed for controlling the loader manipulator, the aligner robot, the shutter, and the vision board, for processing images (for alignment and inspections), and to create a user interface.

Since the cell is face-down during the alignment process, the video camera is mounted below a transparent alignment stage, as indicated in Figure 8. The alignment stage is centrally located between the cell loader, the conveyor belt (for cells that pass vision inspection), and the reject table (for cells that fail vision inspection), to minimize travel time and maximize system throughput.

Spire engineers worked with a team from the University of Massachusetts Lowell (UML) Center for Productivity Enhancement to develop the cell alignment process subsystem. Spire had the lead role in the mechanical engineering aspects, such as the design of the cell aligner robot, the aligner stage, the shutter, and the structural frame. UML selected the camera and the vision board, wrote the initial version of the vision software for cell alignment and inspection, and developed the control software for the aligner robot and the cell loader manipulator.

The alignment process, outlined in Table 4, starts when the loader places a cell on the aligner stage. A shutter closes over the cell to provide a white background and the camera underneath the stage sends an image of the cell's front surface to the vision board for analysis. The image is processed to determine the cell's location in x, y, and θ, and to inspect the cell for defects such as breaks, chips, unrecognizable contact patterns, or upside-down placement. The shutter opens and the aligner robot moves in x and y to the cell's center point (determined by the image analysis) and picks up the cell from the stage. Rejected cells are placed on the reject table, while good cells are placed in the proper location (x, y, and θ) on the conveyor belt.

The aligner robot's x and y axes are stepper motor driven lead screw assemblies, z is air actuated, and θ is stepper motor driven. The three stepper motor controllers communicate with the aligner PC via an RS232 port. Position sensors allow homing, end of travel, and collision prevention functions. A vacuum pick-up end effector was originally fabricated with a design similar to that used in the loader, but changes were made to meet the special needs of the alignment process. For example, a ball bearing mount was replaced with a ball slide for improved mechanical accuracy when

Table 4 *Cell alignment process. Aligner robot motion directions are in parentheses.*

Step	Description
1	Load cell on aligner stage
2	Close shutter to provide white background
3	Acquire cell image
4	Process image to locate and inspect cell
5	Open shutter
6	Move vacuum end effector to cell center (x, y)
7	Pick up cell with vacuum (z)
8	Align and transport cell to conveyor belt or reject table (x, y, θ)
9	Place cell on conveyor or reject table (z)

placing aligned cells, while a white ring was mounted above the dark vacuum pad to aid in imaging the pad during system calibration.

2.2.3.1 Aligner Lighting Evaluations

The initial aligner stage design did not include a shutter. Vision system testing showed that images of cell contact patterns can be readily obtained, since the reflective metal contacts have excellent contrast against the dark active areas of the cell. However, problems were encountered in detecting cell edges, since the ambient background above the cell produces a pattern of light and dark regions (variable pixel intensities) around the cell image. A white shutter was then designed and installed to provide a uniform white background for good contrast around the cell edges. The shutter slides over the back of the cell during image capture and then retracts to allow the cell to be picked up. Limit switches were installed to indicate shutter open and closed positions for rapid sequencing and to prevent collisions with the loader and aligner manipulators.

While the shutter eliminated the primary edge detection problem, further tests identified another source of error. The gap between the cell and the shutter (approximately 3 mm) creates a narrow shadow band of varying light intensity around the cell edges. The vision system sometimes confused this shadow band with the cell edge, causing intermittent alignment errors. Many variations in lighting were tried without success. Finally the shutter was changed to a translucent white material and lights were added above the shutter, providing back lighting in a manner similar to a light table used for viewing slides or transparencies. The back lighting filled in the shadows completely, and reliable cell edge detection was achieved.

2.2.3.2 Aligner Stage Debris Check

The addition of the shutter (described in Section 2.2.3.1) allowed a new self-diagnostic check to be incorporated into the alignment process. The shutter was programmed to close after each cell is picked up from the stage and an image is obtained of the empty stage. The image is processed to check for debris that could be left on the stage if a cell breaks. If debris is found, the machine pauses, an image of the debris is displayed on the video monitor, and the operator is alerted to clear the debris from the aligner stage. The cell that was picked up from the stage is rejected, since it is assumed that the fragment came from that cell. A photograph of the video monitor displaying a cell fragment detected by the debris check routine is provided in Figure 9. Fragments as small as 1 mm^2 can easily be detected.

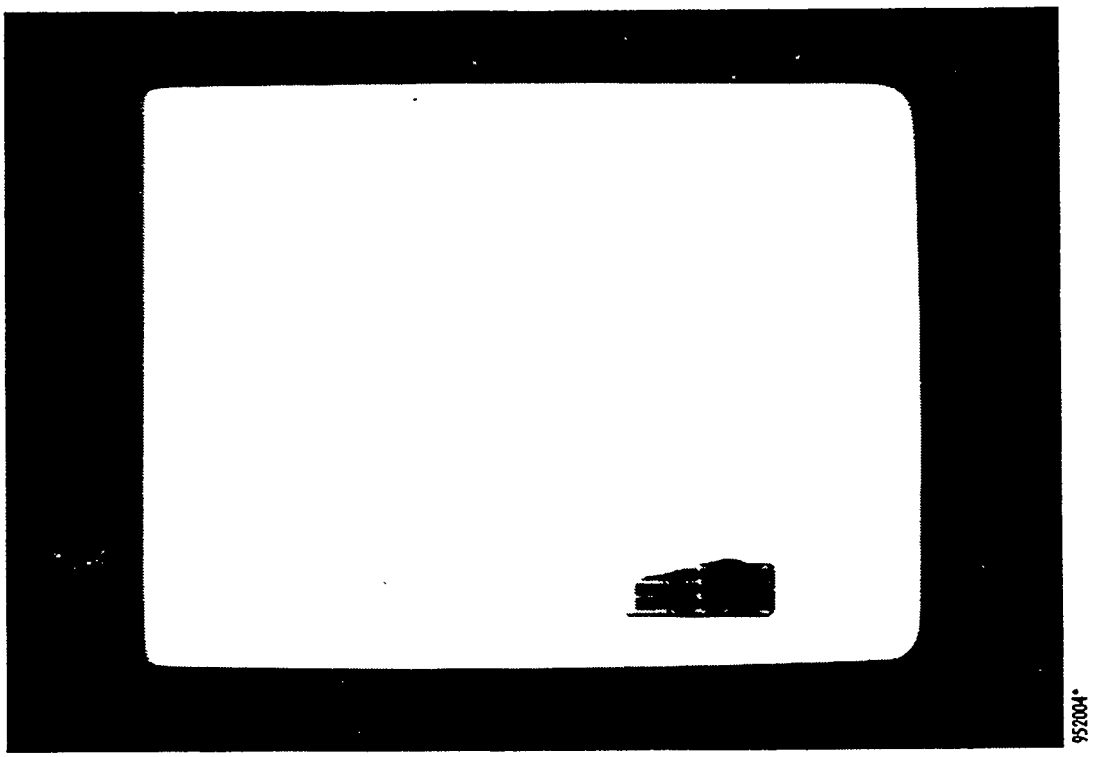

Figure 9 *Cell fragment detected by the debris check routine and displayed on the vision system monitor.*

2.2.3.3 Aligner Mechanical Evaluations

When a cell is picked up from the aligner stage by the aligner robot, the center of the vacuum pad is placed on the center of the cell to simplify the rotational (θ) alignment. The vacuum pad cannot be placed on the cell until after imaging, since the center point of the cell is not known until after the image data are processed. Careful inspection of the pick-up operation showed that cells moved slightly on the aligner stage during placement of the pick-up, introducing an error in cell position. Testing showed that this problem can be minimized to some extent by adjusting the pick-up for parallelism with the stage, but it could not be eliminated.

It was recognized earlier in the program that a vacuum chuck designed into the aligner stage would hold the cell securely and prevent it from being pushed out of position by the pick-up. This approach was not considered, however, since a conventional vacuum chuck would obstruct the view of the video camera mounted underneath the stage. When the importance of holding the cell securely was recognized, a novel vacuum chuck was invented which is transparent to the video camera. The chuck is made from a top glass layer and two layers of clear polycarbonate sheet with intersecting slots and holes. The slots and holes have sharp edges which can be seen faintly on the video monitor, but they do not affect the cell image processing since the images are below the threshold at which they would be recognized as a cell feature. A photograph of the aligner stage with the vacuum chuck and the white shutter is provided in Figure 10.

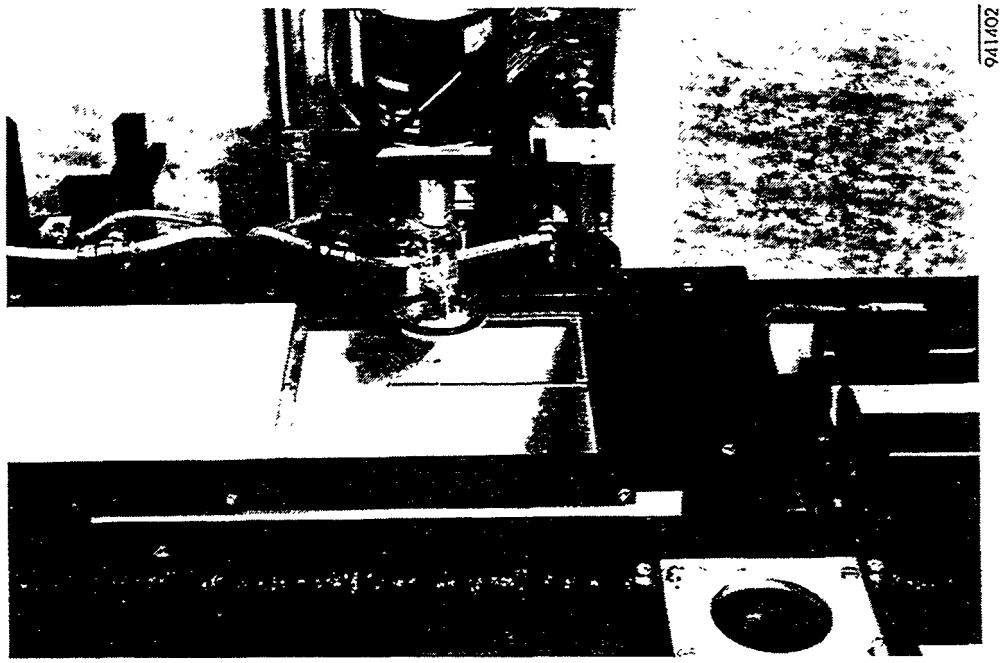

Figure 10 *Aligner vacuum pad over the cell aligner stage. The white shutter is retracted to the left. The stage's vacuum chuck grooves and holes are more pronounced in this photo than they are to the aligner camera due to the camera angle.*

2.2.3.4 Vision System Software Evaluations

The first version of the cell alignment software, written by UML, detected the four edges of a square cell and used this data to calculate the cell's center point and its angle of rotation. The accuracy and repeatability of cell placement was tested and found to be less than required. For example, when the cell-to-cell spacing was set to 0.085", cell string measurements showed spacing variations from 0.075" to 0.110", a range of 0.035". The repeatability of the stepper motors, motor drivers, and mechanisms for both the aligner manipulator and the conveyor belt was measured and verified to be better than ±0.001". Thus the variations were caused by the vision system software. UML tried two alignment algorithms without success, one that used a center-of-mass calculation and another based on intersecting diagonals.

The poor cell alignment results and the lack of robustness (sensitivity to lighting conditions, frequent computer hang-ups, *etc.*) of UML's vision code, despite a large amount of software development and debugging time, forced Spire to pursue an alternative machine vision approach: the use of a commercial vision system. A system was selected that includes a far more sophisticated image processing board with an on-board CPU and a library of high-level software tools available for cell alignment and inspection tasks. A new version of the cell alignment and inspection software was written that uses the new vision processor and tools. Software was also developed in collaboration with UML to link the new image processing software with UML's control software for the loader, aligner robot, and shutter, which was retained. Excellent cell alignment results were obtained during extensive evaluations with cells from six major module manufacturers (Task 15).

A software routine was written for calibrating the aligner robot's coordinate system (in stepper motor counts) with the video camera's coordinate system (in pixels) in x and y space. Another calibration routine was written for finding the center of rotation of the robot's θ axis, which is generally different from the center of the vacuum pad since the pad may not be exactly centered on the motor shaft. These calibration routines involve analyzing images of the aligner vacuum pad on the aligner stage at various positions in x and y (for coordinate system calibration) and with various rotations (for θ calibration). A typical vacuum pad image is provided in Figure 11.

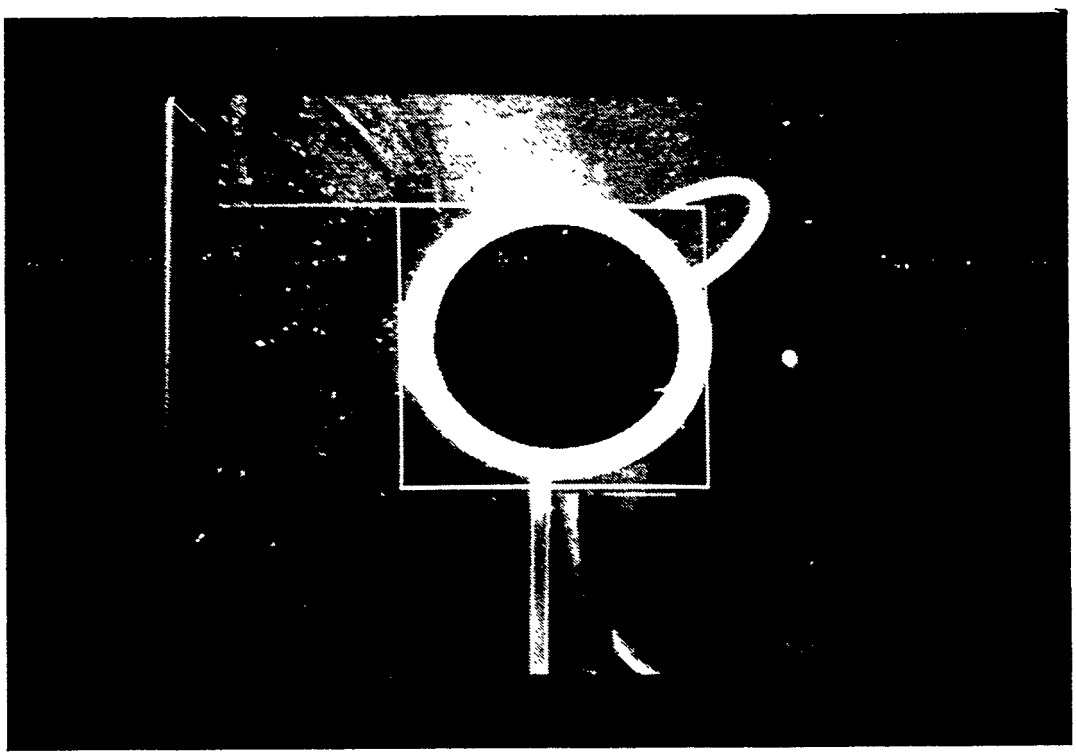

Figure 11 *Aligner vacuum pad image displayed on the vision system monitor. The white box is the search area and the black circle is the area that the vision system identified as the pad. A white ring is mounted behind the vacuum pad for contrast.*

A software routine known as "Train" teaches the vision system the nominal direction of the contact busses, since square cells can be placed on the aligner in one of four rotational orientations. (Cells that have 180° symmetry only have two rotational orientations, but the software was written for the more generalized case.)

The Train routine is run only for the first cell through the Assembler when the aligner software is started up. The top cell in the loader's stack carrier must be placed face down with its busses parallel to the ribbon path. When the top cell is transferred to the aligner stage by the loader manipulator, the vision system acquires an image of the cell and stores a square portion of the image, located near the top left corner of the cell and including a section of the contact bus, as shown in Figure 12. The vision system then rotates the whole cell image three times, in increments of 90°, and a similar square portion is stored each time, resulting in four stored images, or models, one near each corner of the cell.

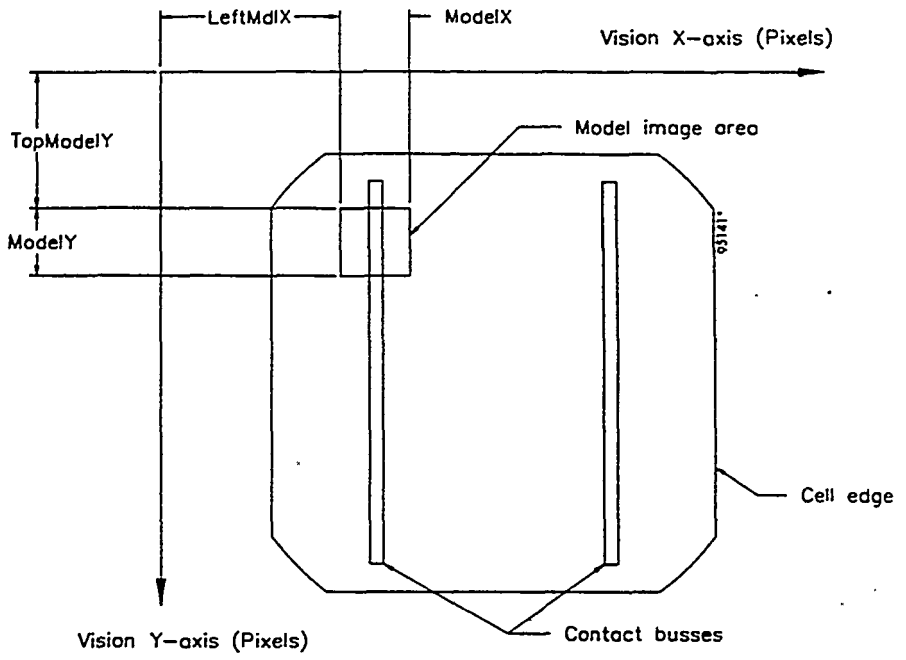

Figure 12 *Position of a typical model image area for finding the nominal orientation of the cell contact. The image size and location are adjustable to suit the cell design.*

The "Align" routine determines each cell's location in x, y, and θ in pixel space. Align first checks the nominal orientation (0°, 90°, 180°, or 270°) of the cell's contact pattern by comparing an image of a region near the top left corner of the cell to the four models stored by the Train routine. The contact busses are then imaged to find their angle of rotation, θ, and the midpoint between the two busses. Three rectangular search boxes are used for this purpose, as shown in Figure 13. The two rectangles on the left bus are used to find θ, while the two top rectangles are used to find x. Finally the cell's location in y is determined by finding the location of two opposite cell edges in the y-axis (in pixel space) and calculating the midpoint of a line drawn between the two edges, as shown in Figure 14.

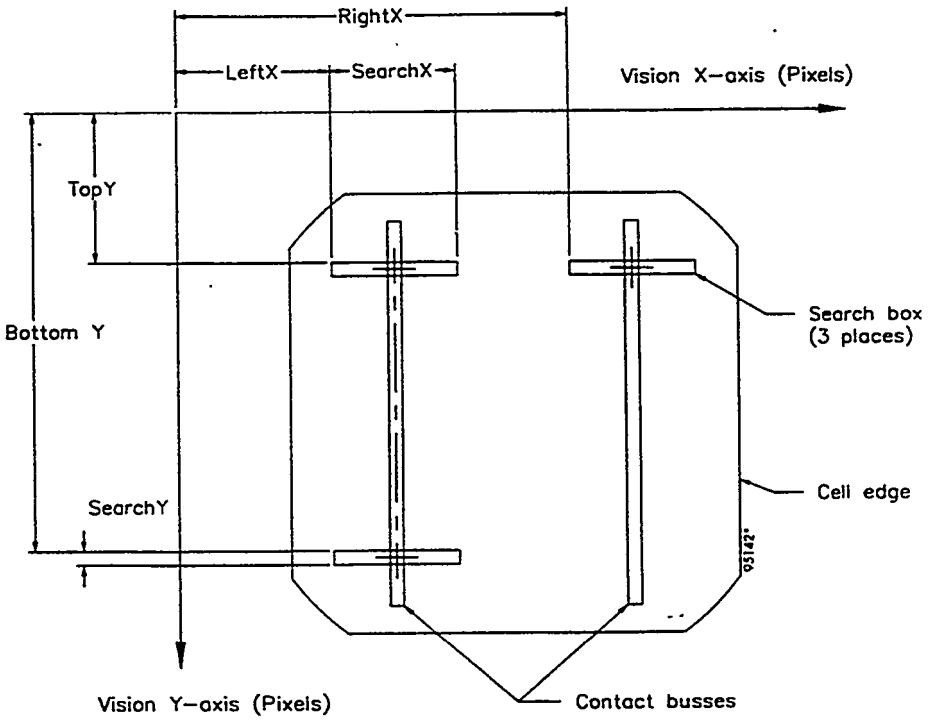

Figure 13 *Bus bar search areas for finding the cell contact location in x and θ. The search area size and locations are adjustable to suit the cell design.*

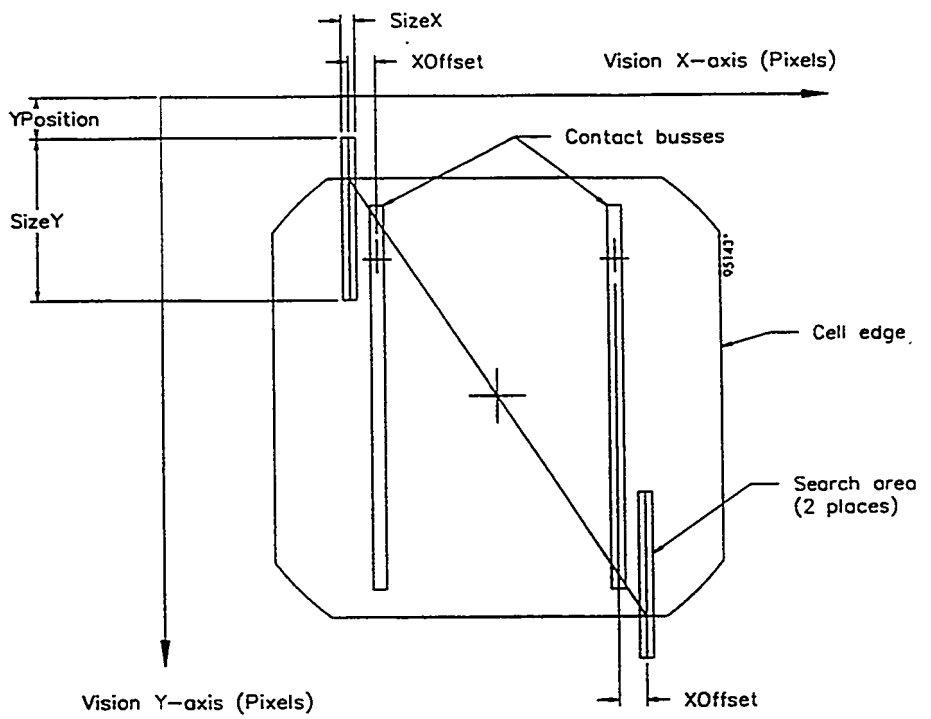

Figure 14 *Edge detection search areas for finding the cell location in y. The search area size and locations are adjustable to suit the cell design.*

The Align routine executes all of the functions illustrated in Figures 12, 13, and 14. A photograph of the video monitor showing the results of the Align routine is provided in Figure 15. The Align algorithm was intentionally designed to provide alignment in the x-axis (perpendicular to the contact bus bars) based on the location of the contact busses, for best alignment with the interconnect ribbons. Since ribbon alignment is not critical along the length of the ribbon, alignment in the y-axis is based on the cell edges, allowing cells to be spaced evenly along the string direction for best appearance in the module.

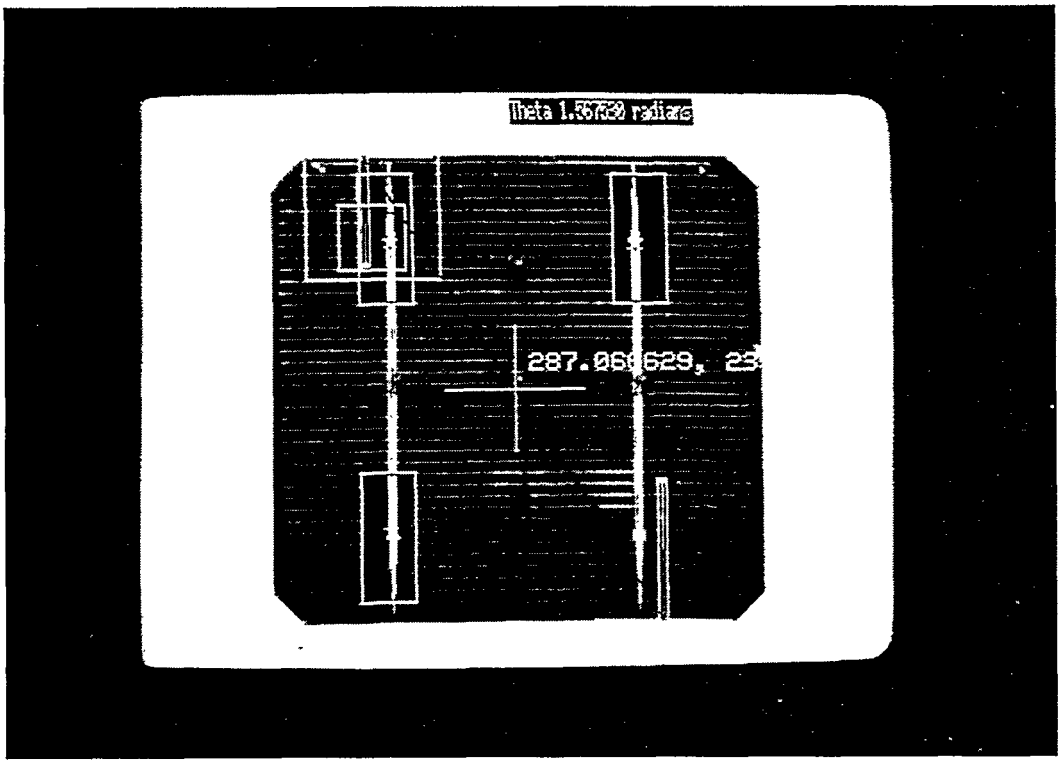

Figure 15 *"Align" routine results displayed on the vision system monitor for a 10 cm square cell.*

The "Inspect" routine checks a cell for chipped edges by measuring the area of the cell's perimeter and comparing it to a user-selected minimum area. The size of the chip that can be detected by this method is limited by the normal variations in cell size that are found in production. For example, the smallest chip that can be identified for a 100 mm square cell with a tolerance of ±0.5 mm is $(100\ mm)^2 - (99.5\ mm)^2 = 100\ mm^2$.

The "Debris Check" routine, described in Section 2.2.3.2, closes the aligner shutter and acquires an image of the stage. Any object found on the stage is displayed as a blinking black and white shape, as shown in Figure 9.

2.2.4 Task 4 - Interconnect Ribbon Handling Process Development

Processing subassemblies for ribbon handling, bending, and cutting were developed in this task. A drawing which labels the major components of the ribbon handling system is provided in Figure 16.

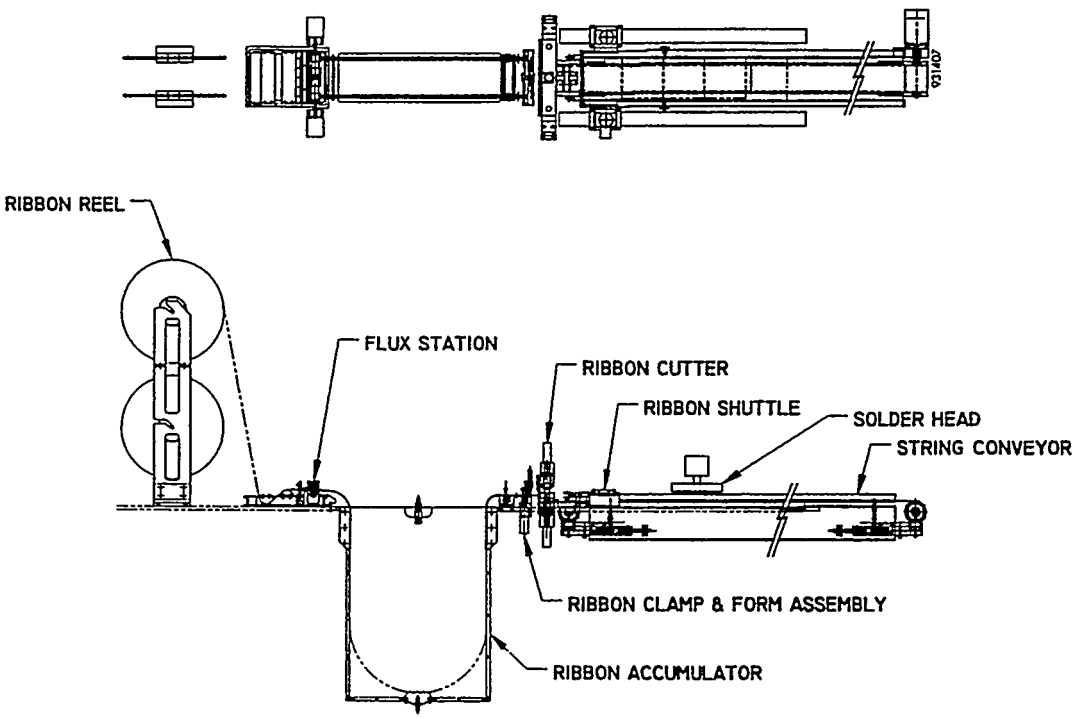

Figure 16 *Components of the ribbon and cell handling system.*

Ribbon material is purchased in reels which are loaded on the ribbon reel assembly. The ribbon travels through the flux station (which includes the ribbon drive assembly), the ribbon accumulators, the ribbon clamp and form assembly, the ribbon cutter, and the ribbon shuttle assembly. These assemblies are integrated to work together automatically under the control of a Programmable Logic Controller (PLC).

As part of the initial design work, a story board was created in CAD to illustrate the sequence of events needed to produce a string of soldered solar cells. The story board was a valuable aid in the mechanical design of the ribbon handling system, as it facilitated the design of mechanisms capable of executing all of the processes needed to produce cell strings in the proper sequence. The process sequence is as follows:

- The ribbon shuttle, consisting of a pair of air actuated mechanical grippers driven by linear motors, pulls two interconnect ribbons a distance at which a stress-relief bend is formed in each ribbon. The ribbons are pulled again to a position at which they are cut. The cut ribbons (also called tabs) are pulled to place them in the desired location for assembly. Linear motors were selected to provide rapid, precise, and programmable positioning of the ribbon.

- A vacuum conveyor belt holds the left ends of the tabs while the grippers open and retract to the right (in Figure 16), dropping the right ends of the tabs onto the belt. The grippers then move left to acquire the ribbons for the next pair of tabs. A cell is placed by the aligner in the first cell position, on top of the first set of tabs. The ribbon forming,

cutting, and placing process is repeated, with the right half of the second pair of tabs placed over the first cell, and the left half placed on the vacuum belt. The vacuum conveyor indexes, carrying the cell and tabs the length of one cell plus the gap between cells.

- The tab fabrication, cell placement, tab placement, and cell indexing processes are repeated as needed to build up a string of the desired length. After several conveyor indexes (three for 10 cm cells) the cell arrives under the light solder head where it is soldered to both the top and bottom tabs in one step. After the last cell in the string is soldered, the conveyor carries the string to the proper location on the belt for removal with the string transfer assembly.

2.2.4.1 Ribbon Reel Assembly

Solder coated copper ribbon material is typically supplied as a coil wound on a cardboard reel. The ribbon reel assembly was designed with a reel diameter capacity of 38 cm (15 inch). The interval between reel changes is a function of reel diameter, machine throughput (seconds per cell), cell size (length of ribbon across the front and back of the cell), spacing between cells, and ribbon thickness (since more thin ribbon fits on a given diameter reel). For example, assuming a 5 s/cell throughput, 102 mm cells, 2 mm spacing, 75 μm thick copper ribbon, and 12 μm thick solder plating, a 30 cm diameter reel will last approximately 2 hours and 40 minutes, while a 38 cm diameter reel will last approximately 5 hours and 25 minutes.

The ribbon reel assemblies are shown in Figure 17. Each of the two reel assemblies (left and right) supports two stock reels (upper and lower) to allow ribbon splicing from the trailing end of ribbon from an empty reel to the leading end of ribbon from a full reel. While the splicing operation is manual, it eliminates a time consuming manual threading operation (through the flux bath, drive rollers, accumulator, clamp and form assembly, and ribbon cutter) which would otherwise be required. Optical end-of-ribbon sensors are provided to signal the operator when a reel is empty. The sensors are mounted between the flux station and the ribbon reels (Figure 17). When a reel empties, the sensor stops the ribbon drive motor from feeding ribbon into the accumulator and signals the operator to splice in a new reel.

2.2.4.2 Ribbon Accumulator Assembly

The ribbon accumulators allow rapid feeding of ribbon by the ribbon shuttle without rapid rotation of the stock reels or rapid transport of the ribbon through the flux bath. The ribbon shuttle can draw upon the ribbon in the accumulators for a short period of time while the operator splices ribbon from a new reel. Part of the two accumulators are shown in the foreground of Figure 18.

Four ribbon sensors are used, two on each accumulator. An optical sensor is located at the bottom of each ribbon loop to turn off the ribbon drive motor (at the flux station) when the accumulator is full. A metal proximity sensor at the top of each accumulator (one is visible in Figure 18) signals the ribbon shuttle to stop extracting ribbon if the accumulator is empty.

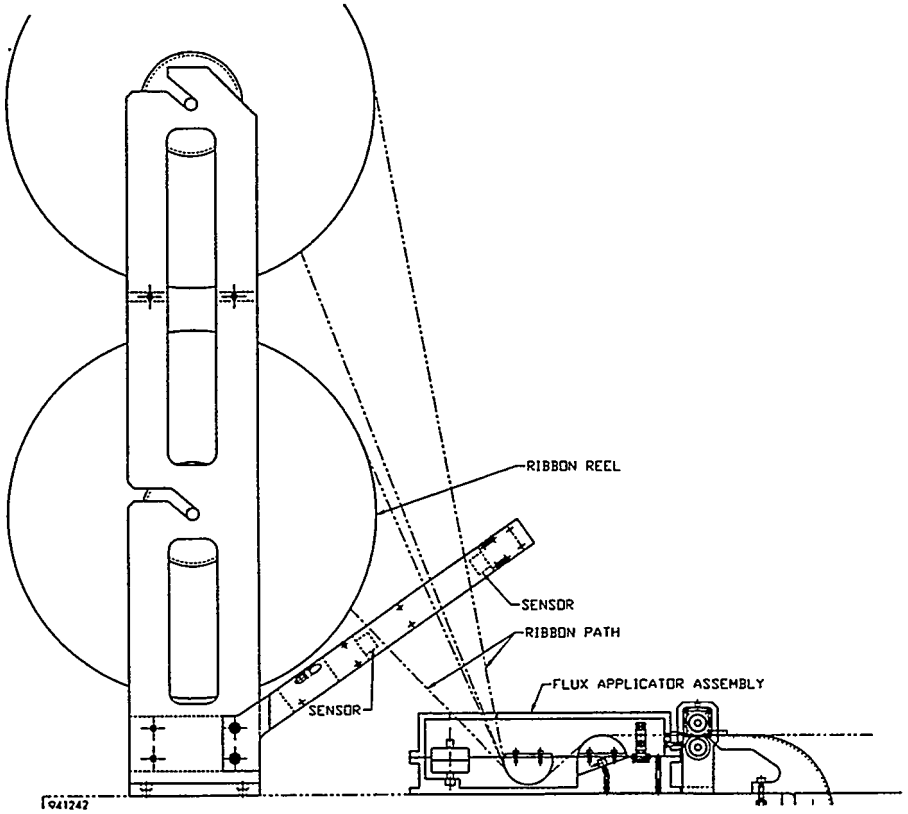

Figure 17 *Ribbon reels, sensors, and flux bath assemblies.*

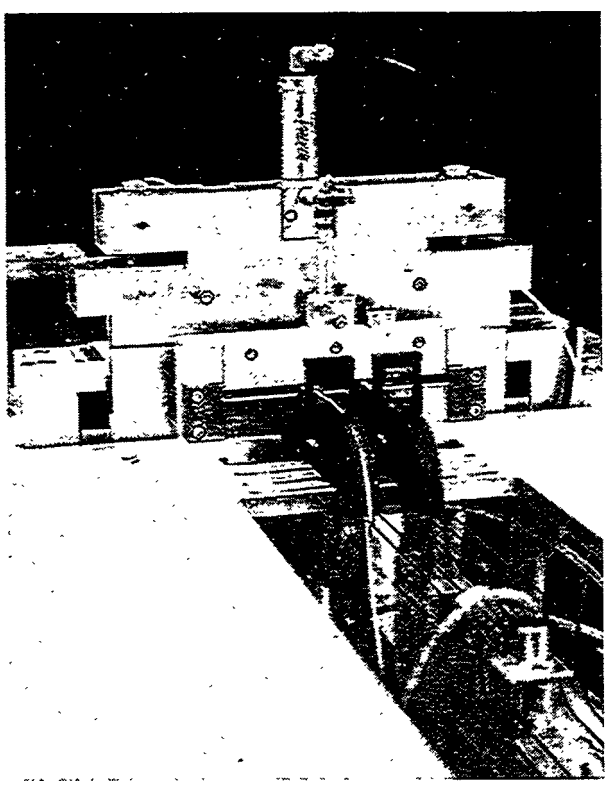

Figure 18 *Photograph of part of the interconnect handling system. From foreground to background: the accumulators, the clamp and form assembly, and the ribbon cutter.*

2.2.4.3 Ribbon Clamp and Form Assembly

The ribbon clamp and form assembly is seen in Figure 18 and in the lay-out drawing provided in Figure 19. The ribbon forming section produces a stress-relief bend in the two interconnect ribbons. A metal die machined with the shape to be transferred to the ribbon is driven upwards by an air cylinder against an elastomeric pad. Initially designed with a urethane pad, ribbon forming tests showed that the ribbons were not obtaining the full die shape, an indication that the urethane pad was too hard. The pad was replaced with a lower durometer O-ring material seated in a captive groove. Tests showed that the metal die and O-ring transfer the bend shape to the ribbon very well. The - O-ring groove design makes maintenance and replacement of the elastomer trivial.

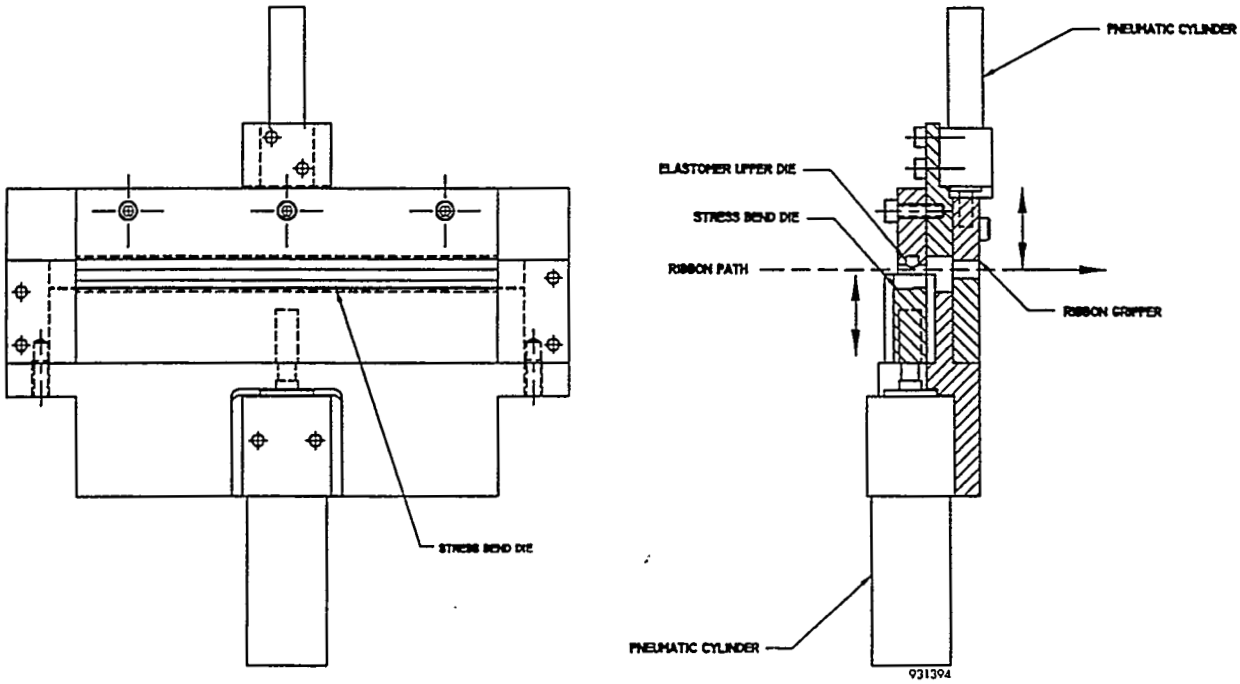

Figure 19 *Ribbon clamp and form assembly.*

The clamp section of the clamp and form subassembly holds the two interconnect ribbons while they are being cut to prevent them from falling under their own weight into the accumulator. The small air cylinder on top of the clamp and form subassembly (Figure 19) actuates the clamp.

2.2.4.4 Ribbon Cutter Assembly

The ribbon cutter assembly cuts the two interconnect ribbons to the desired length. The initial concept had two sets of cutting blades (one set for each ribbon) mounted on horizontal slides so they could retract away from the path of the grippers on the ribbon shuttle assembly. The concept was modified in the final design to eliminate the horizontal motion by using a single large blade set for both ribbons, thereby simplifying the mechanism and increasing its speed. Both top and bottom blades move vertically away from the ribbon after cutting to provide clearance for the grippers on the ribbon shuttle. The blades are mounted on ball bushings and are driven by air cylinders. The assembly is shown in the background of Figure 18.

Since the cutter blades have the potential to cause severe injury, an optical sensor has been installed at the blade opening to detect the presence of an object and prevent the blades from operating. Blade position sensors are also provided to prevent collisions with the ribbon grippers.

2.2.4.5 Ribbon Shuttle Assembly

The ribbon shuttle assembly uses two linear stepper motors to move a pair of pneumatic grippers. Linear stepper motors were chosen for their high speed (up to 150 cm/s) and programmability. The grippers clamp and pull the two interconnect ribbons in selected increments, thereby determining the tab stress-relief bend position, the tab length, and the tab placement position. The grippers are suspended over the conveyor belt on which the tabs and cells are placed for assembly. Position sensors are provided for linear motor homing and end of travel sensing. The grippers have integral position sensors that indicate whether they are open or closed. A photograph of the shuttle assembly is provided in Figure 20.

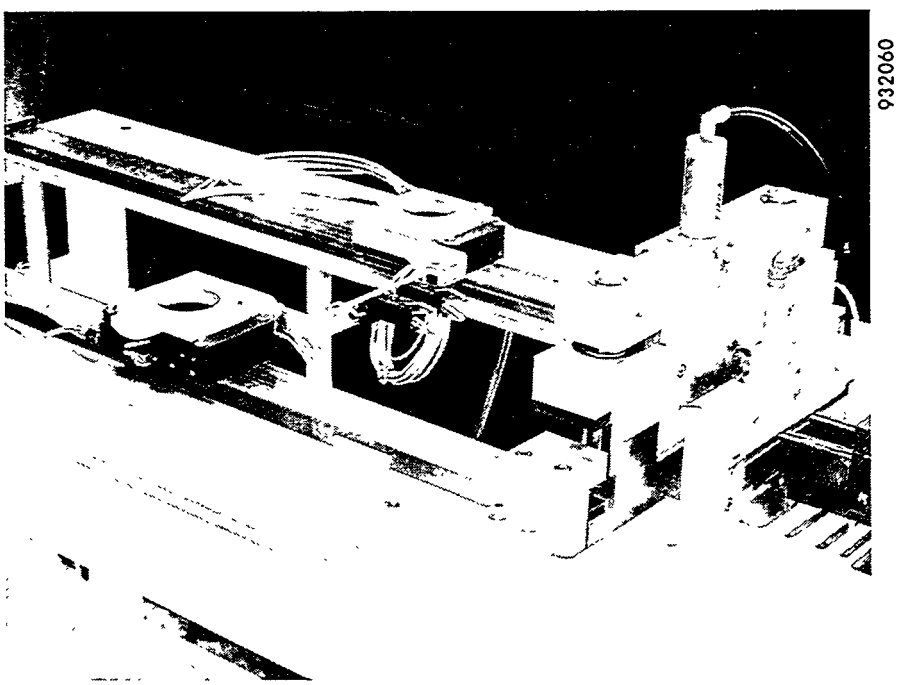

Figure 20 *Ribbon shuttle assembly with grippers open. Ribbon cutter and clamp-and-form assemblies are shown at right.*

2.2.4.6 Ribbon Handling Testing

The large (36 cm diameter) cardboard reels on which the interconnect ribbon is supplied worked fairly well in the winter when the indoor humidity was low, but they bowed severely in the spring when the humidity was high. The outer surfaces of the cardboard absorbed moisture from the air and expanded more than the inner surfaces, pinching the ribbon tightly and causing the ribbon to slip in the drive rollers. The problem was solved by transferring the ribbon from the cardboard reels to reusable plastic reels, which were designed and fabricated for this purpose.

Interconnect ribbon stiffness varies with its thickness and temper. A ribbon curl problem was identified when ribbons with a copper thickness greater than 75 μm were processed. Some ribbon had a coil set (a curl from being wound on the reel) or it acquired a bend as it was pulled around the semi-circular ribbon diverters in the flux bath. The bend was sufficiently large that the ribbon did not lie flat on the conveyor belt, and so could not be held in position by vacuum. A ribbon straightener was designed, fabricated, and installed at the exit of each ribbon accumulator, just before the ribbon enters the bending die. A drawing of the straightener assembly is provided in Figure 21.

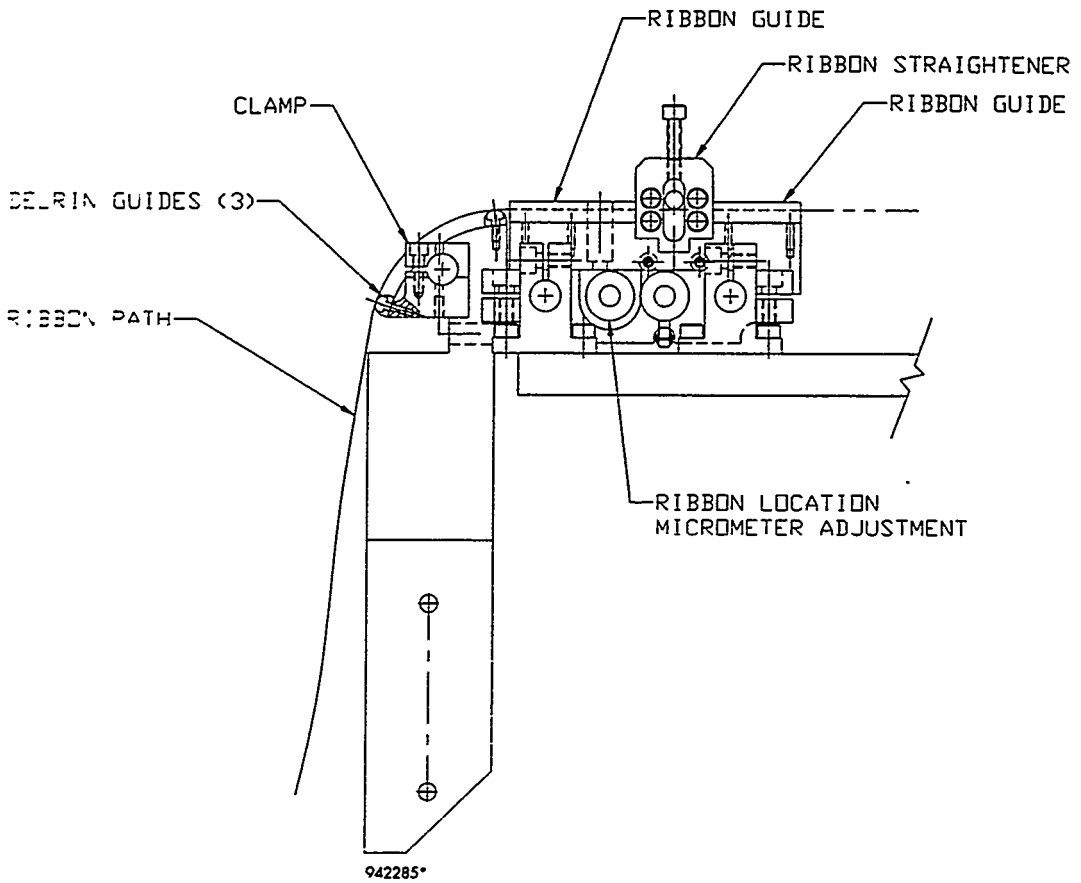

Figure 21 *Ribbon straighteners and adjustable ribbon guides.*

The straightener has two pairs of fixed guide pins between which the ribbon travels. A movable pin can be adjusted to apply a gentle upward or downward pressure on the ribbon, as required, to remove the bend in the ribbon. This assembly was tested and found to be highly effective in straightening the ribbon.

Preliminary processing evaluations indicated that occasionally a tab was missing from a cell in a string. Possible causes for a missed tab include insufficient grip by the ribbon gripper jaws, flux residue in the ribbon guides which causes excess drag on the ribbon when the gripper tries to pull it quickly, or a bend in the ribbon which can make the jaws fail to acquire the ribbon. Efforts were directed towards reducing ribbon drag for the grippers and developing a new ribbon sensor for the gripper jaws.

Ribbon drag was sharply reduced by modifying the exit path on the accumulators. As shown in Figure 21, the ribbon makes a 90° bend when it exits the accumulator and enters the ribbon guides. The friction of the ribbon as it travelled over a large radius aluminum surface accounted for the majority of the ribbon drag, which could overcome the gripper jaw clamping force when the aluminum surface acquired sticky flux residues and the jaws attempted to pull ribbon at high acceleration rates. The curved aluminum surface was replaced with three small Delrin guides, shown in Figure 21 (one of the three guides is hidden behind the object labelled "Clamp"). Since the new guides have a much smaller contact area with the ribbon surface, the ribbon drag was greatly reduced.

The ribbon gripper jaws were modified to add electrical contacts that sense the presence of ribbon. The original aluminum jaws, which can be seen in Figure 20, were replaced with jaws made from a dielectric material. Electrical contacts were installed in the top jaw of each gripper, as shown in Figure 22. When the jaws close, the interconnect ribbon acts as a switch, completing the circuit between the two contacts. Testing showed that the sensors are reliable ribbon indicators. In addition, the metal contacts, made from small set screws, were found to provide a more secure grip than was previously obtained with the original flat-surfaced jaws. The combination of the new jaws and the Delrin guides significantly reduced the frequency of missed tabs to a very low level.

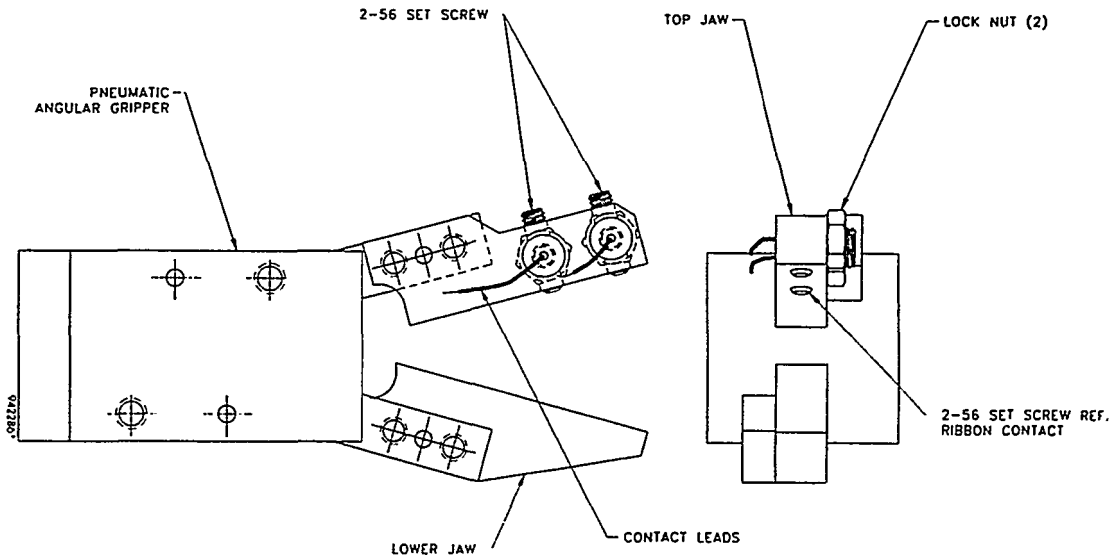

Figure 22 *Ribbon gripper with contacts for sensing ribbon.*

Software was written that checks for the presence of ribbon just before the gripper jaws open to place the ribbon on the conveyor belt, the last step in the process at which the jaws hold ribbon. If ribbon is not sensed at the jaws, the system pauses, an alarm sounds, and a message is displayed that alerts the operator to check for and remove any dropped ribbons. When the operator signals that all is clear, the grippers pull a new pair of ribbons.

Tab position measurements made on cell strings produced during processing trials indicated the need for improved tab placement accuracy. Three approaches to improving alignment were investigated and implemented: increasing the grip on the tabs by the vacuum belt, improving the tab guiding tooling, and reducing the ribbon path height above the conveyor belt.

An inspection of the platen under the conveyor belt revealed that much of the vacuum groove area was not needed for holding tabs and cells. Unnecessary grooves were sealed off temporarily with tape to see if the grip on the tabs provided by the vacuum belt could be improved. An increased force was required to slide a tab across the belt, indicating an improvement in grip. On the basis of this test, a new platen was designed and fabricated which reduced the open area from 68.4 cm^2 to 23.9 cm^2, resulting in a platen with only 35% of the original groove area.

Efforts were also directed towards improving the ribbon guides that provide alignment when the ribbon is acquired by the grippers on the shuttle assembly. Examination of the guides showed that the aluminum sides were wearing from friction caused by the edges of the copper ribbon as it is rapidly pulled through the guides. As a result, the ribbons were no longer accurately positioned, as they had been when the guides were new. Replacement guides were designed to tighter tolerances and with a much longer guiding length than the original guides. The guide material was changed from aluminum to stainless steel to reduce the wear caused by the copper ribbon. As part of the redesign, micrometer adjustments were added to allow the ribbons to be precisely positioned, both for ease in initial set-up and for switching between cells with different tab spacings. A photograph of the new guide assembly is provided in Figure 23.

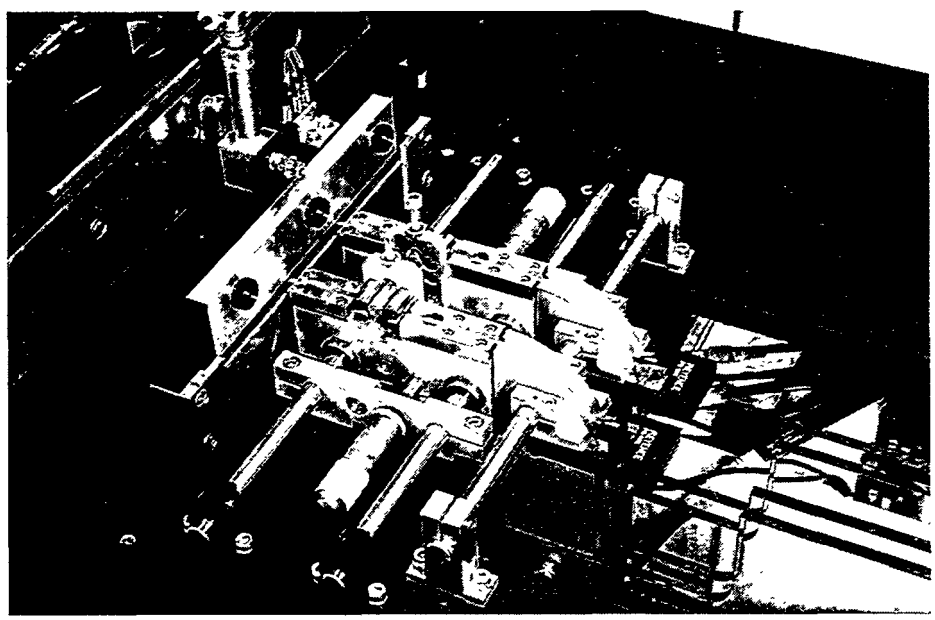

Figure 23 *Ribbon guide assembly with micrometer adjustments. Also note the ribbon straighteners located between two guide sections.*

The accuracy and repeatibility of ribbon placement was measured with the original aluminum guides and remeasured after installation of the longer stainless steel guides. The results are plotted in Figure 24. In both cases the ribbon guides were set to obtain a nominal spacing of 1.90". The spacing between the two ribbons soldered to the front of each cell was measured at the ends of the ribbons. The left graph in Figure 24 shows the distribution of spacing values obtained with the original guides. The ribbon spacing ranged from 1.87" to 1.94" with a standard deviation of 0.017". The right graph shows the distribution of spacing values with the improved guides. The ribbon spacing ranged from 1.88" to 1.92" with a standard deviation of 0.009". Thus the new guides provide more accurate ribbon placement.

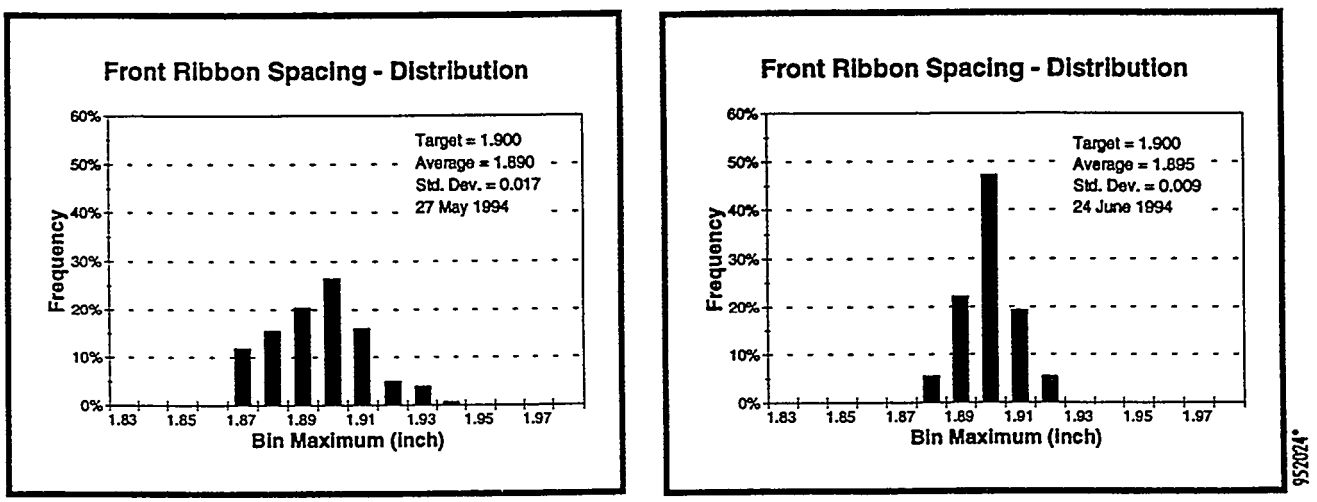

Figure 24 *Ribbon placement measurements before and after ribbon guide redesign. Left: aligned with short aluminum guides. Right: aligned with long stainless steel guides.*

The ribbon gripper design, shown in its second version (with ribbon sensors) in Figure 22, was further modified to allow a reduction in the height of the ribbon path above the conveyor belt. Since tabs are passed from the gripper to the belt, a lower ribbon path reduces tab misalignments. The second version design, represented by the drawing on the left in Figure 25, had upper and lower jaws that opened. The movement of the lower jaw prevented the ribbon path from being closer than 14 mm (0.55") above the belt. The new (third version) of the gripper jaws was designed with a fixed lower jaw, as shown on the right in Figure 25. The fixed jaw enables the ribbon path to be 7 mm (0.27") above the belt, half the original height.

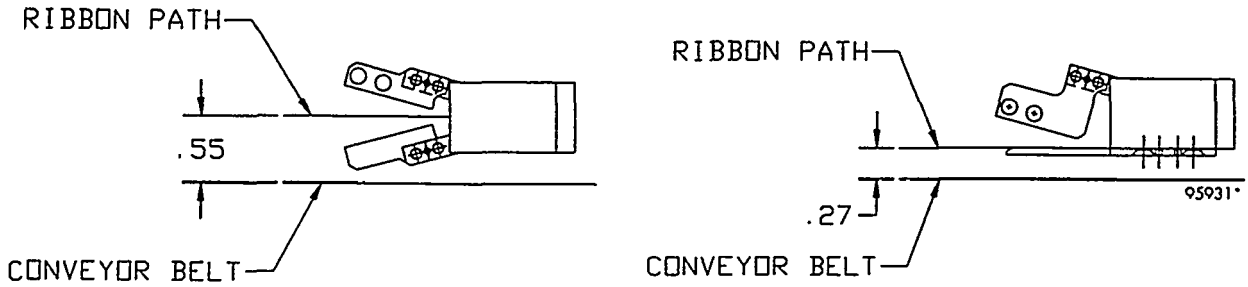

Figure 25 *Ribbon gripper modification to reduce the ribbon path height above the conveyor belt. Left: second version. Right: third version with fixed lower jaw.*

2.2.5 Task 5 - Solder Flux Application Process Development

Flux is required to dissolve the native oxides on the surfaces of the cell contacts and the solder coating on the copper ribbon, allowing the solder to wet to the cell contacts and form a durable bond. Two alternative approaches were considered for automatically dispensing solder flux or solder paste to the solder joints: a syringe dispenser method and a ribbon coating method. In the first approach, syringes located over each interconnect tab and actuated in x and z would dispense lines of flux or paste onto the tabs. A cell would then be placed face down on the coated tabs and the operation would be repeated on the rear surface of the cell before the next set of tabs is placed over the cell.

Spire engineers evaluated commercial equipment that automatically dispenses solder paste and flux for hybrid circuit and surface mount applications. Equipment is available with more than adequate precision and motion control programmability. Unfortunately, if the dispensing syringes were driven at the speeds needed to obtain sufficient throughput for this application (4 s/cell), they would not be able to dispense continuous lines, due to the surface tension and viscosity of the paste or flux.

The use of a greater number of syringes (*e.g.*, six per tab) to simultaneously dispense multiple dots of paste or flux might be capable of meeting the throughput requirement, although the dispensing operations still have to be done in series with the tab placement and cell placement steps. This approach has the drawback that it cannot dispense continuous lines of flux or paste. In addition, the large number of dispensers and controls required for this approach makes it mechanically complex. Such complex systems generally are high in cost and demand frequent maintenance.

The second approach, ribbon flux coating, has a number of advantages over syringe dispensing: it requires minimal mechanism, it adds no time to the assembly process, since it can be done in parallel with the cell and tab placing processes, and it coats both sides of the ribbon with flux. Therefore, ribbon coating was selected for development. In this process, ribbon is pulled through a flux bath as it is fed from the supply reels by a drive roller, as shown previously in Figure 17. In principle, this is a simple method since ribbon must be fed from reels whether flux is applied or not. However, sufficient flux must be applied to the interconnect ribbon for reliable soldering without generating unacceptable flux residues on the cells or on the ribbon feed system components.

A ribbon flux coating assembly was developed as shown in the lay-out drawing in Figure 26 and the photograph in Figure 27. Two pairs of independently-powered drive rollers pull ribbon from reels through a flux reservoir. The ribbons travel around a pair of semi-cylindrical diverters to immerse them in flux. A float switch and a peristaltic pump automatically maintain the proper flux level. A pair of adjustable ribbon guides provide alignment for the ribbon as it enters the drive rollers. A cover with a vent tube are provided to trap and exhaust solvent fumes.

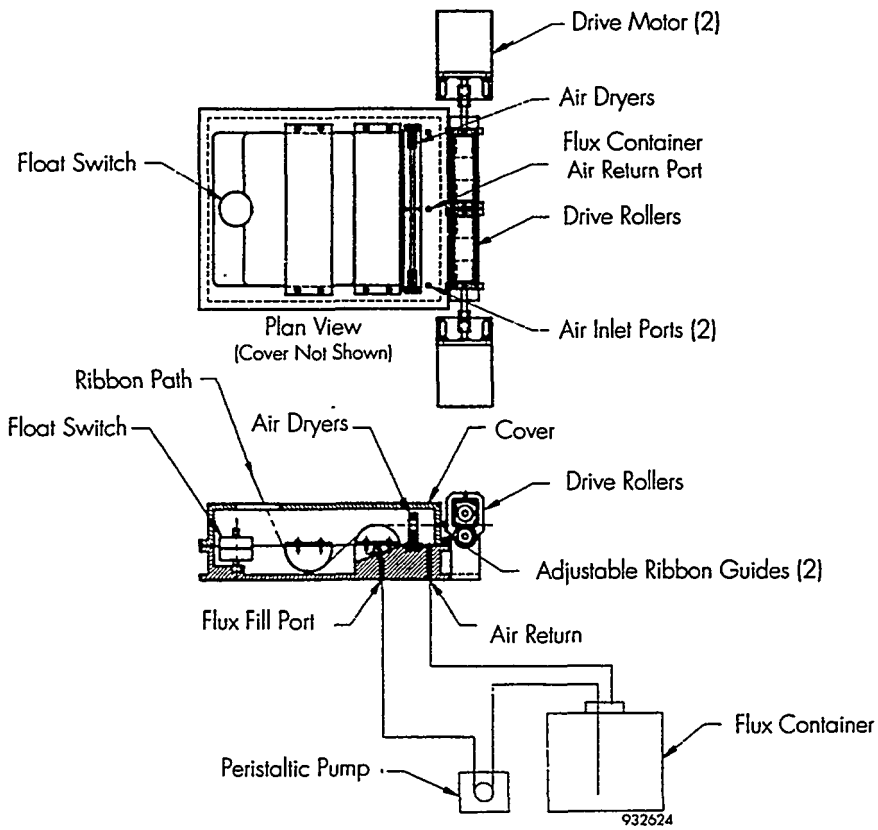

Figure 26 *Lay-out drawing of the flux coating assembly.*

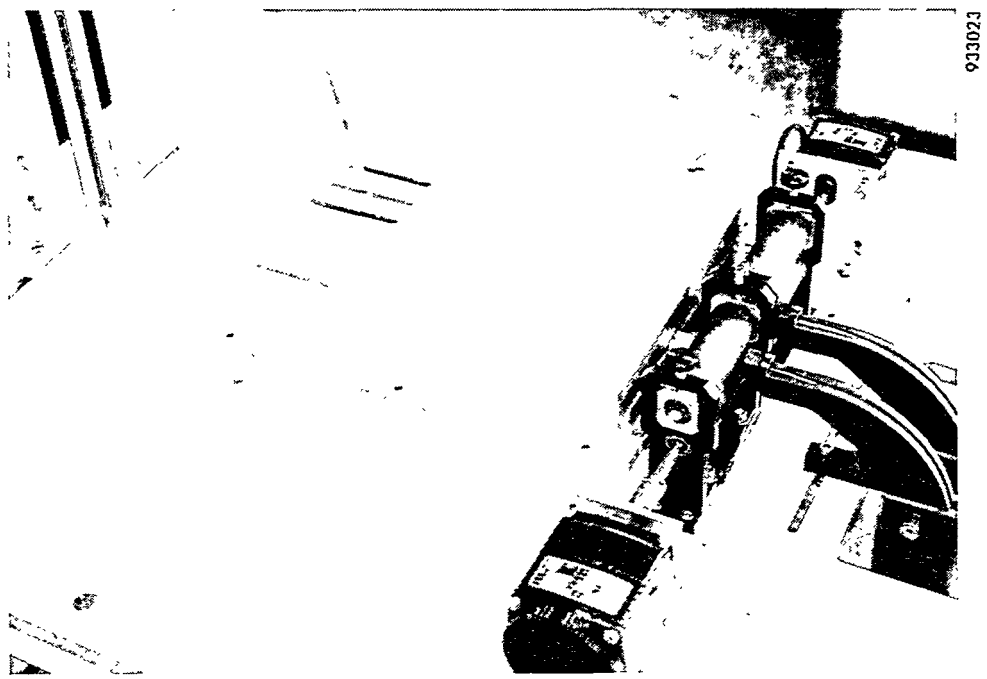

Figure 27 *Photograph of the flux coating subassembly.*

A number of fluxes were tested with varying results. The first flux type, Multicore 2112, fed properly in continuous operation. However, when the rollers sat idle long enough for the flux to dry, the ribbon tended to stick to the rollers and wind around them, due to the tackiness of the dried flux on the rollers. A squeegee type wiper was used to limit the quantity of flux on the ribbon, but insufficient flux was left on the ribbon for soldering.

Several strategies for solving the flux sticking problem were investigated: air jets were added to dry the flux on the ribbon; flux thinner was used to reduce the solids content; and three additional flux types were evaluated. The air jets, mounted between the flux reservoir and the ribbon drive rollers, consisted of two pairs of air nozzles, one above and one below each ribbon, connected to a source of regulated compressed air. Four kinds of non-corrosive fluxes and two flux thinners were tested in the flux station. A summary of the test results is presented in Table 5.

The air dryers were found to be effective in reducing the amount of Multicore 2112 flux on the ribbon as it entered the rollers, but they did not completely eliminate the problem of the ribbon sticking to the rollers. Flux thinner recommended for use with the 2112 was mixed with the flux to decrease the solids content from 12% to 6%. Ribbon feeding tests were repeated but the ribbons still occasionally stuck to the rollers.

Multicore X32-10M flux, a halide-free no-clean flux, had no problems with sticking ribbon to the drive rollers. Unfortunately, this flux did not produce strong solder joints between ribbons and solar cells.

Table 5 *Flux testing summary.*

Flux Type	Solids Content	Solvents	Sticks Ribbon to Rollers	Solderability to Solar Cells
Multicore 2112	12%	Alcohols & ketones	Yes	Fair
Multicore 2112	6%	Alcohols & ketones	Yes	Fair
Multicore X32-10M	2%	Propanol & methanol	No	Poor
Kester 2331	14%	Propanol & glycerol	No	Good
Kester 2331	2%	Propanol & glycerol	No	Good
Kester 920-CXF	4.5%	Propanol	No	Good

The third flux tested was Kester 2331, a neutral pH organic flux. The flux was tested both at full strength and thinned to a 1/6 ratio by volume, decreasing the solids content from 14% to 2%. This flux presented no problems for the ribbon handling system, including the drive rollers. In addition, excellent solder joints were made to cells with this flux. Unfortunately, this flux contains glycerol which leaves a greasy residue on the ribbons after soldering. Since this residue could affect the adhesion of encapsulants, leading to module delamination, an alternative flux was desired.

Kester type 920-CXF flux was obtained for interconnect ribbon coating tests. This flux is a non-corrosive, low-solids, no-clean flux recommended by Solec for use with their cells. The flux was evaluated for compatibility with the ribbon handling tooling and for solderability to Solec and Siemens Solar cells using the light soldering process. The flux contains 4.5% solids and 95% propanol. The best results were obtained with the air jets turned off to leave more flux on the ribbon. Evaluations showed that the flux does not stick the ribbon to the tooling, it does not leave a sticky or greasy residue on the cells after soldering, and excellent solder joints were obtained on a variety of different solar cells. As a result, this flux was selected for use in all of the preliminary and final process evaluations done in this program (Tasks 15 and 16).

2.2.6 Task 6 - Ribbon to Cell Soldering Process Development

The objective of this task was to develop a high throughput, high yield soldering process for thin and standard silicon solar cells. Spire's light soldering technology was adapted for use in this program because it provides a rapid heating capability that generates low mechanical and thermal stress on cells while requiring little maintenance. Conduction preheating was added to further reduce thermal stress and enable increased throughput. A new process was developed in which a cell's front and back contacts are soldered in one heating step, eliminating the second heating step needed for separate front and back soldering processes. Thus simultaneous soldering of the front and back contacts provides higher yield and throughput.

High intensity lamps emitting over a broad spectrum (visible and infrared) provide radiant energy to solder the interconnect ribbons to the solar cells. This light soldering process was originally developed at Spire to replace conduction soldering, in which heated elements physically contact the

ribbons to make discrete solder joints. Light soldering allows continuous solder joints to be made while generating less mechanical and thermal stress, since no direct contact is made to the cell or ribbons for heat transfer. Thermal stress calculations done independently by Franke and Steinbach show that conductive preheating followed by radiative heating (the approach used in this program) generates the least stress of the five cell string soldering processes they considered.[5] The other four processes were three conduction heating methods (heated moving spot, heated bar, and heated multiple spot) and radiative heating without preheating.

An additional benefit of light soldering is reduced equipment maintenance, since it eliminates the frequent cleaning required for the heated elements used in conduction soldering. These elements quickly pick up a layer of molten solder from the ribbon which then oxidizes on the hot elements. Frequent cleaning is required since the oxide is insulating and interferes with good heat transfer.

Components for the two lamp solder head assembly are shown in the lay-out drawing in Figure 28. The assembly includes two high power lamps, air cooling for the lamp seals, protective windows and flux vapor exhausts to keep the lamps clean, and low force springs that hold the tabs in contact with the cell during soldering. The lamp spacing can be adjusted to match the tab spacing.

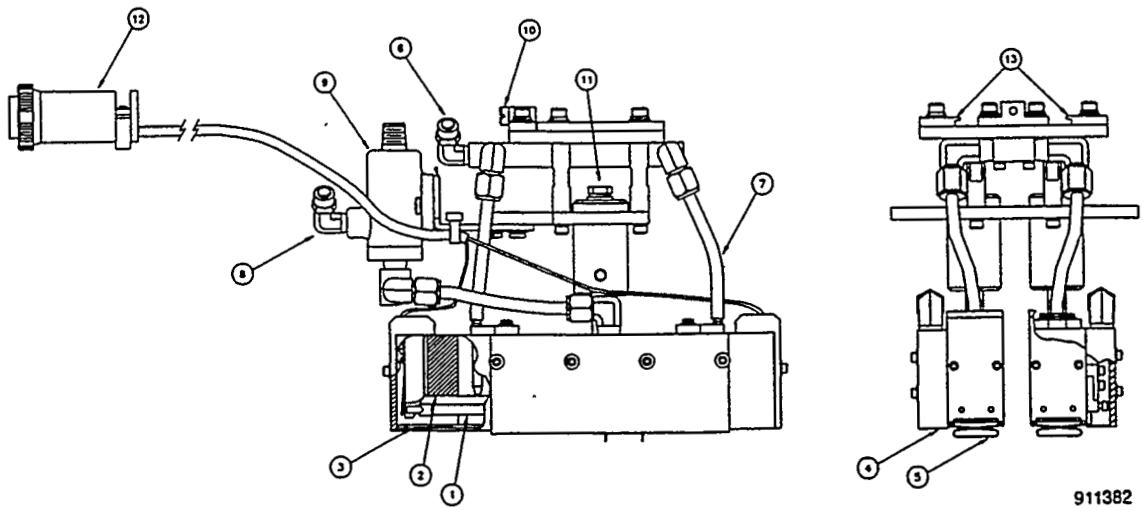

Figure 28 *Two lamp solder head assembly.*

The solder head actuator assembly (Figure 29) moves the solder head up and down for soldering. When the solder head is down, the tab retaining springs lightly press the interconnect tabs onto the cell contacts until the solder freezes. The lamp assembly (Figure 28) slides onto the mounting plate at the bottom of the actuator assembly. An air cylinder drives a ball slide with hydraulic cushions for smooth vertical motion. Air flow control valves regulate the solder head speed, while magnetic reed switches indicate the head position. The solder head, actuator, and mounting hardware are shown installed over the conveyor belt in Figure 30.

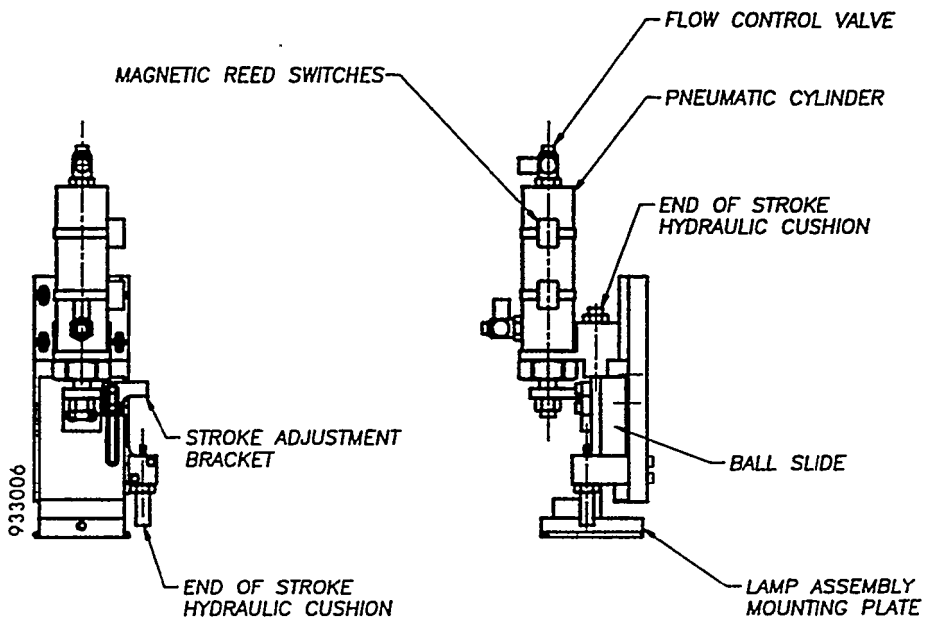

Figure 29 *Solder head actuator assembly.*

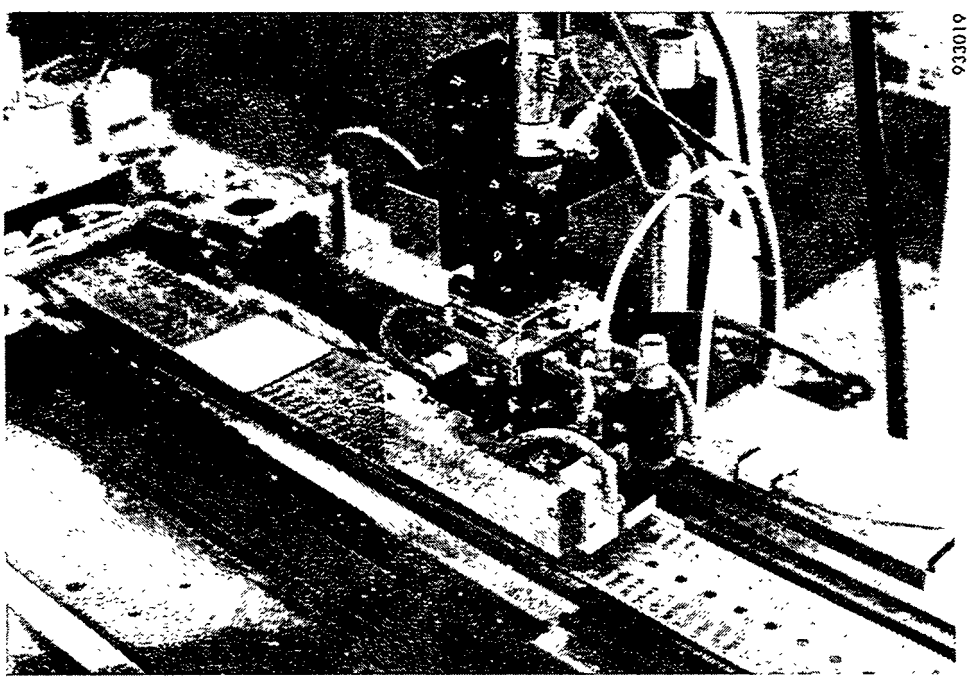

Figure 30 *Photograph of solder head and actuator assemblies.*

New components developed for the soldering process include the heated vacuum platen and the perforated conveyor belt, shown in Figure 31. The platen assembly includes a vacuum blower and plenum, slotted platen, heaters, temperature controller, and thermocouple. The conveyor belt is a metal foil, perforated with vacuum holes for holding the tabs and cells in position and sprocket holes for accurate indexing. The development of these components is described in more detail in Section 2.2.7.

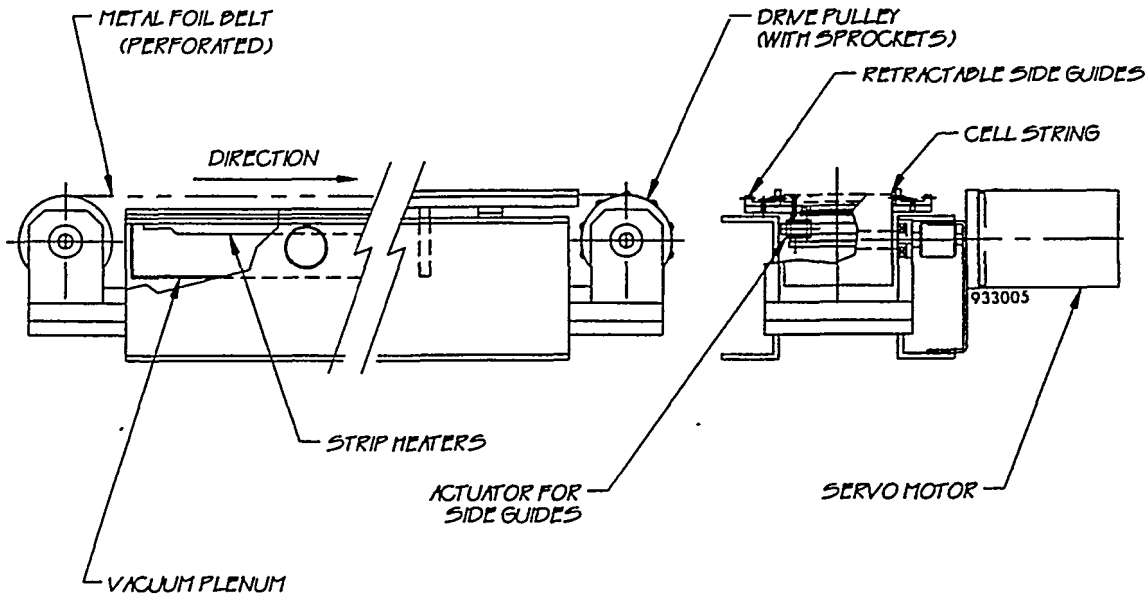

Figure 31 *Conveyor belt assembly with heated vacuum platen.*

The light soldering process developed in this program is as follows. Two flux coated tabs are placed on the vacuum conveyor belt which is preheated to approximately 140°C. A cell is aligned and placed face down on the tabs. Another pair of tabs is placed over the back of the cell and the conveyor belt indexes. The cell placement, tab placement and belt indexing steps are repeated for each cell in the string. The cells reach the solder head after several belt indexes: three for 10 cm cells, as shown in Figure 32. The solder head moves down, allowing the springs to hold the tabs against the cell surface, and the lamps switch to high power to heat the cell (approximately 1.8s) and melt the solder. The lamps then switch back to idle (low power) until the solder freezes (approximately 1.5s), after which the solder head moves up.

Soldering process parameters include the platen temperature for preheating cells and tabs, the voltage on the soldering lamps for heating the cells, the idle voltage on the soldering lamps, the heating time, and the cooling time. These parameters are adjusted for each type of cell to obtain good solder joints. The process parameters used for thin Si cells are listed in Table 6.

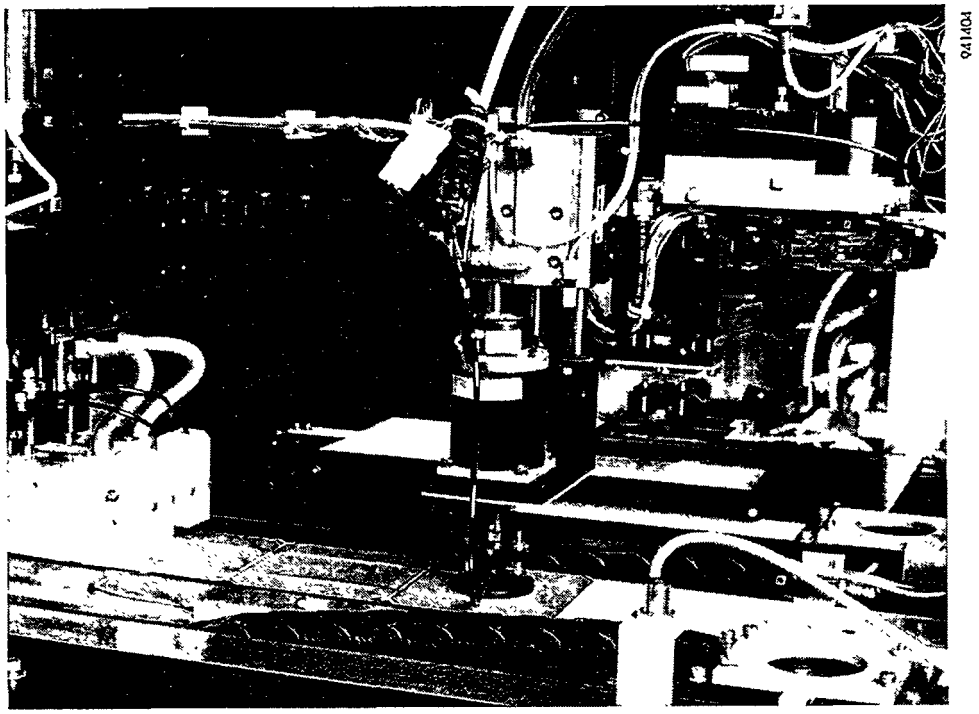

Figure 32 *Cell and tab placement, belt indexing, and soldering.*

Table 6 *Typical process parameters used for soldering thin-cell strings.*

Parameter	Setting or Description
Platen temperature	140°C
Lamp voltage, heating	140 VAC
Lamp voltage, idle	25 VAC
Heating time	1.8 s
Cooling time	1.5 s
Cell type	Solec, 102 mm square, 200 μm Cz-Si thickness
Flux type	Kester 920-CXF
Ribbon type	0.100" x 0.003" Cu with $Sn_{60}Pb_{40}$ coating

A number of cells soldered under the conditions listed in Table 6 were subjected to pull tests to measure the force required to peel the ribbon from the cell. A Chatillon model DFG-10 digital force gauge was used to record the maximum force from each tab pulled. The results, plotted as a histogram in Figure 33, show that good peel strengths were achieved, averaging 432 g for the front contacts and 288 g for the back contacts when pulled at a 90° angle. Pulls at the higher end of the scale (>400 g) typically pull silicon out of the wafer or break the wafer, indicating that the solder joint is stronger than the silicon wafer. The back contacts were weaker than the front due to a lower adhesion of the back contacts to the silicon, as the failure was at the silicon-contact interface, not the solder-contact interface.

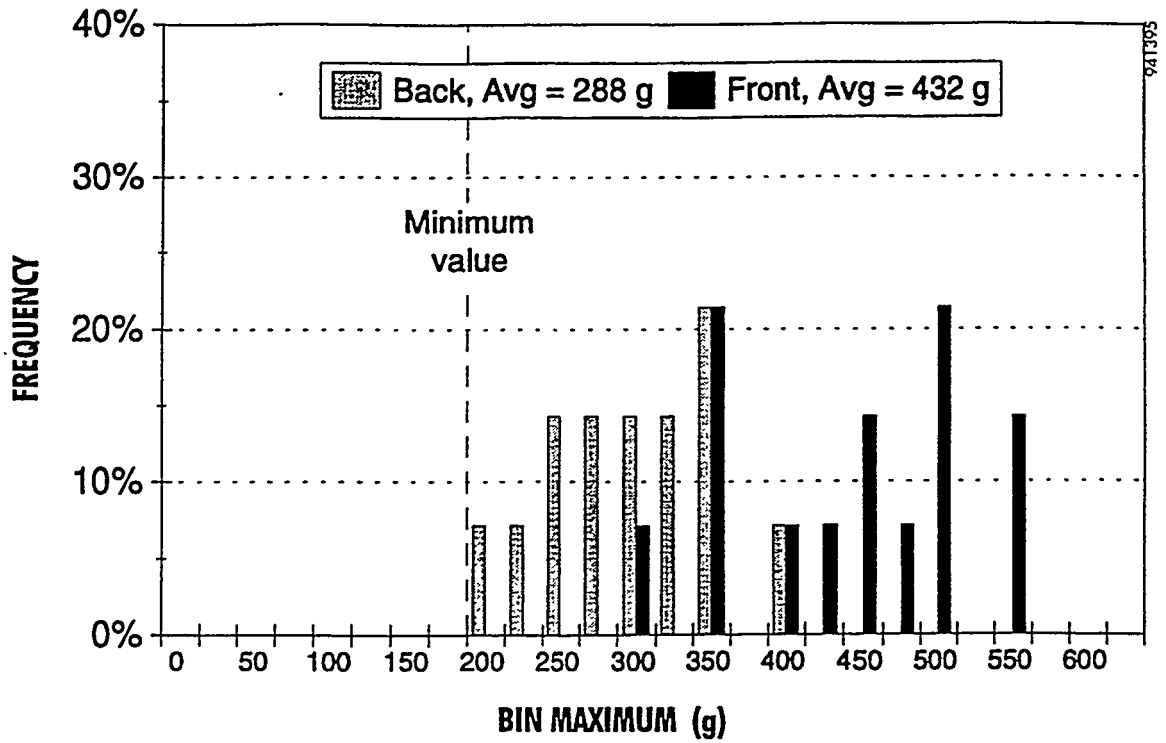

Figure 33 *Solder joint pull strength distribution, 90 ° pull angle; soldering conditions listed in Table 6.*

2.2.7 Task 7 - Cell String Handling Process Development

Cell string handling consists of two tasks: (1) handling cells and interconnect tabs as they are being assembled to produce cell strings, and (2) transporting these strings to the I-V tester and to the array table for placement in module-size arrays. A three meter long vacuum conveyor belt was devised for string assembly, while a linear array of vacuum pads on a four-axis manipulator was developed for string transport.

The method for handling interconnect ribbons and cells as they are being assembled and soldered together is a critical part of the assembly process. A unique conveyor belt system was conceived and developed in this program. The belt system has a vacuum capability for securely holding fragile cells and a heating capability for preheating cells prior to soldering. A diagram showing the important features of the conveyor assembly concept is provided in Figure 31.

A heated vacuum platen supports the conveyor belt over its first 61 cm (24 inches). Electric strip heaters are mounted on the bottom surface of the platen, while a pattern of intersecting slots machined in the platen provides paths for air to flow from the conveyor belt perforations to a vacuum plenum below the platen. The plenum is connected to a high flow vacuum blower. Once the cells are soldered to the interconnecting tabs, the conveyor belt carries them out of the heated and vacuum-ported zone to the area for pick-up by the string transport mechanism.

Tests were done with a prototype belt early in the program to evaluate the feasibility of the conveyor concept. A 91 cm (3 ft) long belt section was fabricated from the same materials and with the same hole pattern required for a full length belt. A shop vacuum was attached to a platen-plenum assembly and tests were done with various ribbons and cells. The belt was found to hold one or more cells very securely, either with or without ribbons, as the belt was moved across the surface of the platen. When only a pair of ribbons was placed on the belt, however, they were held weakly, indicating the need for a stronger source of vacuum. Thus a regenerative blower was obtained which generates lower pressures and higher flows than the shop vacuum. The prototype belt tests indicated that the moving vacuum belt concept works, so a full length belt assembly was designed and fabricated.

The belt is made from stainless steel, formed into a continuous loop by electron beam welding and perforated with holes for vacuum and for mating with a sprocketed drive pulley. The sprockets provide belt indexing accuracy for controlling cell spacing and tab placement. The belt is also coated with Teflon® for protection from chemical attack by flux, to prevent flux from sticking cells to the belt, and for ease of cleaning.

Other details of the conveyor belt assembly were designed, fabricated, and assembled, including the pulleys, belt tracking and tensioning mechanisms, retractable side guides, and conveyor structural elements. A stepper motor is coupled to the drive pulley with a flexible coupling and a 10:1 gear reducer to increase the belt indexing accuracy. The photograph in Figure 34 shows, from right to left, the stepper motor, gear reducer, motor bracket, flexible coupling, pulley mount, and drive pulley. The conveyor belt, mounted on the pulley, has a central row of large holes that function both as vacuum holes for cells and sprocket holes for the ball bearing sprocket teeth pressed into the drive pulley. Patterns of small vacuum holes on either side of the large central holes are used to hold the ribbons on the belt.

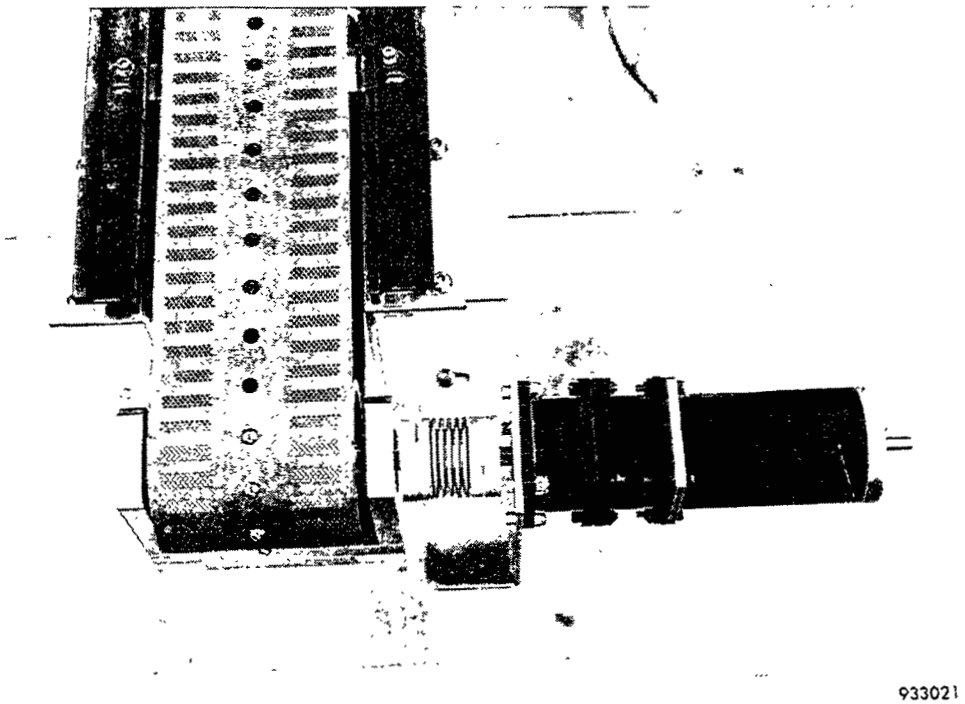

Figure 34 *Drive pulley end of the vacuum conveyor belt.*

When a cell string is completed, it is picked up from the conveyor belt by a string transfer mechanism. The mechanism consists of a linear array of vacuum pick-ups suspended from a four-axis manipulator, as shown in the drawing in Figure 35. After picking up the cell string, the mechanism carries it to the in-line I-V tester for an electrical performance test, and then places the string either on the array table, if the string passes the test, or on the reject table. The lay-out drawing of the complete system (Figure 4) shows a plan view of the cell string conveyor, the string transfer mechanism, the string I-V tester, the string array table, and the reject string table. The system has the capacity to assemble groups of cell strings up to 2.0 m long by 1.4 m wide.

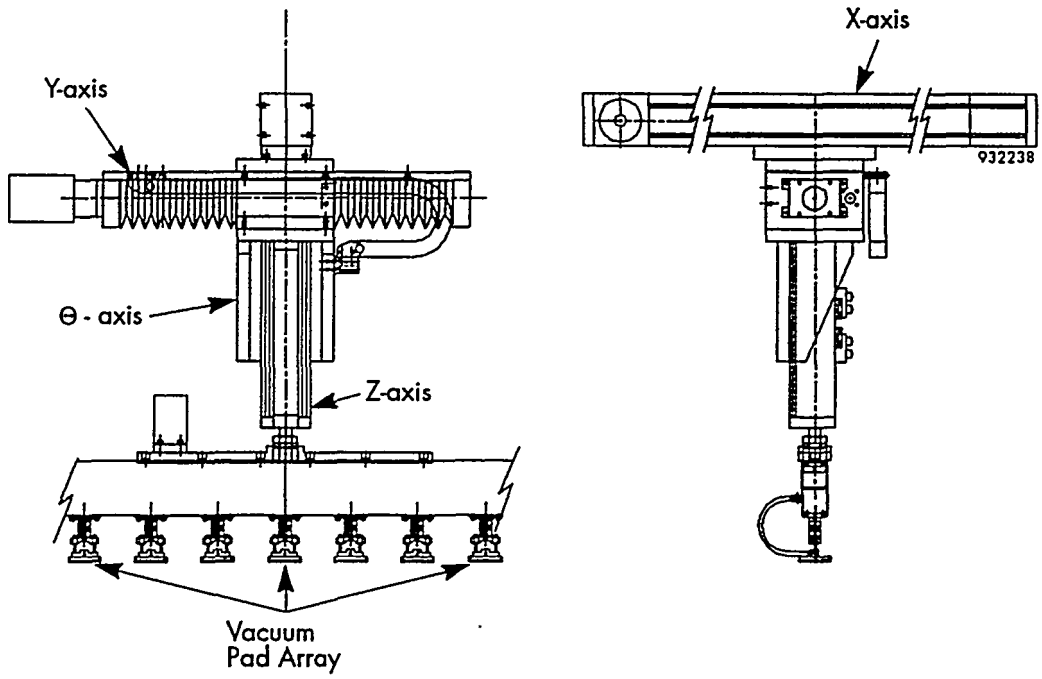

Figure 35 *Cell string transfer assembly.*

The cell string manipulator provides string motion in four axes (x, y, z, and θ). Pneumatic z and θ actuators provide 2.5 cm of z motion and 180° of θ motion. The z motion is used to pick up and place the cell string, while the θ motion allows strings to be placed in alternating plus and minus orientations, a standard technique for arranging strings in series. Both θ and z axes are equipped with position sensors.

The y axis has 20 cm of travel and is driven by a ball screw type of positioner and a stepper motor, similar to those used on the cell aligner robot. Y motion is used if an offset in the string length direction is desired, as is normally the case for round cells.

A belt driven linear positioner is used for the long (244 cm) x motion. The x motion is used to transport a string from the conveyor to the I-V tester and then to either the string array table (good string) or the reject table (reject string). A stepper motor drives a toothed belt that moves a stage along ball bearing ways. The load carried by the x axis stage is sufficiently massive that a 6:1 gear reducer is used to lower the torque requirements for the stepper motor.

An array of vacuum pick-ups is suspended from the 4-axis manipulator. The pick-ups are supported by a two meter long channel designed to allow placement of the pick-ups anywhere along the length of the channel. One pick-up is used for each cell in a string. The pick-ups use a floating mount design similar to that used by the cell loader. A photograph of the string transfer mechanism is shown in Figure 36.

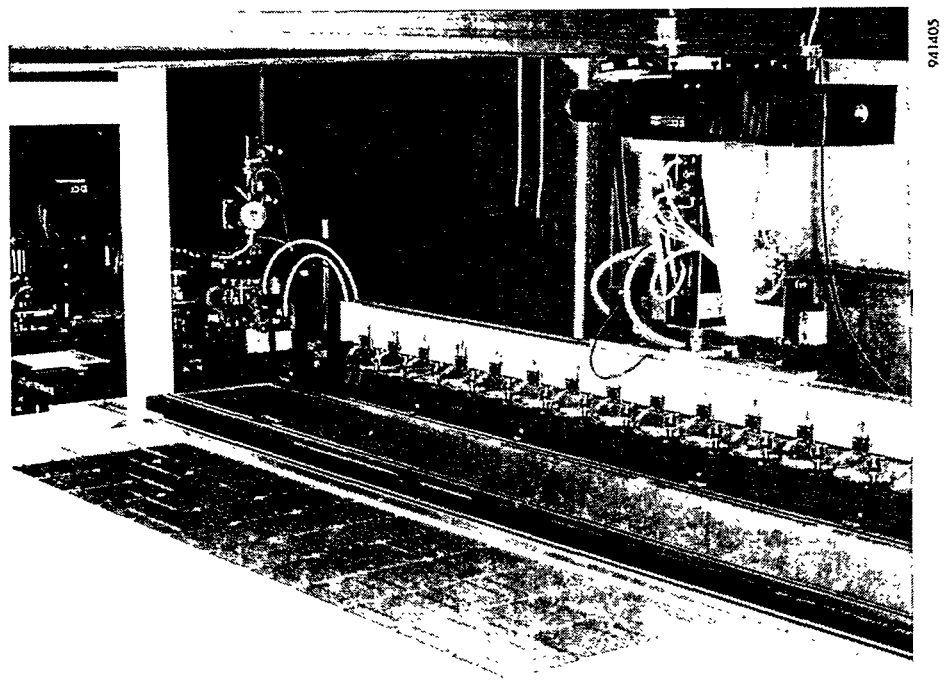

Figure 36 · *String transfer assembly, including the 4-axis manipulator and the cell string vacuum pick-up array.*

A venturi vacuum pump supplies the vacuum used for picking up cell strings. Small manual shut-off valves are installed in the vacuum lines to each vacuum pick-up. These valves allow the string transfer assembly to be configured for different length strings without changing the vacuum line plumbing.

Testing of the string handling process showed that a fairly long time delay was incurred during string placement on the array table. The delay was caused by the time required to vent the vacuum manifold. A vacuum release valve was added that reduced the delay significantly by injecting compressed air into the vacuum manifold when strings are placed.

Vacuum switches were installed on each vacuum pick-up on the cell string transfer assembly. These switches provide a positive indication that all cells in a string are acquired before the string is lifted and transported. They also indicate when the string is released from vacuum during placement on the string array table.

A carrier stop was designed and installed on the string array table to provide a fixed location for the carrier on which cell strings are placed. The carrier stop consists of a rail which extends along the entire length of the array table, at the edge next to the I-V tester, and a plate which has an edge perpendicular to the rail. The plate can slide along the rail to any desired location and is locked in place on the rail with a clamp. A string carrier can be placed in a fixed, repeatable position on the array table by sliding it into the corner formed by the rail and the plate.

2.2.8 Tasks 8 and 13 - In-Line I-V String Testing Development

The need for an illuminated cell string performance test for in-line quality control after string soldering was recommended to Spire by module manufacturers during the Task 1 design definition efforts. As a result, Task 8 was added to Phase I of the program, with work concluding in Phase II under Task 13.

The in-line string current-voltage (I-V) tester measures string electrical performance under simulated sunlight and compares the measured data with three acceptance criteria to determine if the string should be used in a module. Measured values for string open circuit voltage, short circuit current, and maximum power are compared to minimum acceptance values preselected by the operator. If any one of the three measured values does not meet or exceed the corresponding acceptance value, the string is placed on the reject table.

The in-line string I-V tester consists of a xenon light source, optics, power supply, and pulse forming network for producing a uniform one-sun illumination on the cell string; a calibrated reference cell for monitoring the lamp intensity and triggering the measurement; test probes for making contact to the string; an electronic load for sweeping the I-V curve; and a personal computer for controlling the light source, acquiring, analyzing, displaying, and storing data, and comparing string performance with stored pass/fail criteria. Strings up to 15 cm wide by 200 cm long can be tested.

The lamp assembly and enclosure are shown in Figure 37. Two 1 m long xenon arc lamps are mounted end-to-end inside tubular glass spectral filters. Lamp mounts, filter mounts, electrical contacts, cooling jets for the lamp seals, and a glass test stage were designed, fabricated, and installed. The lamp mounts are designed to minimize the space between the lamps for illumination uniformity. Access panels are provided for servicing the lamps.

A new lamp pulse forming network was designed for maximum string testing throughput. In Spire's present sun simulators, used for module testing, the lamp flash rate is 15 Hz, and one data point on the I-V curve is measured during each flash. The standard procedure is to measure 256 data points for each I-V curve, which takes approximately 17 s. Throughput can be increased without a significant loss in accuracy by reducing the number of data points to 100, which reduces the measurement time to 6.7 s. A different approach was taken here to achieve faster throughput: a single flat-peaked light pulse is generated during which a complete I-V curve is measured. The lamps, power supply, and pulse forming network were assembled and tested. Flat, stable light pulses were obtained with a duration of 8 ms at the peak, verifying the design of the pulse forming network.

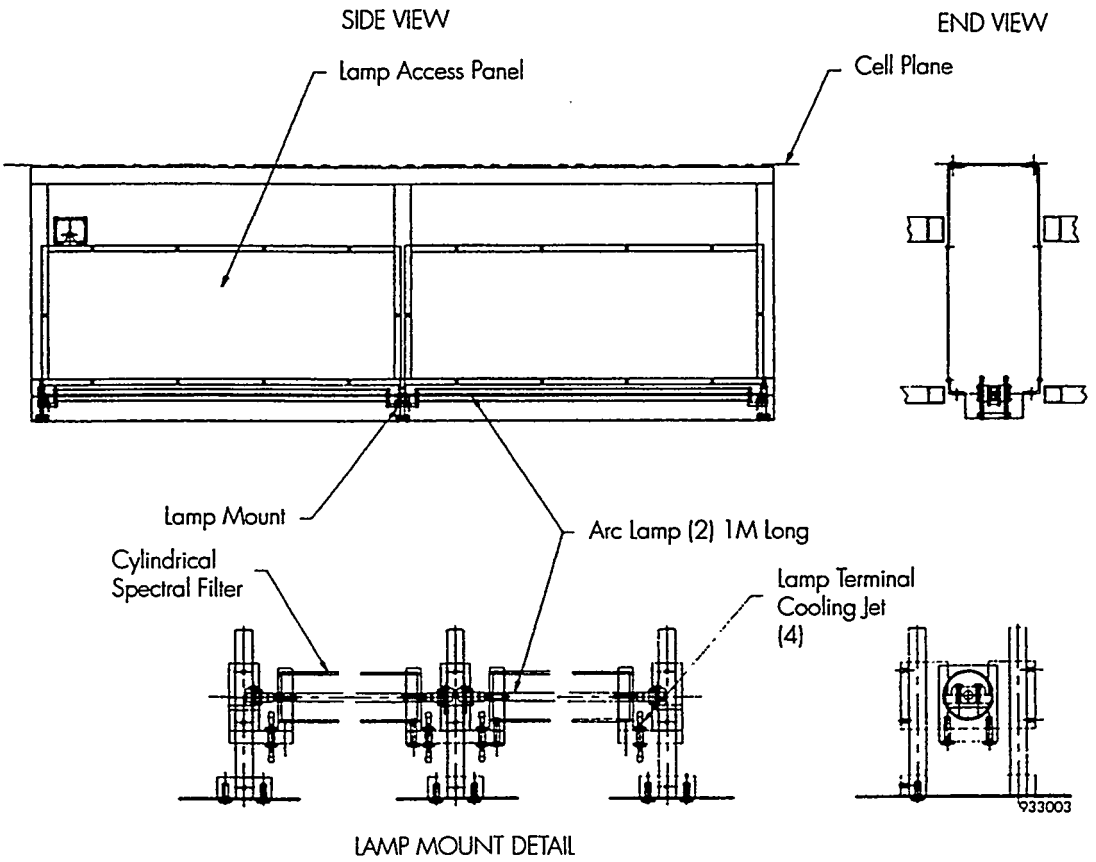

Figure 37 *I-V tester lamp assembly and enclosure.*

A new probe assembly was designed to make electrical connections to the ends of a cell string. The assembly has three spring-loaded contacts at each end of the cell string, two to collect current from the two interconnect tabs and one to sense voltage from one of the tabs, thus providing a four-point (+V, +I, -V, -I) probe arrangement for maximum measurement accuracy. The probes are attached to the beam that holds the cell string on the string transfer mechanism, eliminating the need for separate probe actuators, since the z-motion of the beam is used to press the probes onto the tabs. The two contact assemblies (one at each end of the string) can be mounted anywhere along the beam to match the cell string length. Slotted mounting brackets allow adjustments to be made to the contact spacing (to match the tab spacing) and the contact height.

Circuitry was designed and assembled and software was written for PC control of the electronic load that sweeps the voltage and current across the cell string. Software was also written for measuring I-V curves. During each light pulse, the electronic load sweeps a complete I-V curve from short circuit current (I_{sc}) to open circuit voltage (V_{oc}) while the PC acquires 100 data values (n = 1 to 100) on each of three analog channels: string voltage (V_n), string current (I_n), and reference cell short circuit current ($I_{ref\text{-}n}$). $I_{ref\text{-}n}$ is proportional to light intensity and is monitored to ensure that all measurements are made at levels close to one sun and to allow small corrections to be made in I_n at each I-V data point to compensate for small variations in intensity. Measurements show that $I_{ref\text{-}n}$ varies less than ±2.5% during a 100-point string test. The maximum power point on the I-V curve (P_{max}) is determined by calculating $P_n = V_n \times I_n$ for each data point on the curve and selecting the maximum value. Sample data from a measured string are plotted in Figure 38.

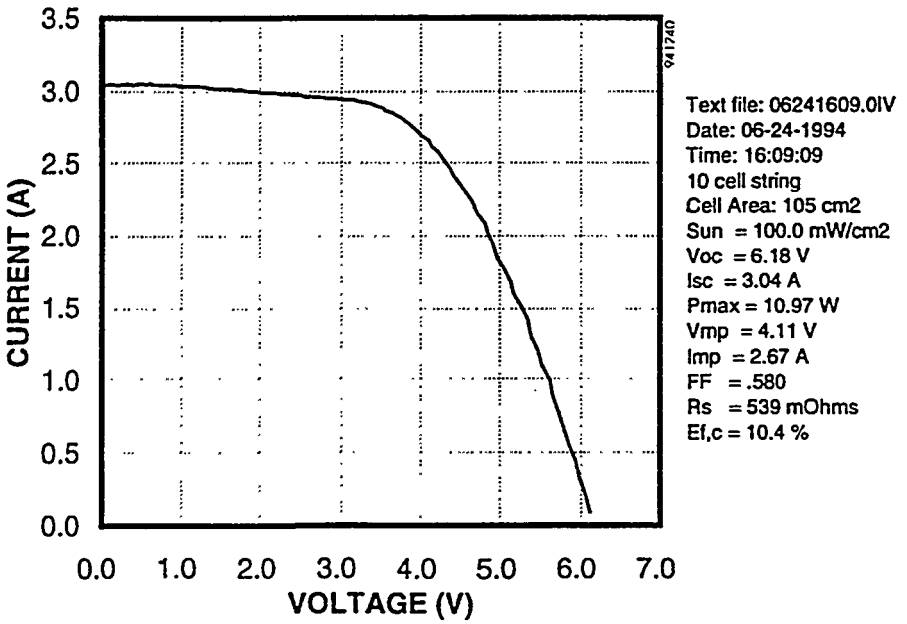

Figure 38 *One sun I-V data measured with string I-V tester. (Note that the low fill factor and poor efficiency of this string were caused by poor cell performance, as determined by individual cell string measurements. Cell and string measurements were in agreement.)*

In production, a display of a full I-V curve is not required on a routine basis. If the string passes the acceptance criteria, a table of significant data is saved in a file on the hard disk and the string is transported to the string array table. If the string fails, the data table and all 100 I-V data points are saved in a file on the hard disk, and the string is transported to the reject table. Examination of I-V curves for failed strings can help the manufacturer to diagnose the cause of string failure.

2.2.9 Tasks 9 and 10 - Process Subassembly Design and Test

Process subassembly design and test activities are described in detail in the above process development sections (Sections 2.2.2 through 2.2.8). Design work included the mechanical design of subassemblies for cell loading, cell aligning, interconnect ribbon handling, ribbon fluxing, ribbon to cell soldering, cell string handling, and in-line I-V string testing. Each subassembly comprises a number of lower-level subassemblies which are listed in Table 7. Electrical and pneumatic controls were designed for each of these subassemblies.

2.2.10 Tasks 11 and 14 - Integrated System Design and System Integration and Test

Under these tasks an integrated system was designed in which the individual process subassemblies were combined to form a single automated system. Integration is required for the mechanical subassemblies and for the pneumatic, electrical, and software systems used for powering and controlling the subassemblies. Integration design work was done in Phase I under Task 11, while system integration and testing were done in Phase II under Task 14.

Table 7 *Subassemblies, automated solar cell assembler.*

Process subassembly	Lower-level subassemblies
Cell loading	Cell stack carriers Carrier shuttle Load stack elevators Two axis pick-and-place manipulator Vacuum end-effector
Cell aligning	Four axis robotic manipulator Vacuum end-effector Video imaging and processing system
Interconnect ribbon handling	Ribbon reels Ribbon accumulators Ribbon clamp and form assembly Ribbon cutting assembly Ribbon shuttle
Ribbon flux application	Flux station Ribbon drive rollers Automatic flux filling system
Ribbon to cell soldering	Two lamp solder head Actuator assembly
Cell string handling	String conveyor Heated vacuum plenum Four axis manipulator Vacuum end-effectors assembly String array table and reject string table
In-line I-V string testing	Sun simulator Test probes assembly Electronic load and measurements

2.2.10.1 Subassembly Integration

Mechanically, all of the process subassemblies listed in Table 7 were designed to mount together on three structural frames which join together to form a single system. One frame supports the loader and aligner subassemblies; the second frame supports the ribbon handling subassemblies, the flux application subassembly, the cell soldering subassembly, and one end of the string conveyor subassembly; the third frame supports the string handling subassemblies, the other end of the string conveyor, the string array table, the reject string table, and the I-V tester subassembly.

Three pneumatic distribution manifolds were designed, one for each of the three structural frames. These manifolds supply the subassemblies with filtered compressed air at the proper pressures and flows. Lubricators were installed on the lines that supply air to actuators for which lubrication is recommended. Pressure switches were installed on critical regulators to signal the control system when the air pressure drops below the level needed for proper operation.

Electrical systems were designed, including an AC power system and wiring for communications between subassemblies. Both the main power distribution box and the PLC, which controls much of the system operation, were mounted in the centrally-located frame that supports the ribbon handling subassemblies. AC outlet boxes and connectors for signal lines were installed in two locations on the ribbon handling frame: where it joins to the loader/aligner frame and where it joins to the string handling/I-V tester frame.

2.2.10.2 Control System and Software

A block diagram of the control system is provided in Figure 39. Software was developed for the supervisory PC for communications with subsystem controllers, including the PLC and stepper motor drivers. A graphical user interface was written in Visual Basic for operator-machine interface functions, which include:

- user inputs for machine set-up, such as cell type, number of cells per string, and number of strings per module
- user commands for system control, such as run, pause, continue, reset motors, and emergency stop
- machine messages during operation, to indicate status (*e.g.*, cell carrier empty or reel out of ribbon) or error conditions (*e.g.*, ribbon dropped or low vacuum on transfer arm)
- control of stepper motor drivers for the ribbon shuttle, the conveyor belt, and the string transfer mechanism

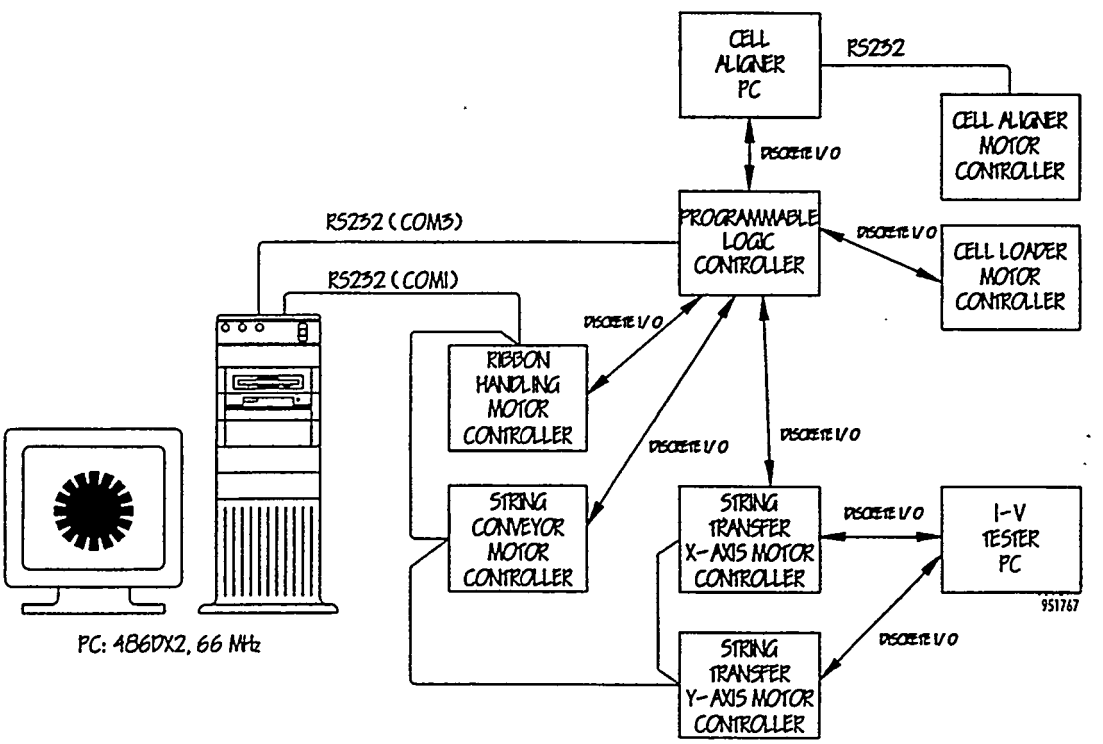

Figure 39 *Assembler control system block diagram.*

The operator issues commands or selects operating parameters from a menu screen, shown in Figure 40. The information is then downloaded to the appropriate subsystem controller.

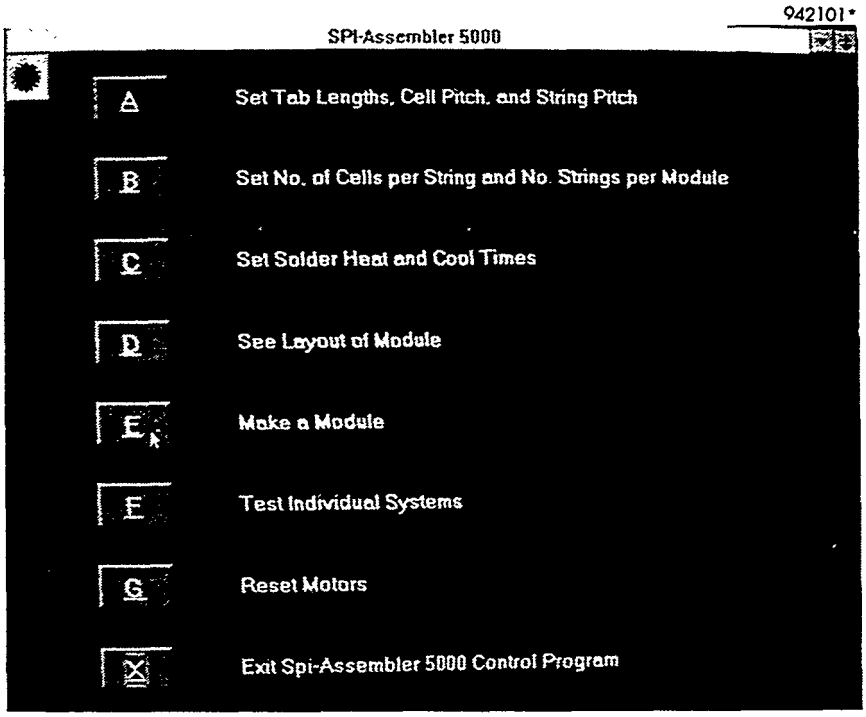

Figure 40 *Main menu screen, SPI-ASSEMBLER 5000.*

Software was developed for the I-V string tester PC, which controls the I-V tester lamps, electronic load, and measurement subassemblies. String pass/fail information is transferred to the string transfer motor controllers for placing each string in the appropriate location.

A graphical user interface and control software were developed for the aligner PC, which controls the cell alignment subassemblies (the aligner robot, vision system, aligner stage vacuum, and aligner shutter) and the cell loader manipulator. The main menu for the cell alignment system is shown in Figure 41.

A control panel was designed to provide a number of operator control functions and displays. A photograph of the panel is shown in Figure 42. Controls are provided to start, pause, and emergency stop the system, reset the stepper motors, and mute an audible alarm. Ribbon controls are provided for manually operating the ribbon drive motors and to toggle the ribbon clamp open and closed. Platen controls are used to set the cell preheat temperature and the platen vacuum level. Solder lamp controls are provided to set and display the lamp voltage levels used during the soldering cycle. The enclosure was mounted on the ribbon handling frame near the ribbon reels.

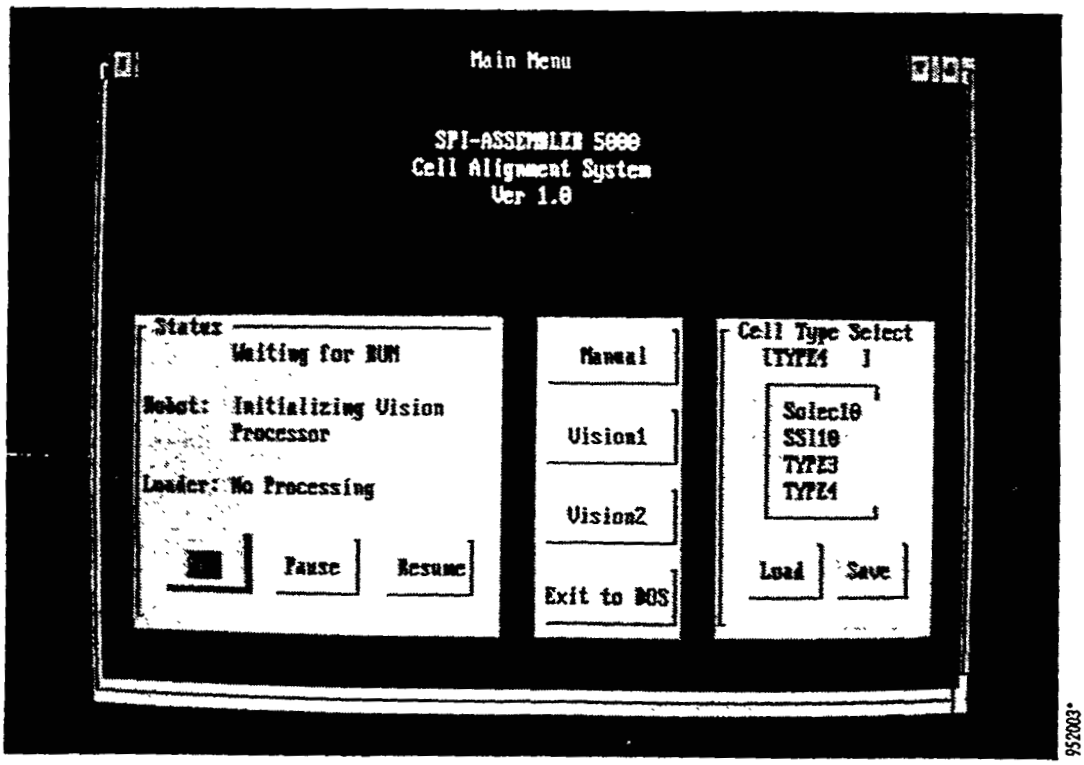

Figure 41 *Main menu screen, cell alignment system.*

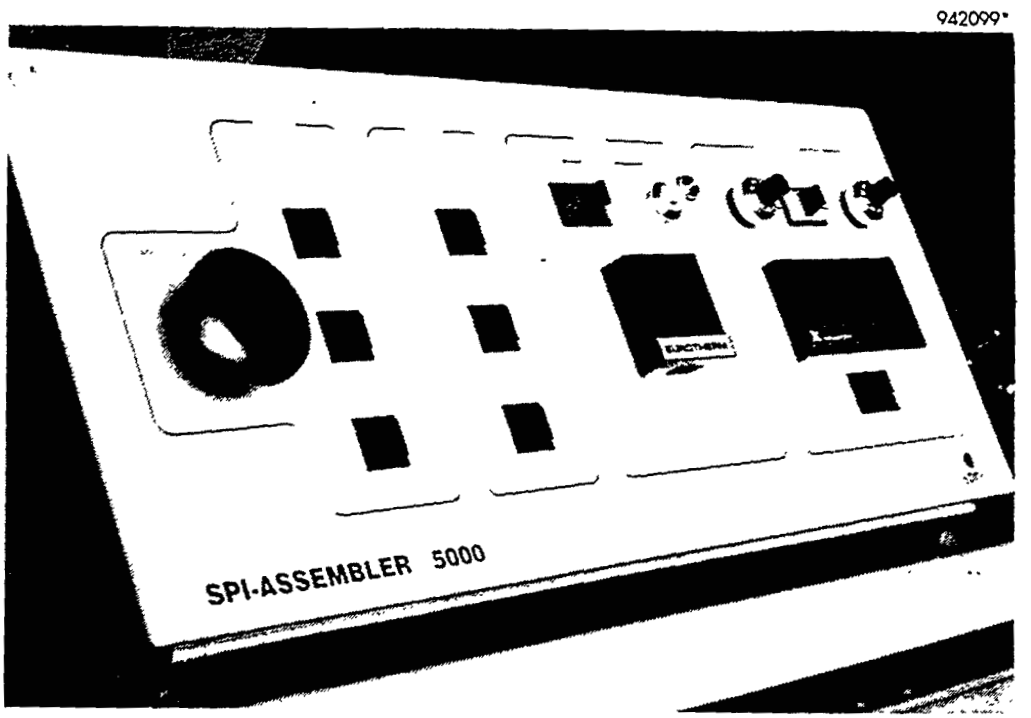

Figure 42 *Control panel, cell assembler.*

2.2.10.3 Safety Systems

Due to the large size of the Assembler system, five large red emergency stop buttons were mounted at various locations around the perimeter of the machine. These buttons are provided for operator safety and equipment protection. One button was mounted on the operator control panel (Figure 42) while the other four were mounted in small boxes located around the machine.

The process control and monitoring programs on the PLC and the PC were enhanced with the addition of 19 different alarm conditions. When sensors indicate an alarm condition, an audible alarm is sounded and a message is displayed on the PC monitor to indicate the source of the alarm. The alarms are grouped into three categories, in order of increasing severity, as follows:

Warning - provides an audible alarm and a message on the PC monitor; machine operation is not interrupted.

Machine Pause - provides an audible alarm and a message on the PC monitor; machine operation is interrupted; motor positions and digital output states are preserved; after the fault is corrected, the operator can resume processing from the point at which the system was interrupted.

Emergency Stop - provides an audible alarm and a message on the PC monitor; machine operation is interrupted; power is removed from all stepper motor drives and all digital outputs; after the fault is corrected the system must be restarted, as for an initial power up.

A list of alarms by category is provided in Table 8.

The Assembler contains a number of mechanisms that operate at high speed or with force sufficient to cause bodily injury. These mechanisms include the cell stack shuttle, the cell loader manipulator, the aligner robot, the aligner shutter, the load elevator, the ribbon clamp and form assembly, the ribbon cutter, and the ribbon shuttle assembly. Two approaches were considered for protecting personnel from injury: an enclosure system and a combination of a light curtain with safety mats.

The enclosure approach requires the design and fabrication of protective panels, windows for observing the system in operation, and interlocked doors for loading cell stacks and for servicing the system. A design evaluation of the enclosure approach indicated that fairly complex (and expensive) sheet metal work would be required. In addition, it would be difficult to design the enclosure system with the desired visibility and ease of access to all of the subassemblies. Experience shows that operators who cannot adequately see or access machinery tend to remove protective covers, creating a hazardous situation.

An alternative plan for combining a light curtain with safety mats was devised. This plan was selected over the enclosure approach, since it provides the necessary protection from moving machinery while allowing excellent visibility in operation and maximum access for servicing. The light curtain consists of a transmitter (a linear array of infrared LEDs), mirrors, a receiver (a linear array of phototransistors), and a controller. The transmitter and receiver were mounted with four mirrors on the Assembler to create a box-shaped light curtain, as illustrated in Figure 43.

Table 8 *SPI-ASSEMBLER 5000 alarm conditions.*

Alarm Level	Alarm Condition
Warning	End of reel, left End of reel, right Loader down - cannot shuttle No cassette loaded IV test failure
Machine Pause	Operator pressed Pause button Ribbon loop too high, left Ribbon loop too high, right Ribbon dropped, left Ribbon dropped, right Low pressure, solder head cooling Low vacuum on platen No vacuum on transfer arm - string not picked up Object in the light curtain
Emergency Stop	Operator pressed one of five Emergency Stop buttons Object between blades Low aligner air pressure Low machine air pressure Low string transfer air pressure

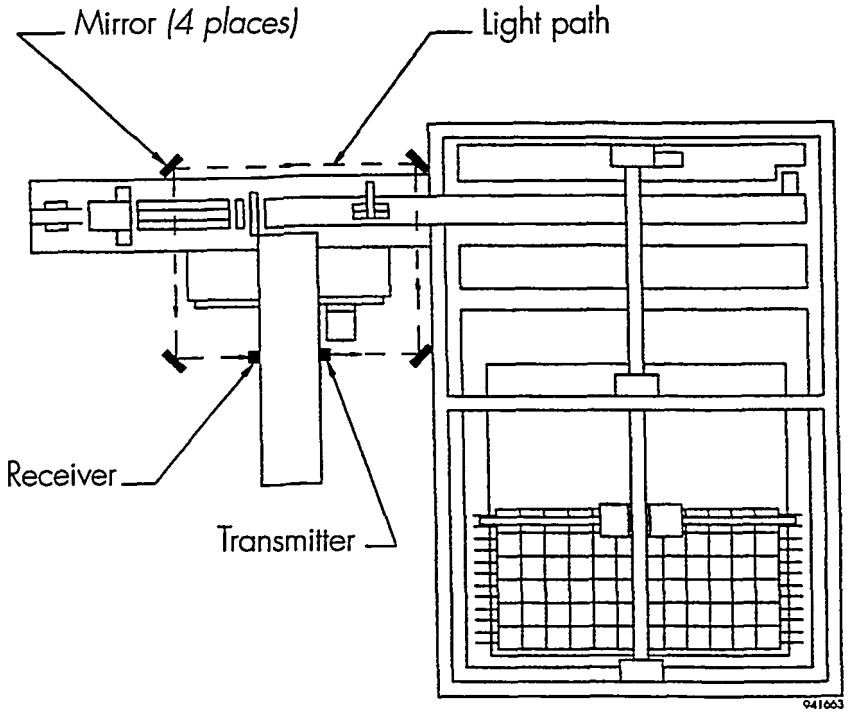

Figure 43 *Safety light curtain arrangement (plan view, not to scale).*

The light curtain encloses the cell loader manipulator, the aligner robot, the aligner shutter, the ribbon clamp and form assembly, the ribbon cutter, and the ribbon shuttle assembly. Any object 19 mm (0.75") or larger that crosses the light beam between the transmitter and the receiver triggers a relay connected to the PLC, which immediately pauses Assembler operation.

Safety mats are rubber floor mats with an embedded switch that closes when pressure is applied by a person standing or walking on any part of the mat. Mats of this type are commonly used to actuate automatic door openers at supermarkets. Two safety mats were installed, one at each of the two cell stack loading areas, such that an operator is required to stand on a mat when loading cells. A mass greater than 6.8 kg (15 lb) on either mat prevents the cell stack shuttle and the load elevator from moving.

2.2.11 Task 15 - Preliminary Processing Evaluation

Preliminary processing evaluations were done with the Assembler at Spire between May, 1994, and June, 1995. During this period, more than 15,000 solar cells were processed from six major module manufacturers. These evaluations were critical not only for process development purposes but also to build manufacturers' confidence in the new processes and equipment.

A summary of the largest evaluation runs is provided in Table 9. The table does not include additional experimental runs of less than 200 cells per run done with Solec, Solarex, and ASE Americas cells. All of the runs in Table 9 were done using solder coated copper interconnect ribbon and Kester 920-CXF flux.

Table 9 *Preliminary processing evaluations at Spire.*

Date	Cell Manufacturer	Cell Type	No. of Cells	Comments
May 94	Siemens Solar	103 mm sq. Cz	1000	97.5% yield, modules made for testing
Sep 94	Siemens Solar	103 mm sq. Cz	2200	98.5% yield, 4 s/cell
Sep 94	BP Solar	125 mm sq. Cz	300	Low yield; 1st run with large area cells
Nov 94	Solec	thin 102 mm sq. Cz	200	98.5% yield on last 132 cells
Mar 95	Solec	thin 102 mm sq. Cz	1100	96.5% yield, 97.8% on last 228 cells; cells have ragged edges
Apr 95	Siemens Solar	103 mm sq. Cz	1200	98.4% yield; for UML solar race car
Apr 95	BP Solar	125 mm sq. Cz	350	98.2% yield, large area cells
May 95	Eurosolare	103 mm sq. Cz	3000	98.3% yield, some chipped cells
May 95	Solarex	114 mm sq. Poly-X	200	100% yield, modules made for testing
Jun 95	ASE Americas	100 mm sq. EFG	2100	98.6% yield
		Total	11,650	

Both thin (200 μm) Cz Si cells from Solec and standard thickness (300 to 400 μm) cells from a range of manufacturers were processed. Yields typically exceeded 98% once some experience was gained. An exception is a group of thin Solec cells that were processed in March, 1995. These cells

had ragged edges caused by the etching process used to thin the silicon wafers to 200 μm. Similar thin Solec cells without ragged edges were processed in November, 1994, with 98.5% yield.

Processing rates of 3.8 to 4.0 s/cell were measured for Siemens cells on a cell-to-cell basis. String-to-string cycle times were 68 s per 12-cell string, equivalent to 5.7 s/cell. This cycle time is longer than the cell-to-cell cycle time due to the present method of string fabrication sequencing. Sequencing improvements have been identified that can reduce string-to-string cycle times.

2.2.11.1 Cell Performance After Processing

Solar cell performance measurements made before and after processing in the Assembler showed no cell degradation. Measurement data taken for 10 thin Solec cells, provided in Table 10, show that the power has increased slightly (2%), mainly due to increased fill factor. This may be caused by an increase in conductivity along the contact busses provided by the interconnect ribbons.

Table 10 *Cell performance after soldering, Solec 200 μm Cz Si cells. Data are average values for 10 cells.*

Measurement	V_{oc} (V)	I_{sc} (A)	FF (%)	P_{max} (W)	Efficiency (%)
Before soldering	0.569	2.792	63.7	1.013	9.69
After soldering	0.571	2.793	64.6	1.032	9.87
Change (%)	+0.4	+0.0	+1.4	+1.9	+1.9

2.2.11.2 PV Module Qualification Tests

Both Siemens Solar and Solarex made modules from cell strings fabricated on the Assembler which they then subjected to accelerated environmental testing per IEC 1215 and IEEE 1262 standards. These tests consisted of thermal cycling, thermal and humidity-freeze cycling, and damp heat soaking. The maximum allowable power loss is 5% for the IEC 1215 testing and 10% for the IEEE 1262 testing. All modules passed both qualification tests, with a maximum power loss of 3.8%. It is significant that the flux residues were not cleaned from the strings prior to encapsulation. Test results are provided in Table 11.

2.2.11.3 Cell String Thermal Stress Testing

Cell strings made with ASE Americas 100 mm square EFG Si cells were subjected to a thermal bond aging test used by ASE for screening solder alloys. Copper interconnect ribbons, 0.10 mm x 1.5 mm (0.004" x 0.060"), were obtained with two types of solder coatings: a standard Sn60/Pb40 alloy and a non-standard Pb-free alloy recommended by ASE. Cell strings were fabricated from both types of ribbon using Kester 920-CXF flux. The strings were not cleaned after soldering.

Table 11 *Results of PV module qualification tests done by Siemens Solar and Solarex on modules made with strings fabricated by the Assembler. SSI data courtesy of J. Hummel and T. Jester, Siemens Solar Industries; Solarex data courtesy of J. Wohlgemuth, Solarex.*

Test	Module Type	Initial Power (W)	Power Change (%)
T-200 Thermal cycling +90°C to -40°C	SSI M55 #1	55.1	-1.5
	SSI M55 #2	54.9	-1.5
	SSI M55 #4	54.8	-0.7
	Solarex MSX-60 #2[a]	60.7	-1.8
T-50 & HF-10 Thermal & Humidity Freeze Cycling	SSI M55 #3[b]	55.2	-3.1
	SSI M55 #5[b]	54.3	-3.4
	SSI M55 #9[b]	55.1	-3.8
	Solarex MSX-60 #1	60.9	-3.5
DH1000 Damp Heat Soak 85°C, 85% RH	SSI M55 #7	55.2	-2.4
	SSI M55 #8	55.0	-1.6
	SSI M55 #10	54.6	-1.5
	Solarex MSX-60 #3	60.7	-3.1

[a]test extended to 400 thermal cycles
[b]test extended to 20 humidity-freeze cycles

Unencapsulated cell strings were subjected to the thermal bond aging test, consisting of a thermal soak at 165°C for 5 hours. Solder joint pull tests were done before and after soaking. As shown in Table 12, the non-standard alloy had significantly fewer weak bonds (pull force < 45 g) after the aging test. On this basis, ASE selected the non-standard alloy for use with its cells.

Table 12 *ASE Americas thermal bond aging test for screening solder alloys. Data courtesy of R. Gonsiorawski, ASE Americas*

Parameter	Front Contact		Back Contact	
	Initial	Thermally Aged	Initial	Thermally Aged
Standard Sn60/Pb40 Solder Coating				
No. of bonds	48	48	48	50
Mean pull force (g)	248	162	200	51
Std. dev.	144	124	162	100
Bonds <45 g	19%	15%	19%	78%
Non-Standard Solder Coating				
No. of bonds	40	40	40	40
Mean pull force (g)	274	305	281	187
Std. dev.	125	120	120	105
Bonds <45 g	3%	5%	3%	8%

2.2.12 Task 16 - Final Processing Evaluation

In June, 1995, preliminary processing evaluations were concluded at Spire and the Assembler was disassembled into its four main parts: the cell loader/aligner assembly, the ribbon handling assembly, the cell-string transport assembly, and the conveyor assembly. The parts were securely packed and shipped to ASE Americas in July to evaluate the Assembler in a production setting. Machine unpacking, assembly, and testing were completed by Spire personnel at ASE. A number of modifications requested by ASE were completed, including the removal of the I-V string tester and the installation of a 15 cm x 200 cm mirror and a Pass/Fail switch box to enable operator visual inspections.

Once the Assembler was operational, preliminary cell strings were fabricated from reject ASE cells. Solar cell loading and aligning worked well, and the interconnect ribbon alignment to the cell front contacts was good. However, two processing problems occurred at higher than acceptable rates: cells were cracking during soldering and solder bonds were being missed at an unacceptable rate on the cells' back contacts. These issues are described in the following sections.

2.2.12.1 Cracked Cells

The ASE cells tend to have terminated edge cracks caused by stresses induced during the ribbon crystal growth and laser cutting processes. In addition, the reject cells used for preliminary Assembler testing probably had a higher frequency of cracks than good cells. An unacceptable number of these cells broke when heated in the soldering process.

The frequency of cell breakage during soldering was significantly reduced by pre-screening the reject cells for terminated cracks. Pre-screening was done by gently flexing the cells, which caused cells weakened by terminated cracks to break easily into pieces.

While the flexing inspection reduced cell breakage considerably, some breakage during soldering was still observed. Given ASE's directive to minimize string rework, the solder lamp heating voltage was reduced (140V to 120V) and the soldering time was increased (1.7 to 3.8 s) to provide a gentler heating profile. Very low breakage rates on the order of 0.3% were obtained in trial runs of several hundred cells under these conditions.

2.2.12.2 Back Contact Solder Bonds

While front side soldering was generally reliable, soldering to the back contacts was less than satisfactory. Testing identified a number of contributing factors, including the small contact pad size, surface irregularities on the pad, camber (in-plane bend) in the interconnect ribbon, and wearing of the ribbon drive rollers.

Several steps were taken to compensate for these factors. ASE redesigned their back contact to have a larger solderable area, which eliminated the problems caused by small pad size and surface irregularities. The camber problem was eliminated by inspecting the interconnect ribbon for compliance with the vendor's specification. The ribbon drive roller problem was caused by a slow disintegration of the roller material where it is in contact with flux. The problem was solved

temporarily by installing a new set of urethane rollers, after which the back contact soldering was noticeably improved. For the long term, Spire is looking into alternative materials that will provide a longer service life.

2.2.12.3 Soldering Process Window

As part of the preliminary process testing, an experimental matrix was done to define a process window within which good soldering is achieved with ASE cells and ribbon. It is important to note that the process parameters used with other manufacturer's cells and ribbon do not apply here, given the unique nature of ASE's EFG ribbon silicon and the higher melting point of the solder alloy that ASE uses.

Strings were fabricated over a range of lamp heating voltages (112V to 125V) and a range of cell heating times (3.7s to 4.1s). The strings were then inspected and the quality of the soldering was rated either excellent (acceptable), good (also acceptable), or poor (unacceptable). The platen pre-heat temperature (140°C) and the cooling time (3.0s) were held constant.

The results of the matrix are plotted in Figure 44. Each bar in the figure represents data for one nine-cell string. The height of the bar is the range of the voltage variation observed for that string. The soldering quality is indicated by the line type: solid for excellent, dashed for good, and dotted for poor. The process window for acceptable strings is indicated by the area between the two slanted dotted lines in Figure 44.

2.2.12.4 Evaluation Run Results

An evaluation run was done with ASE cells which had the newly designed larger back contact pads. The materials and soldering parameters used for this run are listed in Table 13. One hundred and nineteen 9-cell strings were fabricated, for a total of 1071 cells.

Table 13 *Evaluation run materials and soldering parameters.*

Materials and Parameters	Description or Setting
Cell type	ASE 10 cm square EFG, large back contacts
Ribbon base metal	Copper, 0.10 mm x 1.5 mm (0.004" x 0.060")
Ribbon solder coating	ASE-specified alloy, 12 μm (0.0005")
Flux type	Kester 920-CXF
Platen temperature	140°C
Lamp voltage, heating	122 VAC
Lamp voltage, cooling	26 VAC
Heating time	3.8 s
1st cell extra heating time (Δt)	0.4 s (strings 1 to 13); 0.5 s (strings 14 to 119)
Cooling time	3.0 s

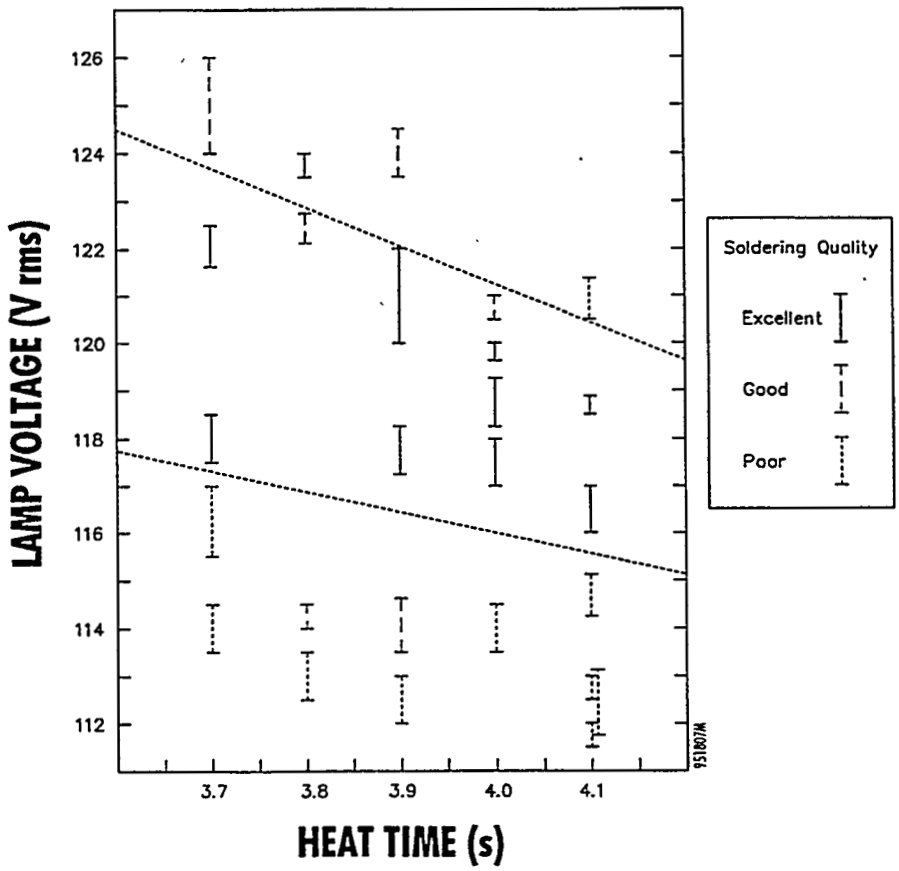

Figure 44 *Soldering process matrix for ASE Americas 10 cm square cells and ASE-selected solder alloy. The process window for acceptable strings is indicated by the area between the two slanted dotted lines. Bar height is the voltage variation observed within each 9-cell string.*

Two adjustments were made to fine-tune the process during the first 26 strings. After placement on the conveyor belt, one of the two ribbons had sufficient coil set (curl) that it was occasionally hit and moved by the ribbon shuttle when the shuttle returned for more ribbon. The ribbon straightener was adjusted to eliminate the curl. A second adjustment was made because the first cell in each string was insufficiently heated to fully melt the solder on the front side of the cell. This occurs because the belt advances between strings (to transport the completed string to the string transfer arm), cooling the platen under the soldering head. The Assembler software has a routine that provides additional heating time (Δt) to the first cell in the string to compensate for this cooling effect. A small (0.1 s) increase in Δt was made after string 13.

A summary of evaluation run yield data is plotted in Figure 45. All of the defects plotted in Figure 45 are reworkable with the exception of cracked cells. The cell yield (percentage of non-cracked cells) in the evaluation run was excellent at 99.3% over all 119 strings. The back bond defect rate was reduced dramatically from previous runs with ASE cells to 0.1% for the last 108 strings and zero for the last 93 strings.

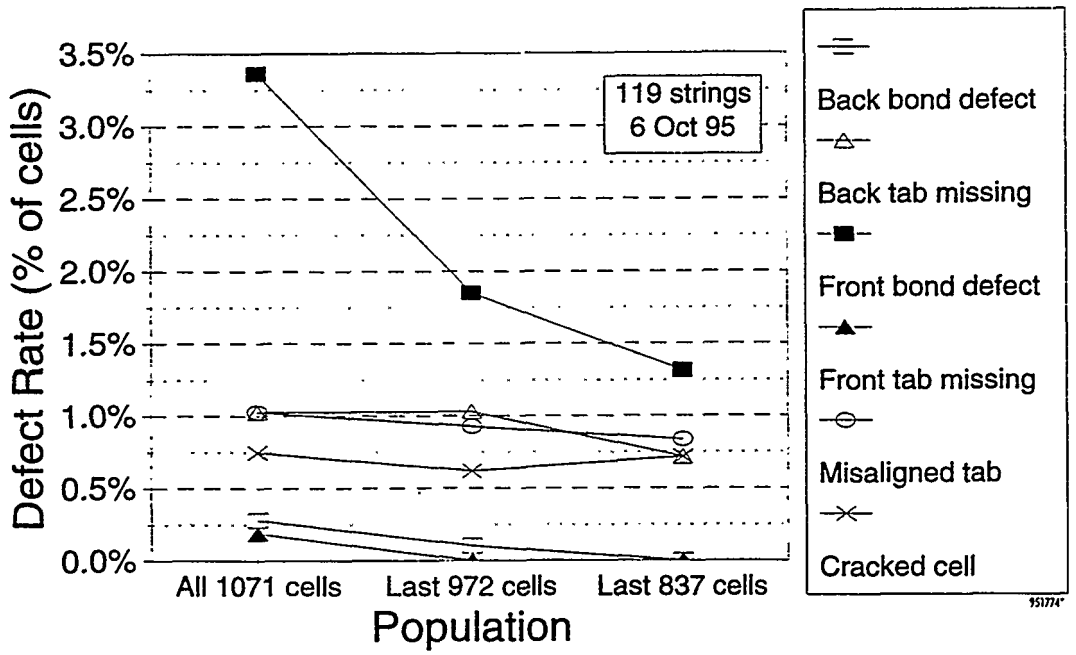

Figure 45 *Evaluation run data, ASE Americas cells, 9 cells/string.*

The cell-to-cell processing time was relatively long at approximately 9 s/cell. This process was developed to obtain high yields with ASE cells, as discussed in Section 2.2.12.1. For comparison, cell-to-cell cycle times of 3.8 to 4.0 s/cell were achieved with single-crystal silicon cells made by Siemens Solar Industries.

Three strings from the evaluation run were selected at random and separated from the product stream for pull testing. Five cells from each string were subjected to pull tests of the front and back contacts using a Chatillon DFG-10 digital force gauge at a pull angle of 90°. The test results, provided in Figure 46, show excellent pull strengths, with average values exceeding 325g for both the front and back contacts. These values are particularly noteworthy given the narrow ribbon width (1.5 mm) used for these strings.

The average front contact pull strength is 357g and the average back contact pull strength is 329g. The data were also divided into left and right categories to probe for any differences that might exist between the left and right ribbons, ribbon handling processes, or solder lamps. The left vs. right data are very consistent for both fronts and backs, well within the standard deviations, indicating no statistical difference between the left and right sides.

2.2.13 Task 18 - System Design Definition for Novel Cells & Bussing

Task 18 has two parts:

- the evaluation of novel solar cells to determine the nature and extent of the constraints and possible options for solar cell interconnection methods and
- a review of manufacturers' requirements for string bussing, defining the range of materials, component geometries, and module configurations an automated bussing system must be designed to process.

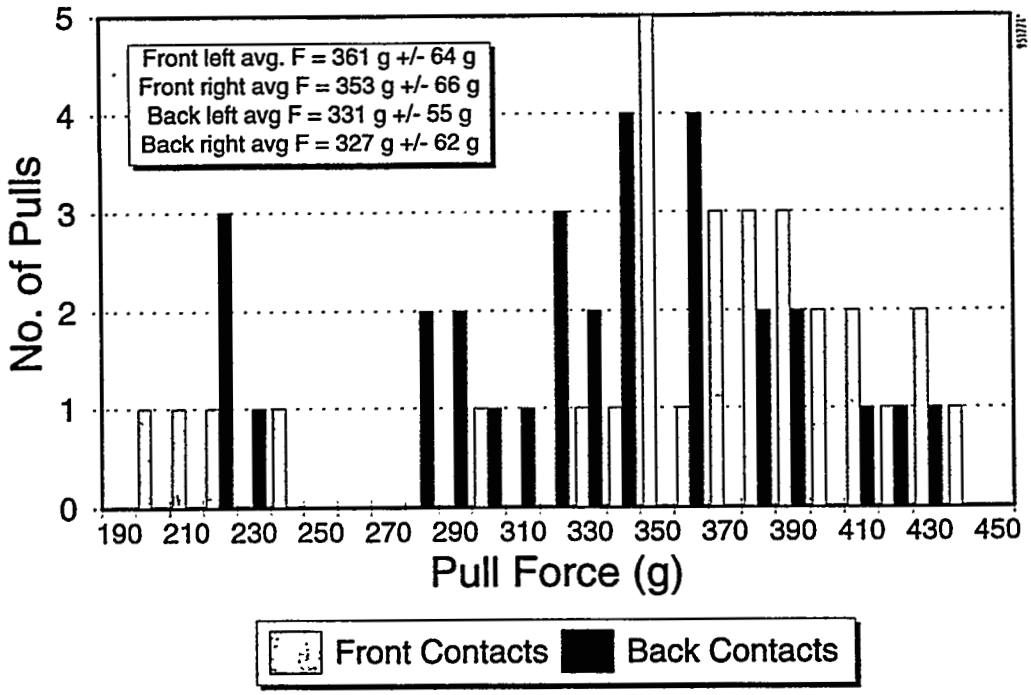

Figure 46 *Histogram of evaluation run pull test data. Pull angle = 90 °.*

2.2.13.1 Novel Solar Cell Soldering Constraints and Options

Spire evaluated novel cell designs from various manufacturers to determine what special constraints these cells may impose on the Assembler. The manufacturers are:

- ASE Americas - polycrystalline EFG ribbon silicon
- AstroPower - thin film polycrystalline silicon on low-cost substrate
- Ebara Solar - thin dendritic web ribbon silicon
- Solarex - cast polycrystalline silicon
- Texas Instruments - silicon spheres on aluminum foil

Spire had discussions with all of these manufacturers and preliminary tests were done on the Assembler with cells from ASE, AstroPower, Ebara Solar, and Solarex. These evaluations indicate that major changes to the Assembler are not required for cells made by ASE or AstroPower.

Initial soldering tests with ASE cells showed that the solder on the interconnect ribbon was melting and conforming to the cell contacts but the joints were weak due to insufficient wetting of solder to the cell contacts. The ribbon drive rollers, which pull the interconnect ribbon through the flux bath, were grooved to provide a thicker flux coating on the ribbon. Ribbon processed with the grooved rollers made larger, more consistent solder joints to the ASE cells.

AstroPower personnel hand-carried a small number of 150 mm square thin film silicon cells to Spire for soldering tests. AstroPower claims that the proprietary substrate material used for their thin film silicon cells has a thermal conductivity that is very similar to silicon's, an important parameter for soldering simultaneously to the front and back contacts. The results of this brief test are encouraging: a string of cells was soldered using parameters developed for single crystal silicon cells, indicating that modifications to the Assembler will not be required for these cells.

Ebara was in the process of changing its cell contact process from evaporation to screen printing. Complete evaluations could not be done since the contact and interconnect designs were not yet finalized. However, 100 Ebara cells with evaporated contacts were obtained to test the Assembler's ability to handle these thin (150 μm) cells. A custom vacuum pick-up and cell stack carrier were designed for the loader, since Ebara's cells are narrow (2.4 cm x 9.8 cm). Cells of this thickness are not only fragile but they can be difficult to pick up from a stack, since lifting the top cell creates a low pressure area underneath that tends to lift additional cells. Loader tests showed that cell breakage was not a problem for these cells, and the loader was able to pick up only one cell at a time.

Solarex's cast polycrystalline silicon wafers contain centimeter-size crystal grains with irregular shapes and different crystal orientations. The angle at which light is reflected from each grain varies, depending on its orientation and the angle of the incident light. Images of these cells obtained by the aligner vision system showed that some crystal grains are brighter than the contact busses. Since the vision system looks for a bright contact bus on a dark solar cell, a bright crystal grain located within the bus bar search area is identified incorrectly as part of the bus, causing a significant error in cell alignment. This problem was solved by repositioning the lamp underneath the aligner stage to obtain a shallower angle of incidence. In this position, the bright reflections from the crystal grains were eliminated and accurate cell alignments were made.

Solarex cells have an antireflection coating over the front contacts which must be removed for soldering. An erasing step, which can be done with a relatively simple mechanism, must be added to the Assembler to remove this coating in the areas where soldering is to be done. Soldering tests showed that solder joint pull strengths are sensitive to the amount of abrasion provided by the erasing process. Good pull strengths were achieved with machine-erased contacts provided by Solarex.

Texas Instruments (TI) cells require substantial modification of the Assembler since TI's aluminum foil interconnects are not solderable. They can, however, be joined by an ultrasonic welding process, a technique used in aluminum foil rolling mills. In principle, an ultrasonic welding head and anvil could be integrated with the Assembler's existing processes, including cell loading, cell aligning, cell string handling, and string transport. Tests were planned for evaluating ultrasonic welding on the Assembler's conveyor belt when word was received, early in 1995, that TI was closing down its photovoltaic activities. As a result, these tests were canceled.

2.2.13.2 String Bussing Requirements

Cell strings are joined together electrically with bus ribbon to complete the module circuit. A survey was distributed to PV module manufacturers to poll their string bussing requirements. The survey solicited information on the bus ribbon and interconnect ribbon materials, the ribbon joining methods used, and the module sizes of interest to the industry. The survey responses were combined to create a generic list that defines the range of requirements applicable to a broad spectrum of manufacturers while protecting the confidential responses of individual companies. The list of bussing requirements is provided in Table 14. This information provides guidance for the design of automated bussing equipment.

Table 14 *String bussing survey summary.*

Parameter	Range of Values
Interconnect ribbon	
Material	Copper, alloy CA-102 or CA-110[a]
Thickness	75 to 125 μm (0.003" to 0.005")
Width	1.5 to 2.5 mm (0.060" to 0.100")
Coating material	Solder, Sn60/Pb40 or other, electroplated or hot dipped
Coating thickness	1.3 to 13 μm (50 to 500 micro-inch)
Bus ribbon	
Material	Copper, alloy CA-102 or CA-110[a]
Thickness	150 to 250 μm (0.006" to 0.010")
Width	2.5 to 6.3 mm (0.100" to 0.250")
Coating material	Solder, Sn60/Pb40 or other, electroplated or hot dipped
Coating thickness	1.3 to 13 μm (50 to 500 micro-inch)
Module size	
Width	23 to 122 cm (9" to 48")
Length	38 to 183 cm (15" to 72")

[a]CA-102 is oxygen-free high conductivity copper; CA-110 is electrolytic tough pitch copper

Busses can be used to connect strings together in series, parallel, or combined configurations. Three general configurations are illustrated in Figure 47. In all cases the bus-length direction is perpendicular to the string-length direction. Lap joints are made between the bus ribbon and the solar cell interconnect ribbons that extend from the ends of each string. Some designs require the attachment of additional bus ribbons (not shown in Figure 47) to provide output to a junction box. Methods for bonding ribbons together were investigated as part of Task 20, Bus Ribbon Bonding.

2.2.14 Task 19 - Bonding Interconnects for Novel Cells

2.2.14.1 Solarex Cast Polycrystalline Silicon Cells

Solarex provided Spire with 11.4 cm square polycrystalline silicon cells for string fabrication on the Assembler. At Spire's recommendation, these cells had slightly longer erased regions over the cells' front contacts (to remove the antireflection coating) for enhanced solderability. Copper ribbon (0.003" x 0.100") with a Sn60/Pb40 coating (0.0005") and Kester 920-CXF flux were used. The soldering parameters were set to 1.7s of heating at a lamp voltage of 140V followed by 2.0s of cooling at 25V, and a 140°C platen temperature.

Four 5-cell strings were fabricated and shipped to NREL as a subcontract deliverable. Thirteen 9-cell strings were fabricated and shipped to Solarex. Solarex fabricated three 36-cell modules from these strings and subjected them to accelerated environmental tests, as described in Section 2.2.11.2. All three modules passed the tests, which included thermal cycling, humidity-freeze cycling, and damp heat soaking. The results of pull tests measured by Spire at a 90° angle were excellent: front contacts averaged 337g (11 pulls), while back contacts averaged 384g (9 pulls).

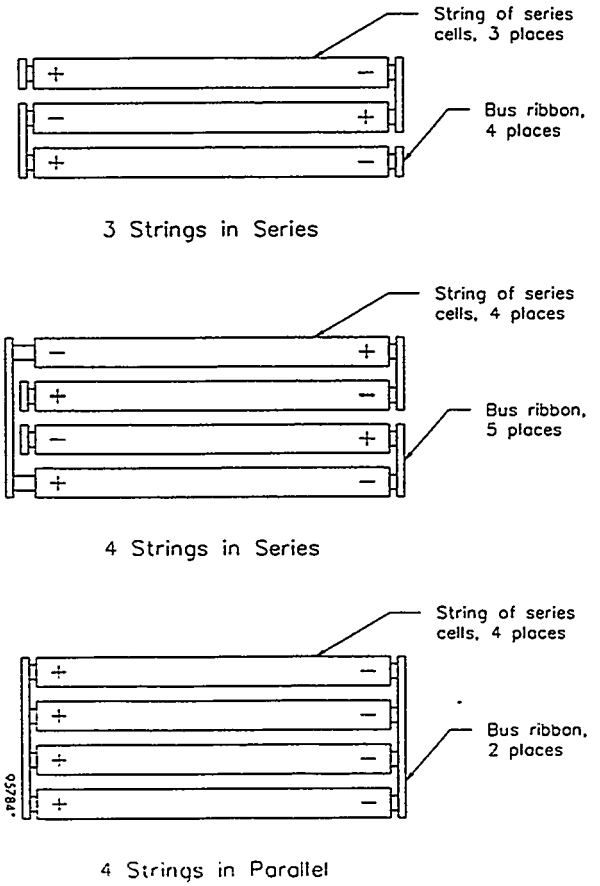

Figure 47 *Typical bussing configurations for PV modules.*

2.2.14.2 ASE Americas EFG Polycrystalline Ribbon Silicon Cells

Two types of ASE cell strings were fabricated on the Assembler at Spire and subjected to thermal bond aging tests by ASE, as described in Section 2.2.11.3. The strings were made with ASE cells and both standard alloy (Sn60/Pb40) solder and non-standard alloy solder. Solder joint pull tests were done before and after thermal aging for each type of solder. The number of weak bonds (less than 45g pull strength) after thermal aging was greatly reduced, from 78% to 8%, as shown in Table 12. On this basis, ASE selected the non-standard alloy for cell string fabrication.

The non-standard solder alloy has a higher melting point that requires longer heating and cooling times. Typical heating and cooling times for standard Sn60/Pb40 solder are 1.7s and 1.5s, respectively. The non-standard alloy requires approximately 3.5s for heating and 3.0s for cooling. Higher lamp power cannot be used to shorten the heating time since it results in increased cell breakage with the EFG cells.

A demonstration run of more than 2100 ASE Americas cells was done at Spire in June, 1995. Copper ribbon (0.004" x 0.060") with the ASE-specified solder coating (0.0005") and Kester 920-CXF flux were used. One hundred and seventeen 18-cell strings were produced. Despite the fragile nature of ASE's EFG ribbon silicon material and the higher melting point of the ASE-specified solder, only 29 cells out of 2106 broke, for a yield of 98.6%. Four 5-cell strings were also fabricated and shipped to NREL as a subcontract deliverable.

2.2.15 Task 20 - Bus Ribbon Bonding

The interconnect ribbons extending from the ends of each cell string are joined to bus ribbons to connect the strings together electrically. Nine different joining processes were identified as possible methods for attaching bus ribbons to interconnect ribbons. These processes were evaluated on the basis of process control and flexibility, throughput, operator safety, equipment cost and complexity, maintenance requirements, power consumption, *etc.* A chart summarizing the advantages and disadvantages of each process is provided in Table 15.

Table 15 *Comparison of bus ribbon joining processes.*

Joining Process		Advantages	Disadvantages
Contact	Hot bar, steady state, reflow soldering	Rapid heating Good temperature control possible Compact size	Periodic maint. for bar cleaning Potential burn hazard Separate cold clamp needed
	Hot bar, pulsed, reflow soldering	Low power consumption Good temperature control possible Safe - cool between cycles	Periodic maint. for bar cleaning Some have long heat-up time
	Parallel gap resistance welding or soldering	Low power consumption Rapid heating Safe - cool between cycles	Periodic maint. for electrode cleaning Hard to control temperature
	Ultrasonic welding or soldering	Fast Safe - no hot parts Flexible - wide range of ribbon materials can be joined without flux	Complex, costly equipment Rigid anvil required under ribbon Periodic maint. for tip cleaning
Non-Contact	Visible or IR light soldering	Non-contact - no tip cleaning	Inefficient energy transfer - ribbons are reflective Clamp needed
	Laser welding or soldering	Non-contact - no tip cleaning Fast	Complex, costly equipment Inefficient power conversion Eye safety hazard
	Hot air soldering	Non-contact - no tip cleaning Inexpensive equipment	Inefficient heat transfer Potential burn hazard Air flow may move parts Compressed air or N_2 required
	RF induction soldering	Non-contact - no tip cleaning Fast? Low power consumption?	Complex, costly equipment RF hazard - shielding required Proximity to other metal parts may cause problems
Mechanical Splice	Crimping	Safe - no hot parts No tip cleaning Fast	Added part needed at each joint Thick splices - hard to laminate Non-metallurgical joint; possible large I^2R losses; reliability Insertion operation needed

Pulsed hot bar reflow soldering rated highly in the ribbon joining process evaluation. Spire contacted several vendors of bonding equipment. Three of these vendors visited Spire to discuss our bus bonding requirements: Unitek Miyachi Corp., Hughes Aircraft Co., and Automation Unlimited. Unitek and Hughes recommended their pulsed heat reflow soldering equipment for this task. Automation Unlimited provides an automated soldering station which dispenses flux core solder which is melted with a standard soldering iron. Spire provided samples of interconnect ribbon and bus ribbon to all three vendors. Bonded samples were prepared by each vendor and returned to Spire for evaluations. Visual inspections and pull tests were done at Spire and 20 samples of bonded ribbons from Unitek and Hughes were sent to NREL as a program deliverable.

The Unitek and Hughes approaches have several advantages over Automation Unlimited's approach. The pulsed heat reflow soldering method (Unitek and Hughes) does not need any additional flux or solder, while the soldering iron method (Automation Unlimited) requires the use of a flux core wire solder, an added materials cost. Also, the systems quoted by Unitek and Hughes are priced in the $9K to $10K range, while the Automation Unlimited system is priced at $28.6K. Finally, pull tests were not done for the Automation Unlimited samples because the joint quality varied due to inconsistent part positioning. Automation Unlimited attributes this to inaccurate tooling, a problem they claim would be corrected if a machine were built for this application.

Pull tests were done on the reflow-soldered ribbons prepared by Hughes and Unitek. No solder or flux was added to the ribbons. The interconnect ribbon is 0.003" x 0.100" copper with a 0.0005" coating of Sn60/Pb40 solder. The bus ribbon is 0.006" x 0.200" copper with a 0.0005" coating of Sn60/Pb40 solder. The interconnect ribbon was coated with flux by the Assembler as would normally be the case at the ends of each cell string. The bus ribbon was solder coated but had no flux coating. Pulls were done at a 90° angle and the peak force was recorded with a Chatillon digital force gauge. The results, presented in Table 16, show excellent pull strengths for both vendors.

Table 16 *Pull test results, bus ribbon to interconnect ribbon solder joints.*

Test	Pull Force (kg)	
	Unitek	Hughes
1	2.07	2.65
2	2.80	2.66
3	3.42	1.82
4	3.20	1.85
5	3.69	2.29
Average	3.04	2.25
Std. Dev.	0.63	0.41

2.2.16 Tasks 12 and 17 - Information Dissemination

Spire actively disseminated information to the PV industry on the activities and results of this program. This work was done under Task 12 (Phase I) and Task 17 (Phase II) of this program with additional support from Spire's ongoing photovoltaic marketing activities. Spire mailed several news releases, produced data sheets and videos, published technical papers, and visited major PV manufacturers throughout the course of the program to keep the PV industry informed.

Four technical papers were published which reported on work done in the program. The papers were presented at the following conferences:

- 12th NREL Photovoltaic Program Review Meeting, Denver, CO (1993)[6]
- NREL Photovoltaic Performance and Reliability Workshop, Lakewood, CO (1994)[7]
- First World Conference on Photovoltaic Energy Conversion, Waikoloa, HI (1994)[8]
- 13th NREL Photovoltaic Program Review Meeting, Lakewood, CO (1995)[2]

An abstract for a paper reporting on processing evaluations with the Assembler was submitted to the 25th IEEE Photovoltaic Specialists Conference to be held in Washington, DC, in May, 1996.[9]

Subcontract reports were written, including 29 monthly reports, two semi-annual reports, and an annual report. Four subcontract review meetings were held, three for the PVMaT Technical Monitoring Team (TMT) and one for a Department of Energy (DOE) peer review, as described below.

- A program review meeting was held for the TMT at Spire, Bedford, MA, on June 2, 1993. Attendees included the members of the TMT (D. Mooney and J. Burdick, NREL, and A. Maish, Sandia) and personnel from Spire (G. Darkazalli, M. Nowlan, S. Hogan, S. Sutherland, J. Murach, and W. Breen) and U. Mass. Lowell (P. Krolak, J. Milstein, and C. Kosta). Program progress and system design concepts were reviewed in detail. A tour of Spire's facilities was conducted, and subassembly components were examined.

- An annual program review meeting was held at NREL, Golden, CO, on December 2, 1993. In attendance were the TMT members (H. Thomas, who replaced D. Mooney, and J. Burdick, NREL, and A. Maish, Sandia), E. Witt, R. Mitchell, and others from NREL, and M. Nowlan from Spire. Videotape and viewgraph presentations were given by M. Nowlan to describe the progress made from January through the end of November, 1993.

- A DOE peer review assessment of this program was held in Englewood, CO on August 11, 1994. The review panel consisted of scientists and engineers with technical expertise in areas related to the program. M. Nowlan of Spire presented the objectives, accomplishments, and current activities of the program through viewgraphs and a videotape of the Assembler in operation. Spire's program later received a Certificate of Appreciation from DOE for achieving the highest rating of the nine programs reviewed by the panel.

- A final program review meeting was held for the TMT at Spire on October 12, 1995. Attendees included the members of the TMT (H. Thomas and J. Burdick, NREL, and A. Maish, Sandia), and personnel from Spire (M. Nowlan, S. Hogan, and G. Darkazalli).

M. Nowlan summarized the objectives, activities, and accomplishments of the program through viewgraphs, slides, and a videotape of the Assembler in operation. A visit was made to ASE Americas, Billerica, MA, to observe the Assembler fabricating strings of ASE cells.

Preliminary and revised specification sheets were prepared to provide information on the automated cell assembly system developed in this program. The system was designated the SPI-ASSEMBLER™ 5000. The specification sheet has been distributed widely to PV module manufacturers. A copy of the current Assembler specification sheet is provided in Appendix A. Spire's contacts with potential customers indicated that some manufacturers prefer to start with a less automated system when production volumes are low to reduce their capital expenditures. As a result, Spire designed and offered a semi-automated system based on the Assembler concept, which was designated the SPI-STRINGER™ 500. A copy of the current Stringer specification sheet is also provided in Appendix A. The Stringer was designed as a modular system, so that optional automation modules (such as ribbon feeding or cell loading) can be added to upgrade the system to a complete Assembler.

Spire exhibited at major international PV conferences in the U.S. and overseas during the course of the program. Spire distributed technical papers describing the work done in this program as well as data sheets on the new cell interconnecting equipment (the Assembler and Stringer). These exhibitions included:

- Soltech '93, Washington, DC (1993)
- 23rd IEEE PV Specialists Conference, Louisville, KY (1993)
- Soltech '94, Ponte Verde Beach, FL (1994)
- 12th European PV Solar Energy Conference, Amsterdam, Netherlands (1994)
- First World Conference on Photovoltaic Energy Conversion, Waikoloa, HI (1994)
- Renewable Energies Asia Pacific, New Delhi, India (1995)
- Soltech '95, San Antonio, TX (1995)

Spire engineers met for discussions on the Assembler with engineers responsible for PV module manufacturing at ASE Americas, AstroPower, Ebara Solar, Siemens Solar Industries, Solarex, Solec International, and Texas Instruments. Extensive processing evaluations were done in Tasks 15 and 16 as described in Sections 2.2.11 and 2.2.12.

At the time that this program ended (October, 1995), information dissemination efforts and processing evaluations (done under Task 15) resulted in the sale of three Assemblers and two Stringers, generating $1.6M in new Spire equipment sales based on technology developed in this program. This amount is roughly equivalent to the total value of the program ($1.52M).

SECTION 3
COST ANALYSIS FOR AUTOMATED SOLAR CELL INTERCONNECTING PROCESSES

A cost study was done to estimate the cost of interconnecting solar cells using the automated processes developed in this program. The study also compared these automated processes with semi-automated and manual interconnection processes. The sensitivity of the cost to production level, labor rate, cell power, yield, and uptime was examined. The study results were originally presented at the 13th NREL Photovoltaics Program Review Meeting in May, 1995.[2] This section provides a summary of the study's major findings.

The three processes considered were as follows:

Manual interconnection - An operator feeds interconnect ribbon from reels, cuts it to the proper length, and forms a stress-relief bend. Flux or solder paste is applied to a solar cell or the ribbon, the ribbon is placed on the cell's front contact bus, aligned, and soldered with a soldering iron. The process is repeated to attach a second ribbon to the cell front. Groups of cells with two ribbons attached are placed face down in an alignment fixture and the ribbons are soldered to the back contacts to complete a cell string.

Semi-automated interconnection with a SPI-STRINGER 500 - An operator turns a roller to pull two ribbons from reels, through a flux bath, and into a cutting/bending tool. A cutting blade and a bending die are attached to a common handle which the operator lowers to cut and bend both ribbons in a single step. Ribbons and cells are hand-placed on a vacuum conveyor belt with the assistance of mechanical guides. A foot switch is pressed to advance the belt, carrying the cells and ribbons under a solder head. The solder head uses high intensity light to solder ribbon to the front and back of the cell in one heating step. The belt motion and the soldering process are automated and programmable.

Fully automated interconnection with a SPI-ASSEMBLER 5000 - Stacks of solar cells are loaded into magazines which are inserted into an automatic loader. The loader transports cells from the stack to an aligner which uses a vision system to locate and inspect each cell. Two ribbons are automatically fed from reels, coated with flux, formed with stress-relief bends, cut to length, and placed on a vacuum conveyor belt. A four-axis robot uses cell location data from the vision system to place the cell in the proper position on the conveyor belt. The belt automatically indexes the cells and ribbons under a solder head which uses high intensity light to solder ribbon to the front and back of the cell in one heating step. The system also provides automated transport of completed strings to an in-line current-voltage tester and to a lay-up table.

Detailed input was provided to a cost model for each level of process automation. Input included materials and consumables costs, labor hours, equipment costs, and spare parts costs. A list of assumptions and rates used for the three levels of automation are provided in Table 17. The yield loss obtained in manual soldering was estimated to be twice as large as that for machine soldering since the light soldering process heats the cell only once to solder all four contact busses (front left and right, back left and right) while applying minimal mechanical contact to the cell.

Table 17 *Cost model assumptions.*

Factor	Manual Tools & Fixtures	Semi-automated Stringer	Automated Assembler
Production uptime (%)	80	80	80
Yield estimate (%)	97	98.5	98.5
Power per cell (W)	1.50	1.50	1.50
Overhead (%)	100	100	100
SG&A (%)	10	10	10
Finance charge (%)	10	10	10
Project life (years)	5	5	5
Operator labor ($/hr)	9.00	9.00	9.00
Annual inflation (%)	3	3	3
Shifts/day	3	3	3
Days/week	5	5	5
Net capacity (kW/yr/shift)	104/person	599/machine	1797/machine

The Spire-developed Investment Analysis - Commercial Model (IACM) was used to calculate the cost per unit of product (dollars per watt of module power) over the plant lifetime. The results of the cost model are graphed in Figure 48. The costs shown are the incremental costs for the process and do not include the solar cell cost. Labor and associated indirect costs dominate the manual process, which totals $0.45/W. Labor costs are significantly reduced for both semi-automated and automated processes, which total $0.16/W and $0.09/W respectively.

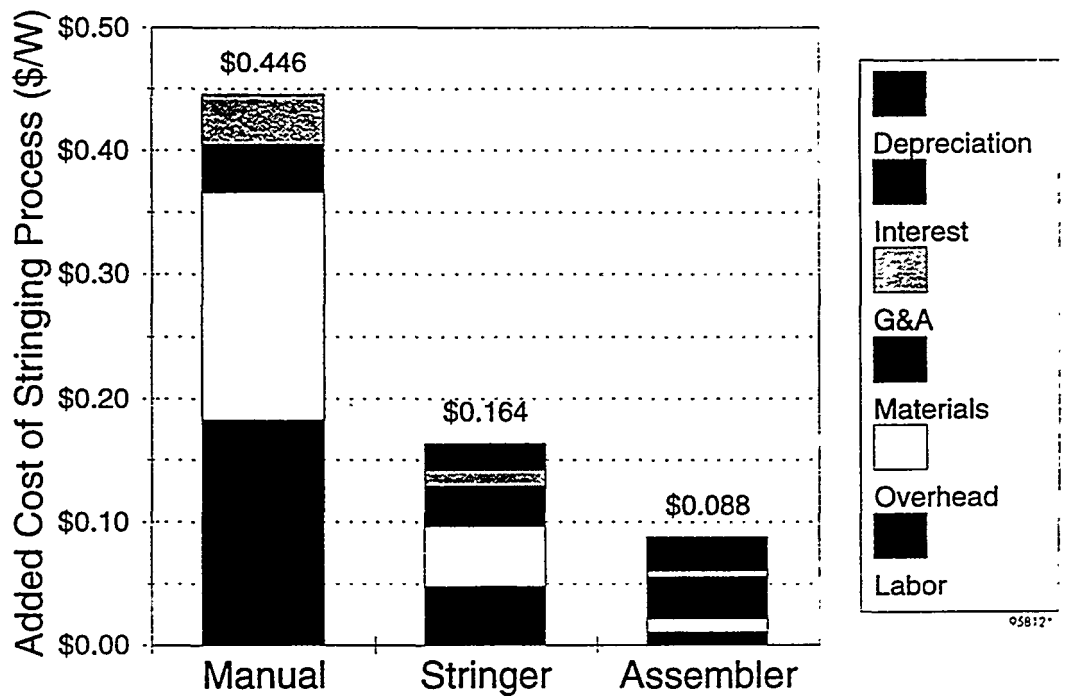

Figure 48 *Comparison of cell interconnection process costs for three levels of automation.*

Inputs to the cost model were modified to plot sensitivities to various factors. Figure 49 shows the effect of running the process at less than full capacity. Full capacity (100% in Fig. 49) refers to 3 shift/day, 5 day/week operation, equivalent to 300 kW/year for manual, 1800 kW/year for semi-automated, and 5400 kW/year for automated processing. The minima evident in the manual and semi-automated curves occur as production fully utilizes one (at 30% capacity), two (60%), or three (100%) shifts of labor. The effect is less noticeable in the automated case (the Assembler) due to the low labor content of the process.

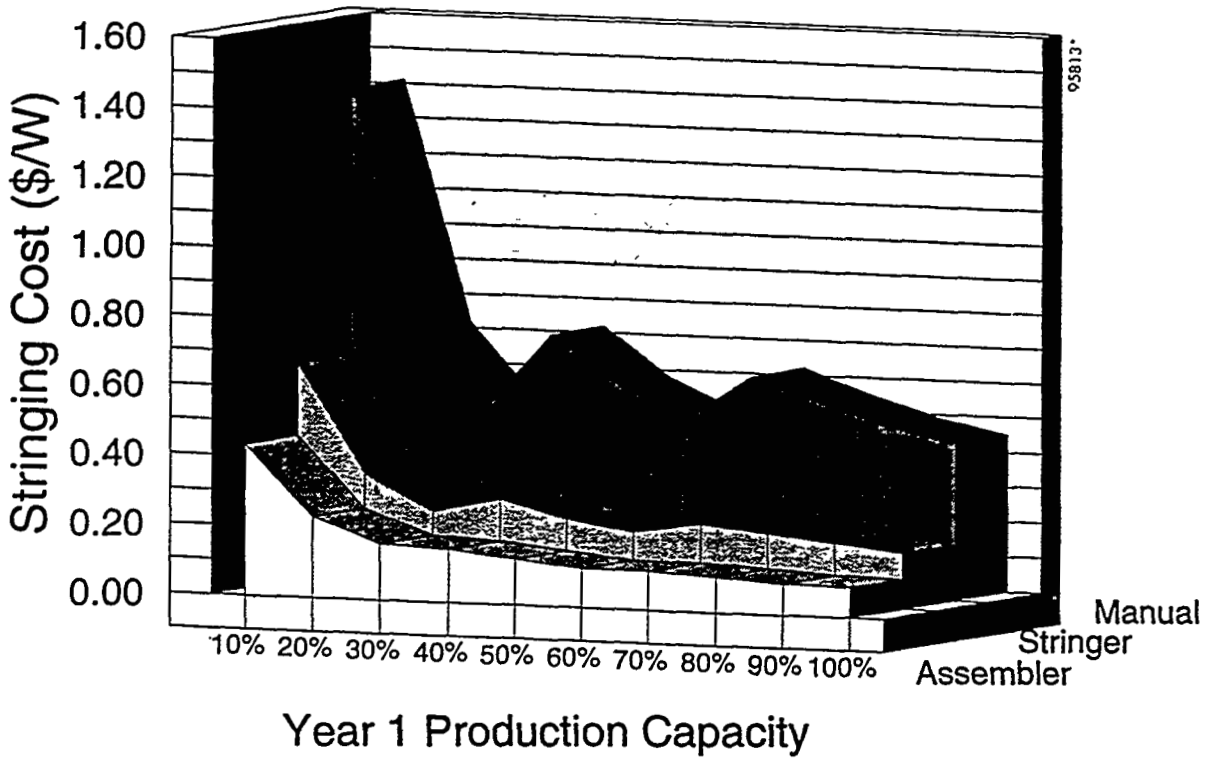

Figure 49 *Cell interconnection process cost vs. production level.*

The cost sensitivity to yield at various factory uptimes is plotted for automated processing in Figure 50. A conservative 80% uptime level has been chosen as the baseline case. Process yields of 98.5% have been demonstrated at Spire with several manufacturers' cells in pilot runs of several hundred to several thousand cells. This number is expected to increase in a production situation where the production volumes are higher and where a machine is dedicated to one or two similar types of cells. Figure 51 shows how the cost of automated stringing varies with changes in cell power, labor rate, and production level.

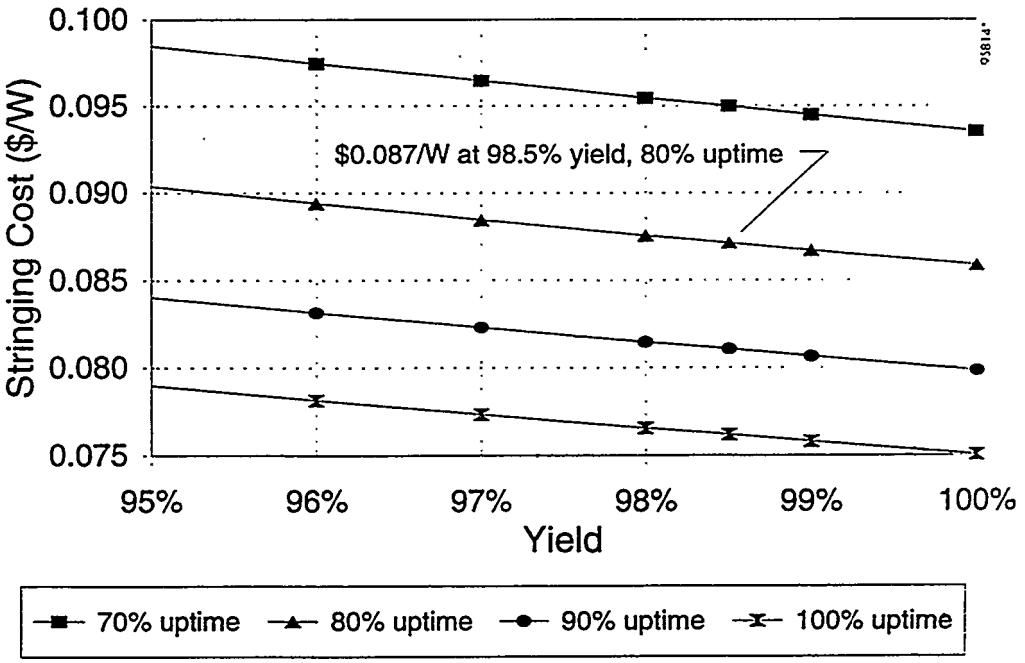

Figure 50 *Automated process sensitivity to yield at various uptimes.*

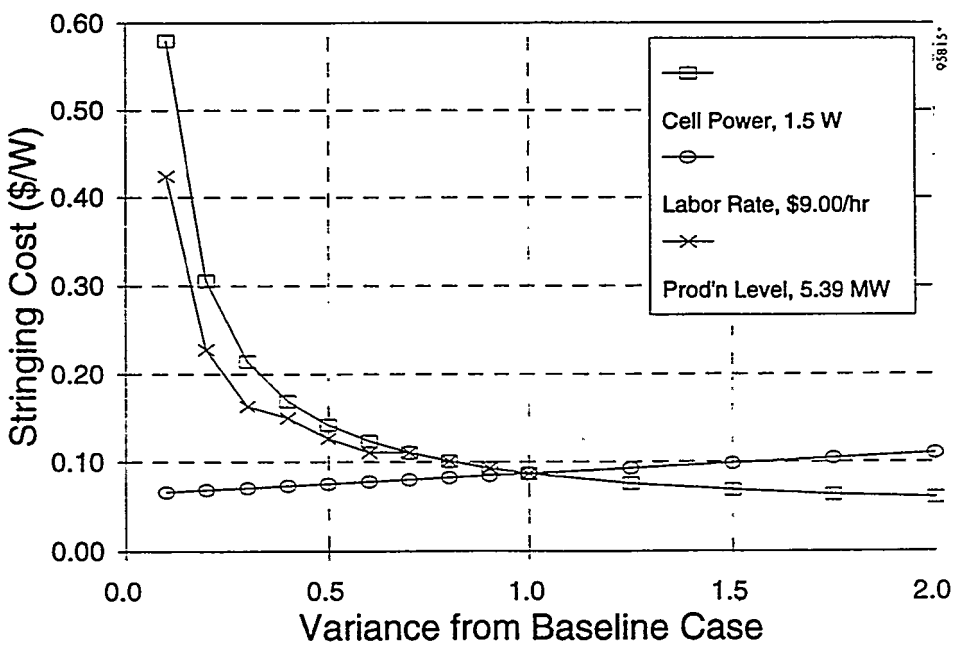

Figure 51 *Automated process sensitivity to cell power, labor rate, and production level.*

SECTION 4
CONCLUSIONS

Spire successfully completed a 34 month program entitled "Automated Solar Cell Assembly Teamed Process Research" as part of the PVMaT Phase 3A project. The team members included lower-tier subcontractors Solec International, who provided thin solar cells for process evaluations, and the University of Massachusetts Lowell's Center for Productivity Enhancement, who assisted with machine vision tasks. Assistance with final processing evaluations was provided by ASE Americas.

A completely new processing system was developed which demonstrated the program objective of developing high yield, high throughput, fully automated processes for tabbing and interconnecting thin and standard silicon solar cells. Low-stress processes were developed for handling cells fabricated from thin silicon wafers with high yield. Cell-to-cell cycle times were measured at 3.8 to 4.0 s/cell, achieving the 4.0 s/cell program goal. Labor content was significantly reduced by combining tabbing and interconnecting into a single automated process.

New automated processes were developed for cell loading, cell aligning, cell inspection, ribbon handling (ribbon feeding, forming, cutting to length), flux application, ribbon-to-cell soldering, cell string handling, and in-line string I-V testing. Flexible automation techniques were incorporated to enable production of a variety of module designs with minimal mechanical adjustments or tooling changes. Some of the low-stress processes that were developed include machine vision cell alignment that eliminates handling cell edges, and a soldering process that combines conductive preheating with a high-intensity light source to solder a cell's front and back contacts in a single heating step.

Processing evaluations were done on the assembly system over a 14 month period. More than 15,000 solar cells from six major module manufacturers were processed through the system, including cells made from monocrystalline Cz Si, polycrystalline cast Si, and polycrystalline EFG ribbon Si. Yields over 98% were achieved with both thin (200 μm) Cz Si cells from Solec and standard thickness (300 to 400 μm) Cz Si, cast Si, and ribbon Si cells from a range of manufacturers.

Solar cell performance measurements made before and after processing showed no cell degradation. Measurement data taken for Solec cells show that the power increased slightly (2%), mainly due to an increase in fill factor. This may be caused by an increase in conductivity along the contact busses provided by the interconnect ribbons.

Both Siemens Solar Industries and Solarex made modules from cell strings fabricated on the assembly system which they subjected to accelerated environmental testing per IEC 1215 and IEEE 1262 standards. These tests consisted of thermal cycling, thermal and humidity-freeze cycling, and damp heat soaking. The maximum allowable power loss is 5% for the IEC 1215 testing and 10% for the IEEE 1262 testing. All modules passed both qualification tests, with an average power loss of only 2.3%.

As a result of the technology developed in this program, Spire has significant new products to offer the PV industry: the SPI-ASSEMBLER 5000 and the SPI-STRINGER 500. Several of these products have already been sold to PV manufacturers.

SECTION 5
REFERENCES

1. U. S. Energy Information Agency data reported by A. L. Frank, Ed., *The Solar Letter*, **5** No. 18 (1995) 259.

2. M.J. Nowlan, S.J. Hogan, and G. Darkazalli, "Cost Analysis of an Automated Process for Interconnecting Crystalline Silicon Solar Cells," proc. 13th NREL PV Program Review Meeting, Lakewood, CO, May 16-19, 1995.

3. Spire Corporation, "Photovoltaic Manufacturing Technology Program," Phase 1 Final Report, SERI Contract XC-1-10057-1 (1991).

4. Fluoroware Wafer Carrier No. PA92-39M-0603 for 100 mm square solar cells.

5. D. Franke and I. Steinbach, "Calculation of Thermal Stresses During the Soldering of Solar Cell Strings," proc. IEEE First World Conf. on Photovoltaic Energy Conversion, Waikoloa, HI, (1994) 1458.

6. M.J. Nowlan, S.J. Hogan, S.F. Sutherland, W.F. Breen, J.M. Murach, and G. Darkazalli, "Development of Advanced Automation Processes for Photovoltaic Module Manufacturing," AIP conf. proc. 306, 12th NREL PV Program Review Meeting, Denver, CO (1993) 287.

7. S.J. Hogan, M.J. Nowlan, T.L. Jester, J.J. Hummel, "Performance and Reliability Testing of Crystalline Silicon Cell Strings Fabricated with a SPI-ASSEMBLER™ 5000 Apparatus," NREL Photovoltaic Performance and Reliability Workshop, Lakewood, CO, September 21, 1994.

8. M.J. Nowlan, S.J. Hogan, G. Darkazalli, S.F. Sutherland, W.F. Breen, J.M. Murach, and J.S. Patterson, "Advanced Automation Techniques for Interconnecting Thin Silicon Solar Cells," proc. IEEE First World Conf. on Photovoltaic Energy Conversion, Waikoloa, HI, (1994) 828.

9. Abstract submitted for publication: M.J. Nowlan, S.J. Hogan, J.S. Patterson, S.F. Sutherland, J.M. Murach, W.F. Breen, and G. Darkazalli, "Processing Evaluations of an Automated High-Throughput System for Interconnecting Crystalline Silicon Solar Cells," submitted to 25th IEEE Photovoltaic Specialists Conf., Washington, DC, May 13-17, 1996.

APPENDIX A

SPECIFICATION SHEETS

SPI-ASSEMBLER™ 5000 AND SPI-STRINGER™ 500

SPI-ASSEMBLER™ 5000

Automated Solar Cell Assembly

The SPI-ASSEMBLER™ 5000 is an automated production machine which interconnects solar cells by soldering flat metal leads, or tabs, to cell contacts. The machine processes solar cells at a throughput of up to 700 cells per hour, resulting in substantial cost savings in high volume production through improved yield and reduced labor.[1]

Solar cells are unloaded from stacks and edge-aligned with a mechanical aligner. Tab material is fed from reels, coated with flux, cut to length, and provided with a stress-relief bend. Tabs and cells are aligned for soldering.

High-intensity lamps in the solder head assembly provide radiant thermal energy to the cell and tabs. Both front and back cell contacts are soldered in a single heating step.

A variety of solar cell sizes and shapes can be processed. The number of cells per string, the number of strings per module, and the string orientation in the module are software programmable. Each completed string is automatically placed in position for module assembly.

Features and Benefits

- ▶ Automated and programmable assembly results in reproducible, high quality soldered cell strings
- ▶ Mechanical snugging system provides cell alignment
- ▶ High-intensity light soldering for improved throughput and yield
  - *Rapid soldering process*
  - *Minimum mechanical force on cell*
  - *Low thermal stress*
  - *Continuously soldered contacts*
- ▶ Software selectable module design
  - *Tab length and stress-relief bend location*
  - *Number of cells per string*
  - *Number of strings per module*
  - *Strings arranged in series or parallel configuration*
- ▶ Adaptable to a wide range of cell and tab designs
- ▶ Controlled by a personal computer with a graphics-based software package

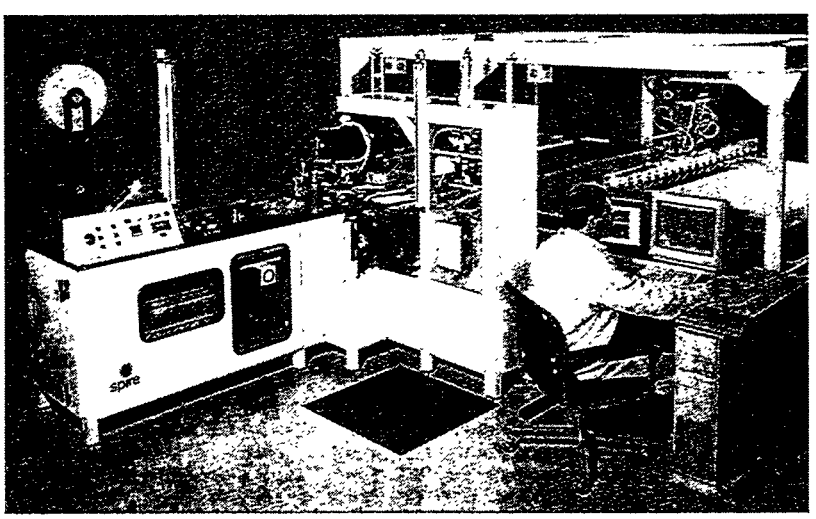

SPI-ASSEMBLER™ 5000 with optional vision system for cell alignment

[1] *M.J. Nowlan, S.J. Hogan, and G. Darkazalli, "Cost Analysis of an Automated Process for Interconnecting Crystalline Silicon Solar Cells," 13th NREL Photovoltaics Program Review Meeting, Lakewood, CO, May 16-19, 1995.*

spire

Spire Corporation/One Patriots Park/Bedford, Massachusetts 01730-2396/USA/617-275-6000/FAX 617-275-7470/email:spire.corp@channel1.com

Specifications

1. Solar Cell Geometry — *square, rectangular, round, or pseudo-square*
2. Maximum Cell Dimensions — *15 cm x 15 cm (6 in. x 6 in.)*
3. Number of Interconnect Ribbons — *2*
4. Maximum Number of Cells per String — *18*
5. Maximum String Length — *200 cm (78.7 in.)*
6. Nominal Throughput — *up to 700 cells/hour*
7. Equipment Dimensions (excluding computer system):
   - *Width* — *488 cm (192 in.)*
   - *Depth* — *315 cm (124 in.)*
   - *Height* — *180 cm (71 in.)*
8. Equipment Weight, Net — *950 kg (2100 lbs.)*
9. Utilities Requirements:
   - *Electricity* — *220 VAC, 60 A, 50/60 Hz, single phase*
   - *Compressed Air*
     - *Pressure* — *500 - 700 kPa (80-100 psi)*
     - *Flow* — *570 l/min. (20 scfm)*

Options

▶ String I-V Test:

A pulsed xenon lamp illuminates the cell string (up to 15 cm x 200 cm), an I-V curve is measured, and the string is placed either in a reject bin or in the proper location for a module, based on user selected criteria.

▶ Vision System for Cell Alignment:

Vision system with CCD camera, electronics, and software provides alignment of cells to tabs using cell pattern information. System also checks for chipped cells and automatically rejects any cells with chips or cells that cannot be aligned.

For additional information and application assistance, please call or fax Photovoltaics Sales.

SPI-STRINGER™ 500

Semi-Automated Solar Cell Stringing

The SPI-STRINGER™ 500 is a semi-automated production machine which interconnects solar cells by soldering flat metal leads, or tabs, to cell contacts. This machine is designed to process standard or thin silicon cells using an automated light soldering sequence.

The number of cells per string, the space between cells, and the soldering process parameters are software programmable. High-intensity lamps in the solder head assembly provide radiant thermal energy to the cell and tabs. Both front and back cell contacts are soldered in a single step.

Solar cells are loaded and aligned by the operator with the assistance of mechanical guides. A separate tab cutting station is included where tab material is fed manually from reels through a flux bath and then manually cut to length and shaped with a stress-relief bend.

Features and Benefits

- ▶ Semi-automated and programmable stringing for reproducible, high quality soldered cell strings
- ▶ High-intensity light soldering for improved throughput and yield
  - *Automated soldering sequence*
  - *Rapid soldering process*
  - *Minimum mechanical force on cell*
  - *Low thermal stress*
  - *Continuously soldered contacts*
  - *No solder paste required*
- ▶ Simultaneous soldering of the front and back contacts to reduce mechanical and thermal stresses on the cells
- ▶ Field adjustable to accommodate a wide range of cell and tab designs
- ▶ Controlled by a personal computer with a graphics-based software package
- ▶ The SPI-STRINGER 500 is upgradable to a fully automated SPI-ASSEMBLER™ 5000

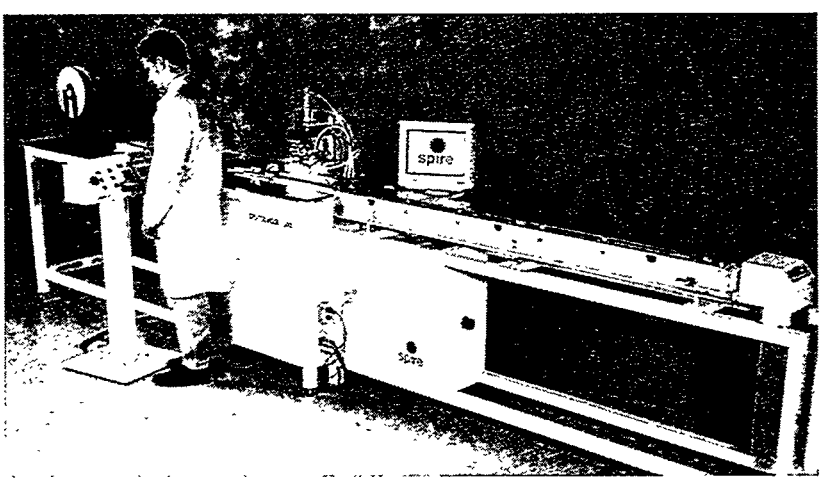

SPI-STRINGER™ 500

spire

Spire Corporation/One Patriots Park/Bedford, Massachusetts 01730-2396/USA/617-275-6000/FAX 617-275-7470/email:spire.corp@channel1.com

Specifications

1. Solar Cell Geometry — *square, rectangular, round, or pseudo-square*
2. Maximum Cell Dimensions — *15 cm x 15 cm (6 in. x 6 in.)*
3. Number of Interconnect Ribbons — *2*
4. Maximum String Length — *210 cm (82.7 in.)*
5. Nominal Throughput — *3 cells/minute*
6. Equipment Dimensions (excluding computer system and console):
   - *Width* — *445 cm (175 in.)*
   - *Depth* — *61 cm (24 in.)*
   - *Height* — *122 cm (48 in.)*
7. Equipment Weight, Net — *475 kg (1050 lbs.)*
8. Utilities Requirements:
   - *Electricity* — *220 VAC, 60 A, 50/60 Hz, single phase*
   - *Compressed Air*
     - *Pressure* — *500 - 700 kPa (80-100 psi)*
     - *Flow* — *57 l/min. (2 scfm)3*

Options

▶ Automated Cell Loading

A robot unloads cells from a cassette, centers the cells, and positions the cells for tabbing.

▶ Computer Automated Tabbing

This option automates the ribbon fluxing, cutting, stress-relief bending, and placement onto the solar cells; two solder coated tabs per cell. The tab length is software programmable. The throughput increases to 10 cells/minute when this option is used in conjunction with automated cell loading.

▶ String Unload Option

A robot transfers the soldered cell strings to a string buffer bin.

For additional information and application assistance, please call or fax Photovoltaics Sales.

Spire Corporation/One Patriots Park/Bedford, Massachusetts 01730-2396/USA/617-275-6000/FAX 617-275-7470/email:spire.corp@channel1.com

About Spire

Spire's innovative products and services provide competitive advantage to our customers in selected growth markets of biomaterials, optoelectronics, and photovoltaics.

Our products include ion beam-based processing services for medical components, compound semiconductor wafers and devices, and photovoltaic module manufacturing equipment - all of which draw on our strong research base and expertise in a variety of thin film technologies.

spire

Spire Corporation/One Patriots Park/Bedford, MA 01730-2396/USA

REPORT DOCUMENTATION PAGE

Form Approved
OMB NO. 0704-0188

1. AGENCY USE ONLY (Leave blank)	2. REPORT DATE	3. REPORT TYPE AND DATES COVERED
	February 1996	Final Subcontract Report, 6 January 1993 - 31 October 1995

4. TITLE AND SUBTITLE

Automated Solar Cell Assembly Teamed Process Research

5. FUNDING NUMBERS

C: ZAG-3-11219-01

TA: PV650101

6. AUTHOR(S)

M.J. Nowlan, S.J. Hogan, W.F. Breen, J.M. Murach, S.F. Sutherland, J.S. Patterson, G. Darkazalli

7. PERFORMING ORGANIZATION NAME(S) AND ADDRESS(ES)

Spire Corporation
One Patriots Park
Bedford, Massachusetts 01730

8. PERFORMING ORGANIZATION REPORT NUMBER

9. SPONSORING/MONITORING AGENCY NAME(S) AND ADDRESS(ES)

National Renewable Energy Laboratory
1617 Cole Blvd.
Golden, CO 80401-3393

10. SPONSORING/MONITORING AGENCY REPORT NUMBER

TP-411-20794

DE96000537

11. SUPPLEMENTARY NOTES

NREL Technical Monitor: Holly Thomas

12a. DISTRIBUTION/AVAILABILITY STATEMENT

12b. DISTRIBUTION CODE

UC-1250

13. ABSTRACT *(Maximum 200 words)*

This report describes work performed by Spire Corporation over a 34-month program. The work included the development of a completely new processing system that demonstrated the program objective of developing high yield, high throughput, fully automated processes for tabbing and interconnecting thin and standard silicon solar cells. High yield, low-stress processes were developed for handling cells fabricated from thin silicon wafers. The new system incorporates new automated processes for cell loading, cell aligning, cell inspection, ribbon handling (ribbon feeding, forming, cutting to length), flux application, ribbon-to-cell soldering, cell string handling, and in-line string I-V testing. The system incorporates flexible automation techniques to enable production of a variety of module designs with minimal mechanical adjustments or tooling changes. A cost analysis comparing manual, the new semi-automated, and the new fully automated processes indicated $0.45/W for the manual case, $0.163/W for the semi-automated case, and $0.087/W using the fully automated equipment.

14. SUBJECT TERMS

photovoltaics ; solar cells ; automated assembly ; teamed research

15. NUMBER OF PAGES
84

16. PRICE CODE

17. SECURITY CLASSIFICATION OF REPORT	18. SECURITY CLASSIFICATION OF THIS PAGE	19. SECURITY CLASSIFICATION OF ABSTRACT	20. LIMITATION OF ABSTRACT
Unclassified	Unclassified	Unclassified	UL